Dynamics of Saline Water Evaporation from Porous Media

A thesis submitted to The University of Manchester for the degree of Doctor of Philosophy
in the Faculty of Science and Engineering

2018

SALOMÉ M. S. SHOKRI-KUEHNI

School of Chemical Engineering and Analytical Science
The University of Manchester
Sackville Street, Manchester, M13 9PL, UK

TABLE OF CONTENTS

Page

ABSTRACT 4
DECLARATION 5
COPYRIGHT STATEMENT 6
DEDICATION 7
ACKNOWLEDGMENTS 8
INTRODUCTION 10
1.1. Pure water evaporation from porous media 10
1.2. Saline water evaporation from porous media 12
1.3. Aim and Objectives 14
1.4. Overview of the dissertation 15
1.5. References 16
ROOF COOLING BY DIRECT EVAPORATION FROM A POROUS ROOF LAYER 20
2.1. Abstract 23
2.2. Introduction 24
2.3. Experimental Considerations 27
2.4. Results and discussions 31
2.4.1. Evaporative mass losses 31
2.4.2. Thermal signatures during drying of porous media 33
2.5. Summary and conclusions 45
2.6. Acknowledgement 46
2.7. References 47
NEW INSIGHTS ON EFFECTS OF NACL CONCENTRATION AND PRECIPITATION ON SALINE WATER EVAPORATION FROM POROUS MEDIA 52
3.1. Abstract 55
3.2. Introduction 56
3.3. Experimental considerations 58
3.4. Results and discussions 59
3.4.1. Challenges of describing saline water evaporation from porous media .. 59
3.4.2. Effects of the precipitated salt at the surface on the evaporative fluxes .. 62
3.4.3. Evolving precipitated salt layers at the surface and their effect on the evaporation rate 66
3.4.4. Thermal signature of the contribution of precipitated salt to the evaporative rate 67
3.5. Summary and conclusions 70
3.6. Acknowledgement 71
3.7. References 71
3.8. Supporting Information 74
IMPACT OF TYPE OF SALT AND AMBIENT CONDITIONS ON SALINE WATER EVAPORATION FROM POROUS MEDIA 79
4.1. Abstract 82
4.2. Introduction 83
4.3. Theoretical considerations 84
4.3.1. Pure water evaporation from porous media 84
4.3.2. Saline water evaporation from porous media 87
4.4. Experimental considerations 89

4.5. Results and discussion 92
4.5.1. Scaling behaviour of pure water evaporation 92
4.5.2. Scaling behaviour of saline water evaporation 93
4.5.3. Precipitation dynamics and the evaporative mass losses 97
4.5.4. Effects of type of salt on the evaporation behaviour 102
4.6. Summary and conclusions 107
4.7. Acknowledgement 108
4.8. Appendix 108
4.8. References 109
IODINE K-EDGE DUAL ENERGY IMAGING REVEALS THE INFLUENCE OF PARTICLE SIZE DISTRIBUTION ON SOLUTE TRANSPORT IN DRYING POROUS MEDIA 114
5.1. Abstract 117
5.2. Introduction 118
5.3. Results and Discussion 119
5.3.1. Quantitative characterisation of ion transport in porous media 119
5.3.2. Solute concentration profiles 123
5.3.2. Estimating the dispersion coefficient 126
5.4. Methods Summary 132
5.5. References 134
5.6. Acknowledgment 138
5.7. Supplementary Information 139
SUMMARY AND CONCLUSIONS 140
6.1. Future work 142

FINAL WORD COUNT: 30’456

ABSTRACT

of thesis submitted by **Salome M. S. Shokri-Kuehni** for the Degree of **Doctor of Philosophy** and entitled "Dynamics of Saline Water Evaporation from Porous Media" on 21st March 2018.

Saline water evaporation from porous media with the associated salt precipitation patterns is frequently observed in a number of industrial and environmental applications and it is important in a variety of topics including, but not limited to, water balance and land-atmosphere interaction, terrestrial ecosystem functioning, geological carbon storage, and preservation of historical monuments. The excess accumulation of salt in soil is a global problem and is one of the most widespread soil degradation processes. Thus, it is important to understand the dominant mechanisms controlling saline water evaporation from porous media.

This process is controlled by the transport properties of the porous medium, the external conditions, and the properties of the evaporating fluid. During saline water evaporation from porous media, the capillary induced liquid flow transports the solute towards the evaporation surface while diffusive transport tends to spread the salt homogeneously thorough the porous medium. Therefore, the solute distribution is influenced by the competition between the diffusive and convective transport. As water evaporates, salt concentration in the pore space increases continually until it precipitates. The formation of precipitated salt adds to the complexity of the description of saline water evaporation from porous media.

In this dissertation, the effects of salt concentration, type of salt, and the presence of precipitated salt, on the evaporation dynamics have been investigated. The obtained results show that the precipitated salt has a porous structure and it evolves as the drying progresses. The presence of porous precipitated salt at the surface causes top-supplied creeping of the evaporating solution, feeding the growth of subsequent crystals. This could be visualized by thermal imaging in the form of appearance and disappearance of cold-spots on the surface of the porous medium, brought about by preferential water evaporation through the salt crust. My results show that such a phenomenon influences the dynamics of saline water evaporation from porous media. Moreover, a simple but effective tool was developed in this dissertation capable of describing the effects of ambient temperature, relative humidity, type of salt and its concentration, on the evaporative fluxes.

Additionally, pore-scale data obtained by synchrotron x-ray tomography was used to study ion transport during saline water evaporation from porous media in 4D (3D space + time). Using iodine K-edge dual energy imaging, the ion concentration at pore scale with a high temporal and spatial resolution could be quantified. This enabled us to reveal the mechanisms controlling solute transport during saline water evaporation from porous media and extend the corresponding physical understanding of this process. Within this context, the effects of particle size distribution on the dispersion coefficient were investigated together with the evolution of the dispersion coefficient as the evaporation process progresses.

The results reported in this dissertation shed new insight on the physics of saline water evaporation from porous media and its complex dynamics. The results of this dissertation have been published in 3 peer-reviewed journal papers together with one additional manuscript which is currently under review.

DECLARATION

I declare hereby that no portion of the work referred to in this thesis has been submitted in support of an application for another degree or qualification of this or any other university, nor any other institute of learning.

COPYRIGHT STATEMENT

i. I The author of this thesis (including any appendices and/or schedules to this thesis) owns certain copyright or related rights in it (the "Copyright")[1] and s/he has given The University of Manchester certain rights to use such Copyright, including for administrative purposes.

ii. Copies of this thesis, either in full or in extracts and whether in hard or electronic copy, may be made only in accordance with the Copyright, Designs and Patents Act 1988 (as amended) and regulations issued under it or, where appropriate, in accordance with licensing agreements which the University has from time to time. This page must form part of any copies made.

iii. The ownership of certain Copyrights, patents, designs and trademarks and other intellectual property (the "Intellectual Property") and any reproductions of copyright works in the thesis, for example graphs and tables ("Reproductions"), which may be described in this thesis, may not be owned by the author and may be owned by third parties. Such Intellectual Property and Reproductions cannot and must not be made available for use without the prior written permission of the owner(s) of the relevant Intellectual Property and/or Reproductions.

iv. Further information on the conditions under which disclosure, publication and commercialisation of this thesis, the Copyright and any Intellectual Property and/or Reproductions described in it may take place is available in the University IP Policy (see http://documents.manchester.ac.uk/DocuInfo.aspx?DocID=487), in any relevant Thesis restriction declarations deposited in the University Library, The University Library's regulations (see http://www.manchester.ac.uk/library/aboutus/regulations) and in The University's policy on Presentation of Theses.

[1] This excludes the chapters which are already published in academic journals for which the publisher owns the copyright

DEDICATION

To my husband and my daughter

ACKNOWLEDGMENTS

The arrival of this day, on which I am about to submit my PhD thesis, is the result of many decisions, experiences, encounters, and relations. I would like to acknowledge some of them.

Firstly, I would like to express my gratitude to The Leverhulme Trust for funding this research.

I would like to acknowledge and sincerely thank Professor Colin Webb and Dr Nima Shokri, for their supervision and kind support during my studies at the University of Manchester. Further, I would like to thank my collaborators, Professor Elie Bou-Zeid, Professor Muhammad Sahimi, Dr Thomas Vetter, Dr Mansoureh Norouzirad, and Ms. Mina Bergstad. It was an honour to work with them.

In addition, I would like to thank Professor Majid Hassanizadeh and Dr. Laurence Stamford for accepting to review and evaluate the present work.

I am grateful to Professor Dani Or, for introducing me to the academic world and Professor Tim Dransfield for supporting my first attempts at research. I would like to express my appreciation to Dr Kofi Osei-Bonsu, Dr Harris Sajjad Rabbani, Ms. Mina Bergstad, and Mr. Abdulkadir Osman for their support and friendship during the years in JCB.

Furthermore, I thank my family. I am grateful to my parents, René Kuehni and Hanni Golling, for all they did, and to Dr Doris Aebi for choosing to become my second mother and for always being there. My father is the wisest person I know, I consider myself lucky beyond words to be his daughter and his trust was the greatest gift of all. I thank my siblings, Olivia, Regina, and Philippe, for always being on my side. I am grateful to Madar joon, Pedar joon, Neda Shokri, and

Nazanin Shokri, for all their love. I would also like to acknowledge Terry Rotherham, for changing the way I think and see the world.

Acknowledgment does not quite convey the deep gratitude, respect, and admiration I feel towards my co-supervisor, Dr Nima Shokri. In his role as my academic advisor he challenged me and pushed me and led me to achievements beyond anything I ever thought myself capable of. Moreover, long before taking on this role as my academic advisor he was my husband. He motivated, encouraged, and enabled me to enter university and pursue a degree in science. Most importantly, after the birth of our daughter he repeatedly compromised his own career development to support mine. I am proud of him for all he did to make this work possible and I know without him I could not be the person I am today.

This brings me to my daughter, Delphi Everest Dana. During the past three years, the picture of my daughter at scientific conferences has become a familiar sight. She is quietly playing in the poster hall, strolling with her papa through mixers, attending gala dinners, all with a charming smile. I could not have done any of this without her being the most accommodating, flexible, and sunny-natured child imaginable. However, I am not completing this work despite having had a child during my PhD, but because of it. When I am tired, she makes me strong. When I am frustrated, she is my motivation to try again. Her entire person, the joy she brings, humbles me and for her I am better and better again.

Chapter 1

INTRODUCTION

Evaporation from porous media is an important topic relevant to many environmental, engineering, and hydrological processes including land-atmosphere interactions, drying of powders, foods, and building materials, evaporative cooling and water management which influences crop production, vegetation and plant growth. Thus, it is important to understand the mechanisms controlling drying of porous media under a given boundary condition.

The evaporation process is controlled by the transport properties of porous media, the properties of the evaporating liquid, and the external conditions (e.g. ambient temperature and relative humidity, wind, radiation). In most environmental and hydrological applications the evaporating liquid is either pure water or saline water. Therefore, in the following a brief introduction about pure water evaporation and saline water evaporation from porous media is presented.

1.1. Pure water evaporation from porous media

Early stages of evaporation from porous media saturated with pure water are marked by a relatively high and rather constant evaporation rate, the so-called stage-1 evaporation. This period of evaporation is controlled by the external conditions. During stage-1, liquid water is transported by capillary induced liquid flow from a receding drying front (i.e. the interface between saturated and unsaturated zone) to the surface of the porous medium where the liquid vaporization occurs. At a certain drying front depth (which is controlled by the pore size distribution of the porous medium), the capillary connection between the wet zone at the bottom of the porous medium and the surface is disconnected due to the interaction between capillary, viscous and gravity forces. At this point, the liquid meniscus recedes from the surface to a level

below the surface of the porous medium forming a new vaporization plane. When all continuous liquid pathways are disconnected from the surface, this marks the onset of the so-called stage-2 evaporation. During this period, liquid water is transported by capillary induced liquid flow from the wet zone at the bottom to this new vaporization plane followed by the liquid evaporation and then vapour diffusion through the overlying dry surface. The vapour diffusion through porous media during stage-2 reduces the evaporation rate significantly compared to the stage-1 evaporation. Figure 1.1 shows qualitatively the processes occurring during stage-1 and stage-2 evaporation.

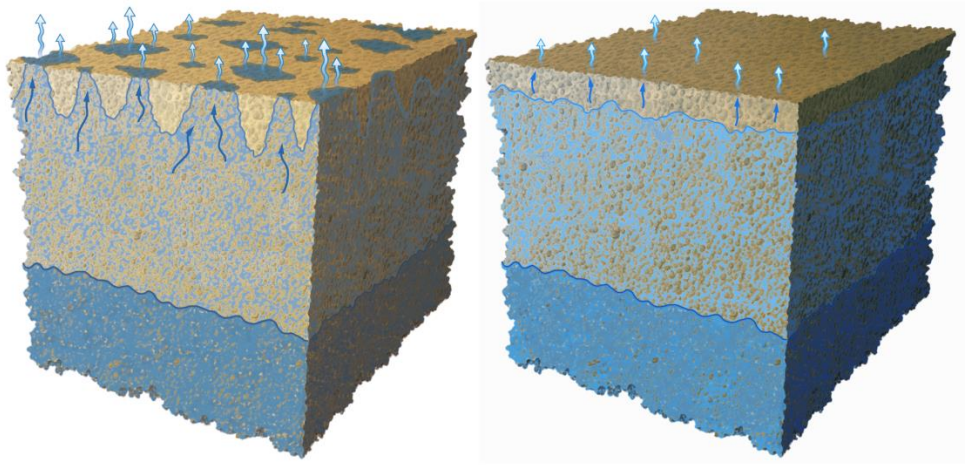

Figure 1.1. A conceptual picture illustrating the mechanisms occurring during (left) stage-1 and (right) stage-2 evaporation from porous media (after Shokri and Or [2011]). During stage-1, liquid vaporization occurs at the surface and the process is controlled by the external conditions (e.g. relative humidity and ambient temperature). During stage-2, a new vaporization plane is formed below the surface and the process is influenced by the vapour diffusion from the newly formed vaporization plane to the surface of porous media.

Although the evaporation process from porous media saturated with pure water is a relatively well-understood process [Laurindo and Prat, 1998; Saravanapavan and Salvucci, 2000; Yiotis et

al., 2006; Lehmann et al., 2008; Smits et al., 2012; Or et al., 2013; Haghighi et al., 2013], much less is known when the porous medium is saturated with saline solution, which is the main focus of this dissertation.

1.2. Saline water evaporation from porous media

Salt transport and precipitation during evaporation from porous media is of major concern in many processes such as soil salinity, terrestrial ecosystem functioning, durability of building materials and preservation of historical monuments, CO2 sequestration and crop production [Scherer, 1990, 2004; Rodriguez-Navarro and Doehne, 1999; Prasad et al., 2001; Il'Ichev et al., 2008; Nachshon et al., 2011a; Derluyn et al., 2011]. High salinity in the root zone severely impeded normal plant growth and development, resulting in reduced crop productivity. Salt-affected land is considered as an ecosystem under stress, where decreases in the nutrient cycling, and increases in the dominance of exotic biota are evident. Such effects can adversely change disease prevalence in plant, animal, and human populations [Jardine et al., 2007]. Therefore, it is very important to understand the saline water evaporation from porous media with the associated precipitation patterns.

During saline water evaporation, the ions are transported by convection toward the vaporization plane via capillary induced liquid flow while diffusion tends to spread the ions homogenously across the entire space. Therefore, the ion distribution is controlled by the competition between the convective and diffusive transport. When convective transport is dominant, the ions are preferentially deposited close to the surface of porous media. As water evaporates, salt concentration in the pore space increases continually. When the salt concentration at the surface substantially exceeds the solubility limit, it precipitates [Desarnaud et al., 2014; Shokri-Kuehni et al., 2017]. This is called efflorescence, and it refers specifically to evaporative driven soluble

salt from the interior of the porous medium to the surface where evaporation occurs [Guglielmini et al., 2008].

In addition to the parameters influencing the pure water evaporation from porous media (some mentioned above), the saline water evaporation is influenced by the type of salt, salt concentration, as well as the complex dynamics of precipitation during evaporation. Within this context, various aspects of saline water evaporation from porous media have been investigated in recent years. For example the effects of parameters such as particle size distribution (Norouzi Rad et al., 2015), relative humidity and temperature (Gupta et al., 2014; Shokri-Kuehni et al., 2017), mixture of salt (Jambhekar et al., 2016), wettability (Chapuis and Prat, 2007; Bergstad and Shokri, 2016), structure of porous media (Nachshon et al., 2011a, 201b, Bergstad et al., 2017) have been studied.

The majority of previous studies investigated how different parameters influence the salt precipitation patterns, but much less is discussed in literature about how the precipitated salt influences the evaporation rates and dynamics. According to the classical description, one would expect to observe reducing evaporation rate as the salt concentration increases in the evaporating liquid because the presence of salt reduces the saturated vapour pressure (thus reducing the difference between the saturated vapour pressure and the relative humidity which is the driving force for the evaporation) but several recent papers showed that this is not necessarily the case (Eloukabi et al., 2013). In other words, increasing salt concentration may not result in decreasing evaporation rate which is a counter-intuitive finding and requires further attention and investigation.

Another important aspect of saline water evaporation is to understand how ions are transported during evaporation. This influences the ion distribution, precipitation patterns and ultimately the

evaporation rate. Accurate pore-scale information will be helpful to extend the physical understanding of the mechanisms controlling ion transport during evaporation. Such information will be useful to develop predictive models capable of describing saline water evaporation at micro- and macro-scale. Without such knowledge, the modelling efforts will rely on adjusting parameters.

1.3. Aim and Objectives

Motivated by the importance of the saline water evaporation from porous media in various environmental and engineering applications, the key objectives of the present dissertation were to enhance our physical understanding of the processes controlling saline water evaporation from porous media. One of our key objectives was to determine how the presence of salt influences the evaporation rate from porous media. To address this question, we investigated this process at pore- and macro-scale using state-of-the-art technologies such as synchrotron X-ray tomography and high resolution thermal imaging combined with well-controlled laboratory experiments.

Within this context, the specific objectives of this research were to determine:

1- How the presence of precipitated salt influences the drying process.

2- How the type of salt and concentration influences the evaporation rate.

3- How ions are transported and distributed at the pore scale during saline water evaporation and how the pore-scale behaviour influences the macroscopic observations.

In addition to the above objectives focused on saline water evaporation, I looked into the drying of sand layers saturated with pure water for potential applications in evaporative cooling. This is explained in Chapter 2.

1.4. Overview of the dissertation

This PhD research was started with exploring the possibility of using porous layers saturated with pure water for evaporative cooling purposes and how the transport properties of porous media may impact the performance of such layers. The next step was to use saline water instead of pure water in the evaporating layers. However, switching the evaporating liquid from pure to saline water raised several interesting questions about how the presence of ions and in particular the precipitated salt at the surface influences the evaporation dynamics. Due to the lack of knowledge on this topic, the rest of this PhD research was focused on describing the dynamics of saline water evaporation from porous media with a particular focus on how the presence of ions, their concentration as well as the precipitated salt influences the drying dynamics. Moreover, the link between the pore-scale processes occurring during saline water evaporation and the macroscopic behaviour was investigated. Therefore this PhD dissertation is structured as following:

Chapter 1 provides a brief introduction about the pure water and saline water evaporation from porous media.

Chapter 2 is about potential application of evaporating sand layers saturated with pure water for evaporative cooling practices. In this chapter, the effects of particle size distribution on the drying dynamics and its cooling potentials are discussed. This chapter was published in "Energy and Buildings".

Chapter 3 is about the dynamics of saline water evaporation from porous media. In this chapter, the contribution of the precipitated salt at the surface to the saline water evaporation is discussed. Thermal imaging is used in this chapter to provide experimental evidence for contribution of precipitated salt at the surface to the evaporation process. Additionally, a conceptual picture is

proposed to describe the drying curve during saline water evaporation from porous media. This chapter was published in "Geophysical Research Letters".

Chapter 4 is about the effects of salt concentration and type of salt on the saline water evaporation from porous media. An equation is proposed in this chapter that enables us to quantify the effects of various parameters such as type of salt, salt concentration, relative humidity and ambient temperature on the evaporation dynamics. The proposed tool is validated using comprehensive series of experimental data. This chapter was published in "Advances in Water Resources".

Chapter 5 is about ion transport in porous media during evaporation. In this chapter, pore-scale analysis is performed using data obtained by synchrotron X-ray tomography to delineate the mechanisms controlling ion transport during saline water evaporation from porous media. This information is useful to describe the saline water evaporation process with the associated precipitation patterns at the macro-scale. Moreover, in this chapter, using the obtained pore-scale information we could investigate effects of particle size on the dispersion coefficient and how it varies over time during saline water evaporation from porous media. This chapter is currently under review for publication.

Chapter 6 consists of a summary of the research undertaken, reviews the conclusions reached, and offers recommendations on future work to be undertaken.

1.5. References

Bergstad, M., D. Or, P.J. Withers, and N. Shokri (2017), The influence of NaCl concentration on salt precipitation in heterogeneous porous media, Water Resour. Res., 53, 1702–1712.

Bergstad, M., N. Shokri (2016), Evaporation of NaCl solution from porous media with mixed wettability, Geophys. Res. Lett., 43, 4426–4432.

Chapuis, O., M. Prat (2007), Influence of wettability conditions on slow evaporation in two-dimensional porous media, Phys. Rev. E, 75, 046311, doi:10.1103/PhysRevE.75.046311.

Derluyn, H., T.A. Saidov, R.M. Espinosa-Marzal, L. Pel, and G.W. Scherer (2011), Sodium sulfate heptahydrate I: The growth of single crystals, J. Crystal Growth, 329, 44-51.

Desarnaud, J., H. Derluyn, J. Carmeliet, D. Bonn, and N. Shahidzadeh (2014), Metastability limit for the nucleation of NaCl crystals in confinement, J. Phys. Chem. Lett., 5(5), 890–895.

Eloukabi, H., N. Sghaier, S. Ben Nasrallah, and M. Prat (2013), Experimental study of the effect of sodium chloride on drying of porous media: The crusty–patchy efflorescence transition, Int. J. Heat Mass Transfer, 56(1–2), 80–93.

Guglielmini, L., A. Gontcharov, A. J. Aldykiewicz Jr., and H. A. Stone (2008), Drying of salt solutions in porous materials: Intermediate-time dynamics and efflorescence, Phys. Fluids, 20, 077101, doi:10.1063/1.2954037.

Gupta, S., H.P. Huinink, L. Pel, K. Kopinga (2014), How ferrocyanide influences NaCl crystallization under different humidity conditions, Cryst. Growth Des. 14 (4), 1591–1599.

Haghighi, E. , E. Shahraeeni, P. Lehmann, D. Or (2013), Evaporation rates across a convective air boundary layer are dominated by diffusion, Water Resour. Res. 49, 1602–1610.

Il'Ichev, A.T., G.G. Tsypkin, D. Pritchard, and C.N. Richardson (2008), Instability of the salinity profile during the evaporation of saline groundwater, J. Fluid Mech., 614, 87–104.

Jambhekar, V.A., E. Mejri, N. Schröder, R. Helmig, N. Shokri (2016), Kinetic approach to model reactive transport and mixed salt precipitation in a coupled free-flow-porous-media system, Trans. Porous. Med., 114(2), 341–369.

Jardine, A., P. Speldewinde, S. Carver, and P. Weinstein (2007), Dryland salinity and ecosystem distress syndrome: Human health implications, EcoHealth, 4, 10–17.

Laurindo, J. B., and M. Prat (1998), Numerical and experimental network study of evaporation in capillary porous media: Drying rates, Chem. Eng. Sci., 53, 2257– 2269, doi:10.1016/S0009-2509(97)00348-5.

Lehmann, P., S. Assouline, D. Or (2008), Characteristic lengths affecting evaporative drying of porous media, Phys. Rev. E, 77, 056309.

Nachshon, U., N. Weisbrod, M.I. Dragila, and A. Grader (2011a), Combined evaporation and salt precipitation in homogeneous and heterogeneous porous media, Water Resour. Res., 47, W03513.

Nachshon, U., E. Shahraeeni, D. Or, M. Dragila, and N. Weisbrod (2011b), Infrared thermography of evaporative fluxes and dynamics of salt deposition on heterogeneous porous surfaces, Water Resour. Res., 47, W12519, doi:10.1029/2011WR010776.

Norouzi Rad, M., N. Shokri, A. Keshmiri, P. Withers (2015), Effects of grain and pore size on salt precipitation during evaporation from porous media: A pore-scale investigation, Trans. Porous. Med., 110(2), 281-294.

Or, D., P. Lehmann, E. Shahraeeni, and N. Shokri (2013), Advances in Soil Evaporation Physics—A Review. Vadose Zone J. 12.

Prasad, A., D. Kumar, D.V. Singh (2001), Effect of residual sodium carbonate in irrigation water on the soil sodication and yield of palmarosa (Cymbopogon martinni) and lemongrass (Cymbopogon flexuosus), Agr. Water Manage., 50(3), 161-172.

Rodriguez-Navarro, C., E. Doehne (1999), Salt weathering: influence of evaporation rate, supersaturation and crystallization pattern, Earth Surf. Process. Landforms, 24, 191-209.

Saravanapavan, T., G. D. Salvucci (2000), Analysis of rate-limiting processes in soil evaporation with implications for soil resistance models, Adv. Water Resour., 23, 493– 502.

Scherer, G.W. (1990), Theory of drying, J. Am. Ceram. Soc., 73, 3-14.

Scherer, G.W. (2004), Stress from crystallization of salt, Cem. Concr. Res., 34, 1613–1624.

Shokri, N., D. Or (2011), What determines drying rates at the onset of diffusion controlledstage-2 evaporation from porous media?, Water Resour. Res., 47, W09513.

Shokri-Kuehni, S.M.S., T. Vetter, C. Webb, N. Shokri (2017), New insights into saline water evaporation from porous media: Complex interaction between evaporation rates, precipitation and surface temperature, Geophys. Res. Lett., 44, 5504–5510.

Shokri-Kuehni, S.M.S., M. Norouzirad, C. Webb, N. Shokri (2017), Impact of type of salt and ambient conditions on saline water evaporation from porous media, Adv. Water Resour., 105, 154-161.

Smits, K.M., V.V. Ngo, A. Cihan, T. Sakaki, T.H. Illangasekare (2012), An evaluation of models of bare soil evaporation formulated with different land sur- face boundary conditions and assumptions. Water Resour. Res. 48, W12526. http://dx.doi.org/10.1029/2012WR012113.

Yiotis, A. G., I. N. Tsimpanogiannis, A. K. Stubos, and Y. C. Yortsos (2006), Pore-network study of the characteristic periods in the drying of porous materials, J. Colloid Interf. Sci., 297, 738–748.

Chapter 2

ROOF COOLING BY DIRECT EVAPORATION FROM A POROUS ROOF LAYER

In this chapter, the evaporation process from porous media saturated with pure water is investigated. The idea is to explore the potential of a layer of drying porous media for evaporative cooling practices and to create an effective system for reducing heat flux through roofs into buildings by utilizing their evaporation capabilities. Within this context, the effects of particle size distribution on the drying behaviour of the porous medium as well as on its cooling potential for evaporative cooling were investigated.

Evaporation experiments using three samples of sand differing in particle size distribution were conducted. Customized rectangular columns were used to pack sand particles saturated by pure water. The sand columns were equipped with thermocouples at top and bottom of the column designed to measure soil temperature. Metal halide lamps and pyranometers were used to boost the evaporation and record the shortwave radiation, respectively. Moreover, a thermal camera was used to record the temperature dynamics at the surface of the sand columns. In addition to the container packed with sand grains, in each round of the experiment, an empty column was used whose bottom was covered by roofing felt and the temperature at the bare roof was recorded during the experiment. The columns sat on top of a table and were exposed to the same negligible heat flux from below. This setup enabled us to evaluate the potential and performance of evaporating sand layers for evaporative cooling practices.

The obtained results illustrate a strong correlation between the temperature dynamics and the evaporative mass losses. During stage-1 evaporation (when the liquid water is transported to the surface where liquid vaporization takes place), the surface is partially wet. This reduces the

temperature compared to the bare roof. During this period the temperature remains relatively constant. Our results show that the end of stage-1 evaporation marks the time when temperature begins to rise at the surface and bottom of the drying porous media due to the loss of liquid continuity with the surface, which eventually reduces the surface water content. Our results show that as long as the evaporation process is during stage-1 evaporation, the temperature at the surface of the "treated roof" (i.e. the roof with the overlying drying porous media) is lower than the bare roof. Since the sand sample with smaller particle size illustrates longer stage-1 evaporation, the low temperature period lasts longer in the case of fine-textured porous media. This result confirms the importance of transport properties of porous media on the performance of such a roofing system. An efficient porous medium for this application should present relatively long stage-1 evaporation otherwise the influence of the presence of the porous medium will be minor.

Roof cooling by direct evaporation from a porous roof layer

Salomé M.S. Kuehni (1), Elie Bou-Zeid (2), Colin Webb (1), Nima Shokri (1)

(1) School of Chemical Engineering and Analytical Science, University of Manchester, Manchester, M13 9PL, UK

(2) Department of Civil and Environmental Engineering, Princeton University, Princeton, NJ 08544, United States

This chapter has been published in Energy and Buildings.

Shokri Kuehni, S.M.S., E. Bou-Zeid, C. Webb, N. Shokri (2016), Roof cooling by direct evaporation from a porous roof layer, Energy and Buildings, 127, 521-528.

2.1. Abstract

As the world continues to urbanise, significant challenges are arising to environment, energy and water sustainability in cities. One of the most challenging consequences of increased urbanisation is increased energy consumption adversely affecting the quality of life, environment and public health. This motivated many researchers to find innovative methods to reduce energy consumption in buildings for cooling practices. In this paper, a series of experiments was conducted to investigate the performance of an evaporative layer of porous media and the effects of its particle size on reducing the roof surface temperature. To do so, customised rectangular Plexiglas columns were packed with three types of sand with well-defined particle size distribution saturated with water with all boundaries closed except the top, which was exposed to air for evaporation. The obtained results revealed the great potential of drying porous media to reduce the heat flux through roof via utilising a part of the energy for liquid vaporisation. As particle size decreased the temperature of roof remained lower than the bare roof for a longer time as a result of the presence of more liquid pathways connecting the receding drying front to the evaporation surface, which kept the surface wet for a longer time. Our results present new insights about the physical mechanisms controlling the performance of drying porous media to regulate roof surface temperature.

2.2. Introduction

Increasing energy efficiency is an immediate priority to cut carbon emissions, secure energy as well as save on energy bills. Over the past few decades, the improvement of living standards and the affordability of air conditioning have led to a considerable increase in the energy consumption related to space cooling. Additionally, the so-called urban heat island effect, resulting from increased urbanisation, contributes to making cities several degrees hotter than their rural surroundings [1-3]. This increases energy consumption for cooling of residential and commercial buildings. Therefore, developing novel approaches to improve cooling energy efficiency of buildings is essential to meet our low carbon economy targets. This will become even more important in the near future with the increase in climate change, not only in hot, but also in temperate climates such as in the UK [4,5].

Traditionally, roofs in some mid and high latitude locations consist of envelope materials (such as clay and asphalt) with a relatively high absorption coefficient, transferring large amounts of heat to the building. This leads to warmer indoor spaces in the summer and as a result higher demands for air conditioning. Roofs can represent up to 32% of the horizontal surface of built-up areas [6] and are important determinants of energy flux and heat transfer through the building envelopes. The roof offers the greatest opportunities for improving the cooling of buildings. It is the building element that is most exposed to the sky. Therefore, significant efforts have been made to reduce this heat load by improving roof design [7,8]. As a result of such efforts, several methods have been proposed. The so-called ‘green roof’ is an example of such a design [9,10]. A green roof is a roof that contains a soil (growing media) and vegetation layer as its outermost surface, allowing better regulation of building temperatures [9]. Although use of green roofs provides significant benefits, not only in energy consumption but also in urban

microclimatological and environmental terms [11], some disadvantages have been noted as well. Installation cost is elevated and maintenance of the green roof system, i.e. watering and replacing the old plants, is required regularly at additional cost. Besides, in terms of building structure, enhanced structural support is required to accommodate green roof systems to ensure sufficient capacity to resist weight load under the soil and vegetation and avoid collapse [12], further adding to the cost.

Other examples of alternative roofs include roof ponds and evaporation-based roof cooling systems [7, 13]. While no porous medium is used in these evaporative roof systems, latent heat of evaporation remains the main mechanism used to cool the building roof [14], as with green roofs. Crawford and da Silva [13], among many others, studied the capability of a roof-based evaporative pumping system to lower thermal loadings imposed on the interior of a building to reduce energy consumption as a result of air conditioning. Jain [15] presented thermal models to evaluate the performance of various passive cooling roof systems including bare roof, wetted roof surface, and evaporative cooling using water pond with movable insulation and concluded that a roof pond with movable insulation offers an efficient method for roof cooling.

There are many papers that investigated evaporation-based (green or otherwise) roof cooling systems and a comprehensive review is beyond the scope of the present paper. But in general, the effectiveness and viability of these types of roofs depend very strongly on the local settings such as local climate, native vegetation, and water availability [1, 16, 17]. It should be also noted that the very concepts of these types of roofs are designed for regions with abundant rainfall and water resources, and with native vegetation species that produce high cooling by evapotranspiration (in the case of green roofs). Considering the rising temperature trends even in

temperate cities (e.g. London), it is important to develop innovative, sustainable and cost-effective approaches capable of cooling buildings under a variety of conditions.

Recently, there have been some efforts to evaluate the performance of porous materials to be used on roofs (without vegetation) to create an effective system for reducing heat flux through buildings by utilizing their moisture absorption and evaporation capabilities [12]. A robust explanation and quantitative tool to predict the performance of a given drying porous media on reducing the heat flux through buildings are still missing due to a lack of deep physical understanding of how the thermal performance of drying porous media is affected by their transport properties, the properties of the evaporating fluid, and the external boundary conditions [18-22].

Typically the evaporation rate from initially saturated porous media is relatively high and is controlled by the atmospheric condition, the so-called stage-1 evaporation. During this period, liquid water is transported toward the evaporation surface via the capillary induced liquid flow connecting a receding drying front, marking the interface between the saturated and unsaturated zone [23], to the evaporation surface where liquid vaporization takes place supporting the evaporative demand. At a certain drying front depth or surface water content, the liquid continuity between the drying front and the evaporation surface is ruptured as a result of the interplay among the upward capillary force and the downward gravity and viscosity forces. Consequently the liquid meniscus recedes from the surface to a level below the surface forming an overlying thin dry layer. This marks the end of stage-1 evaporation [24]. When all liquid meniscuses are disrupted, a new vaporization plane forms very close to the surface which marks the onset of the so-called stage-2 evaporation. During this period, liquid is transported from the saturated zone to the new vaporization plane formed inside the porous medium followed by

liquid vaporization at that level and vapour diffusion through the overlying dry layer [25]. Stage-1 and stage-2 evaporation are limited by the atmospheric conditions and the transport properties of porous media, respectively [26-28].

In the present paper, a novel approach was proposed to reduce the energy consumed for cooling buildings by utilizing drying porous materials (with no vegetation) on roofs. By consuming a part of the radiative energy received at the roof surface for liquid vaporization, the evaporative porous layer reduces the heat flux through the roof, as well as the convective heating of the outdoor space that results in the urban heat island effect [29]. The main appeal of this approach compared to green roofs is that brackish or salt water can be used for evaporation (it can thus be used in dry coastal areas), no maintenance of vegetation is required, and the roof depth can be quite small since it does not need to support a root layer (posing lesser constraints on the built structure). Therefore, motivated by the importance of developing low-energy methods for cooling buildings, the specific objectives of the present paper are a) to evaluate the application of drying porous media on moderating the temperature of irradiated surfaces under laboratory conditions and b) to investigate the effects of particle size on the performance of the drying porous media for this purpose. This paper is a first step in a larger effort aimed at developing such evaporative roofs.

2.3. Experimental Considerations

All experiments were conducted in the Multiphase Flow and Porous Media research laboratory in the School of Chemical Engineering and Analytical Science at The University of Manchester. An experimental setup was developed to investigate the thermal performance of drying porous media, in terms of moderation of the roof surface temperature and reducing heat fluxes towards the indoor space. The experimental station is shown in Figure 2.1.

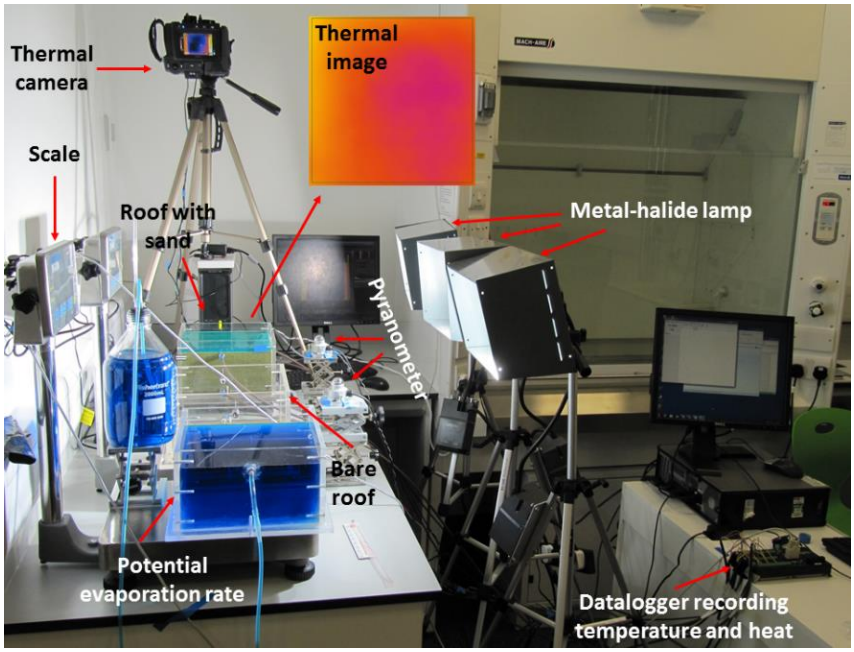

Figure 2.1. Experimental setup. The container filled with dyed water was used to measure the potential evaporation rate. The container packed with sand particles (labelled as "Roof with sand") was used to investigate the performance of drying porous media in reducing the surface temperature compared to the bare roof (the middle column). A thermal camera was fixed on top of the roof covered with drying porous media. Metal halide lamps were used to heat the containers. Two pyranometers were used to measure the radiation flux (they were positioned parallel to the roofing surfaces to capture the flux normal to these surfaces). The column packed with sand grains was equipped with thermocouples at the surface and bottom of the column. Additionally, a heat flux sensor was buried in the middle of the sand column. The data measured by the thermocouples, heat flux sensors and the pyranometers were recorded using a datalogger connected to a PC.

Three samples of quartz sand differing in particle size distribution referred to as coarse, medium and fine sand were used to pack the customized Plexiglas containers (150 mm in height, 250 mm in width and 250 mm in length). Figure 2.2 shows the particle size distribution of the sand samples used in our experiments (provided by the manufacturer).

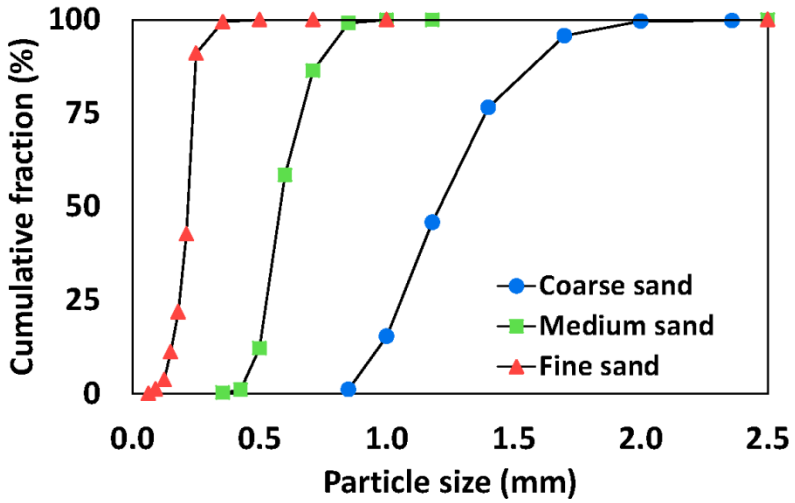

Figure 2.2. Particle size distribution of different sands used in the experiments.

The container was packed with sand grains saturated with deionised water following the procedure described in Grapsas and Shokri [30]. To measure the evaporation rate, the containers were mounted on digital balances (with accuracy of 0.1 g) connected to a computer to record the mass every 5 minutes during the experiments. The container was closed to mass transfer from all boundaries except the top, which was exposed to air for evaporation. The container packed with sand grains was equipped with thermocouples specifically designed to measure soil temperature (105E Type E Thermocouple, Campbell Scientific) with the accuracy of 0.5ºC. The thermocouples were placed at the surface and bottom of the sand pack to measure the temperature at these two locations every 5 minutes during the course of the experiment. The data were recorded using a datalogger (CR1000, Campbell Scientific). In addition, a thermal camera (FLIR T650sc, FLIR Systems, Inc.) with a thermal sensitivity (at 30 °C) of less than 30 mK and a resolution of 640×480 pixels was fixed above the packed sand to record the dynamics of temperature evolution at the surface every 30 minutes. A square heat flux sensor (35.1 mm by 35.1 mm) with a thickness of 2.8 mm (Wuntronic GmbH, Germany) and accuracy of 5%

connected to the datalogger was placed in the middle of the sand pack to measure the heat flux during the evaporation process every 5 minutes.

In addition to the container packed with sand grains, in each round of the experiment two more containers (with the same dimensions as mentioned above) were used to measure the potential evaporation rate and the temperature at the bare roof as illustrated in Figure 2.1. A thermocouple was placed on the surface of the bare roof (covered by roofing felt) to record the dynamics of the roof temperature during the experiment. To measure the potential evaporation rate, the 3rd container was mounted on a digital balance (to record the mass every 5 minutes), filled with dyed water (3 mL per litre), and connected to a Mariotte siphon (also mounted on the same balance) that maintained the water surface in the container at a fixed height [31].

To simulate the solar radiation, three metal halide bulbs were used (EYE Color Arc PAR36, Iwasaki Electronic Co., Japan), which were fixed on customized stands facing toward the containers as illustrated in Figure 2.1. Two pyranometers (Hukseflux, The Netherlands) were used to measure the shortwave radiation from the bulbs. The pyranometers were connected to the datalogger to record the data every 5 minutes during the course of the experiment. Special attention was given to establish equal radiation to the containers by adjusting the position and height of the solar lights, until similar radiation data were recorded by the two pyranometers.

Using the described experimental station, three rounds of experiments were conducted with the fine, medium, and course sand. The obtained results are explained next.

2.4. Results and discussions

2.4.1. Evaporative mass losses

The data measured by the balance were used to calculate the cumulative mass loss and the evaporation rate during each round of the experiment. Figure 2.3 illustrates the obtained results.

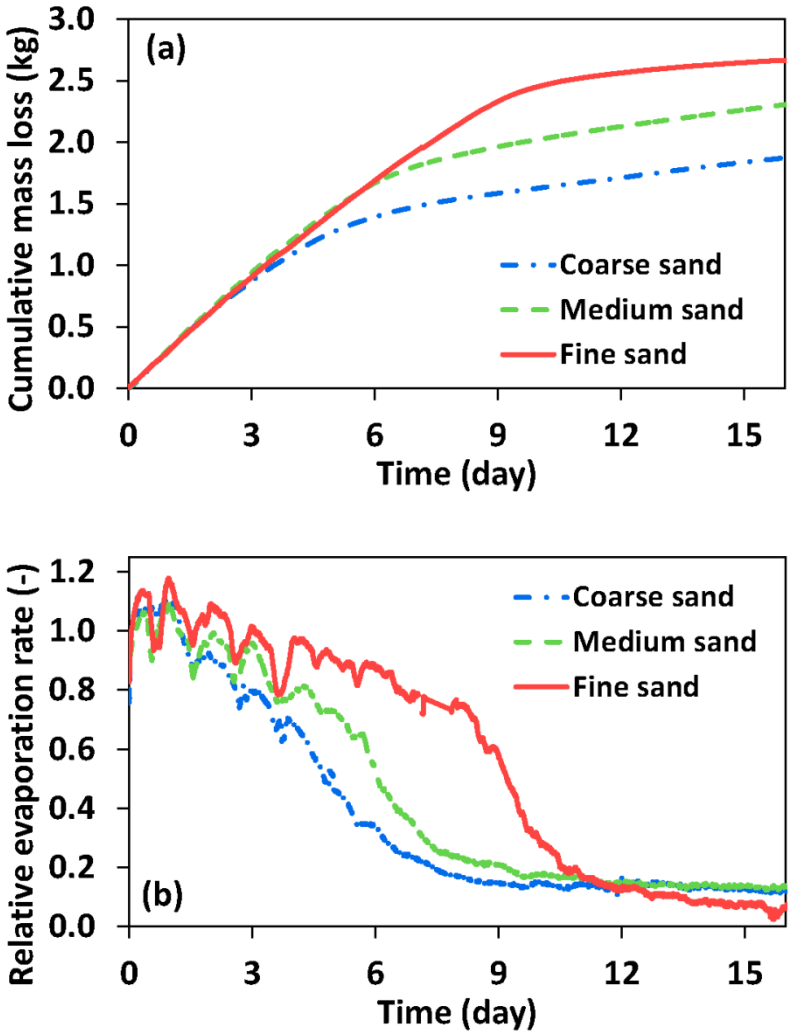

Figure 2.3. (a) The measured cumulative evaporative losses during the experiments with the roofs filled with the coarse, medium and fine sand. The finer the particles, the longer the duration of stage-1 evaporation. (b) The evaporation rates measured during drying of the coarse, medium and fine sands placed over the roofs. Note that the drying rate was scaled by the measured potential evaporation rate from the container filled with water. This dimensionless rate is referred to as "Relative evaporation rate".

During the experiments, we did not control the air speed, ambient temperature, or relative humidity. The average ambient temperature during the experiments with the coarse, medium, and fine sand was 27.8, 29.4 and 30.1 ºC, respectively and the average relative humidity during the experiment with the medium and fine sand was 20% and 17%, respectively (unfortunately due to a technical problem, we could not continuously measure the ambient relative humidity during the experiment with the coarse sand, but we expect it to be in the same range and the differences have minimal impact on our results). The measured ambient temperature and relative humidity were obviously different from the outdoor values as the experiments were conducted in the laboratory.

As mentioned earlier, the stage-1 evaporation is controlled by the external conditions. The slight differences and fluctuations observed in the measured evaporation rates during stage-1 in our experiments are due to the fluctuation in air speed, ambient temperature and relative humidity. Also, this implies that when extrapolating to the performance in the outdoors, the influence of higher air speeds would be to increase evaporation and further boost the effectiveness of the evaporative roofs. One can estimate this increase to be about 25% based on the relation between the Penman and Priestly-Taylor evaporation models, where a factor of 0.25 is used to model the contribution of the wind advection term.

According to Figure 2.3(a), in all cases the slopes of the cumulative mass loss curves were initially high and equal (indicating a high evaporation rate which corresponds to the stage-1 evaporation). As mentioned earlier, during this period the drying process is dominated by capillary induced liquid flow from the drying front (the interface between saturated and unsaturated zone) to the surface maintaining a high evaporation rate despite the receding drying front. As shown in Figure 2.3, in all three cases investigated in the present work, the stage-1

evaporation is followed by a transition period and stage-2 evaporation. This figure clearly illustrates the effect of the texture of the porous medium on the drying behaviour such that the medium with finer pores exhibits longer stage-1 evaporation. The relative evaporation rate in Figure 2.3(b) was calculated by scaling the measured evaporation rate in each case by the potential evaporation rate measured from the container filled with water.

Similar behaviour was observed in other studies [24, 25]. Stage-1 evaporation ends when the upward capillary force transferring the liquid to the surface for vaporization is balanced by the downward gravity and viscous forces. The latter is negligible in sandy media due to the large pore sizes [24]. In porous media with finer pores such as clay, the upward capillary force maintains the hydraulic continuity over longer distances, prolonging the stage-1 evaporation (for more discussions about the effects of pore size distribution on the prolongation of stage-1 evaporation see Or et al. [30] and references therein). Figure 2.3 illustrates the influence of the pore size on the dynamics of the transition from stage-1 to stage-2 evaporation. The results show a sharper and shorter transition period as particle size (and probably the width and tale of the pore size distribution) decreases.

Different drying dynamics, as influenced by the particle size distribution, reflect different liquid phase distribution through the drying porous media. This will influence the temperature distribution as well as heat flux through the drying porous media, as will be discussed in the next section.

2.4.2. Thermal signatures during drying of porous media

Figure 2.4(a) presents the recorded radiation flux by the pyranometer located in front of the bare roof in each round of the experiment and Figure 2.4(b) shows the radiation flux recorded by the

pyranometer placed in front of the container packed with sand grains, scaled by the radiation flux received by the bare roof. The recorded radiation flux is not similar to the values typically observed in outdoor spaces. In our experiments the radiative flux was limited by the capacity of the metal halide lamps used in our experiments. However, this difference in the radiative fluxes does not influence the process and physics explained in this paper. Although slight differences were observed between the radiation flux toward the bare roof in each round of the experiment (due to the slightly different environmental conditions), the scaled radiation flux in Figure 2.4(b) is very close to 1 in all cases. This indicates an equal amount of radiation to the two containers used in each round of the experiment and enables us to accurately evaluate the effects of the presence of a drying porous medium, together with the effect of its particle size distribution on the roof surface temperature.

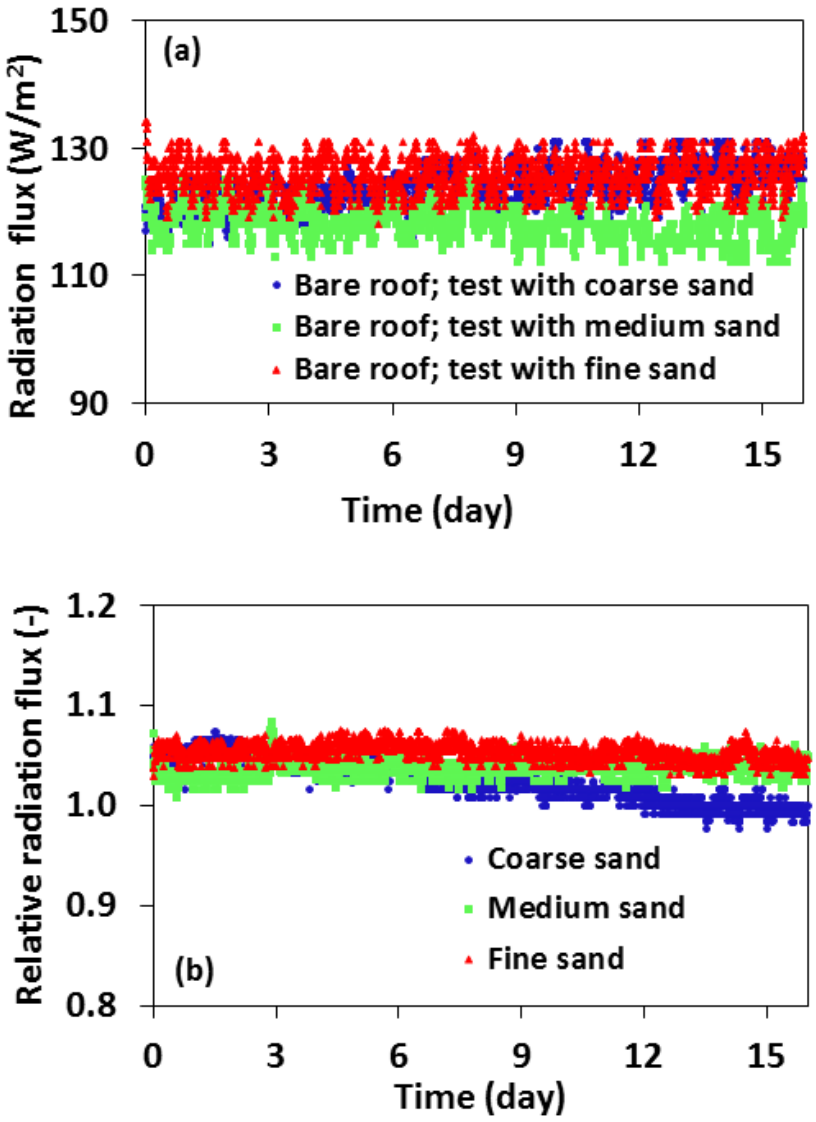

Figure 2.4. (a) Radiation flux toward the bare roofs measured by the pyranometers during the experiments with the coarse, medium and fine sand as illustrated in the legend. (b) The radiation flux toward the roof filled with sand particles scaled by the radiation flux received by the bare roof. The closeness of the value of this relative radiation flux to 1 indicates equal radiation toward the two containers (i.e. bare roof and the one filled with drying porous media).

Although the radiation flux in each round of the experiment was relatively constant (as shown in Figure 2.4), the ambient temperature, air speed, relative humidity, and also potentially ambient

radiation, were not constant in our experiments, causing some fluctuations in the recorded bare roof temperature by the thermocouple as illustrated in Figure 2.5. The attribution of the fluctuations to environmental conditions is supported by the clear diurnal cycle in the temperature plots.

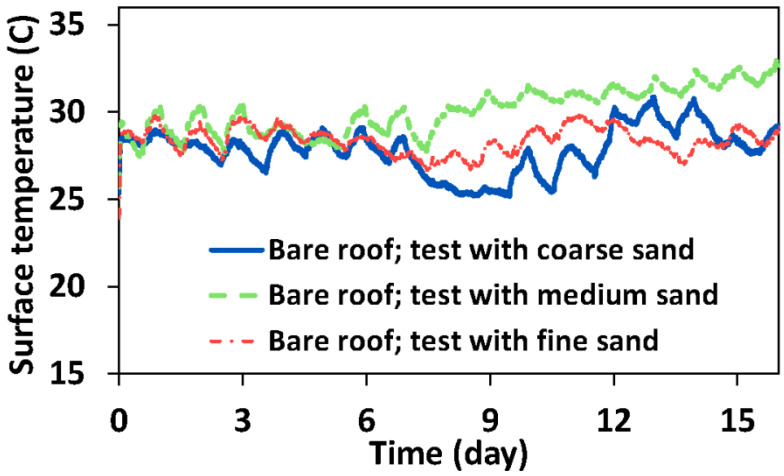

Figure 2.5. Evolution of the surface temperature of the bare roof measured during the experiments with coarse, medium, and fine sand. The observed temperature fluctuation is due to the fluctuation of the ambient conditions.

The temperature of the bare roof in each round of the experiment served as a reference, to evaluate the performance of the drying porous media with a given particle size distribution in moderating the surface temperature. In other words, the measured temperature profiles through the drying porous media are scaled by the recorded temperature of the bare roof in each round of the experiment, enabling us to evaluate the influence of the particle size distribution on the performance of the drying porous media.

The temperature profiles through each drying container were different due to the different drying behaviour of porous media as influenced by the particle size distribution. Figure 2.6 shows the spatial and temporal distribution of temperature at the surface of the drying porous media during

evaporation under the same cumulative evaporative mass losses (hence at different times for the different experiments).

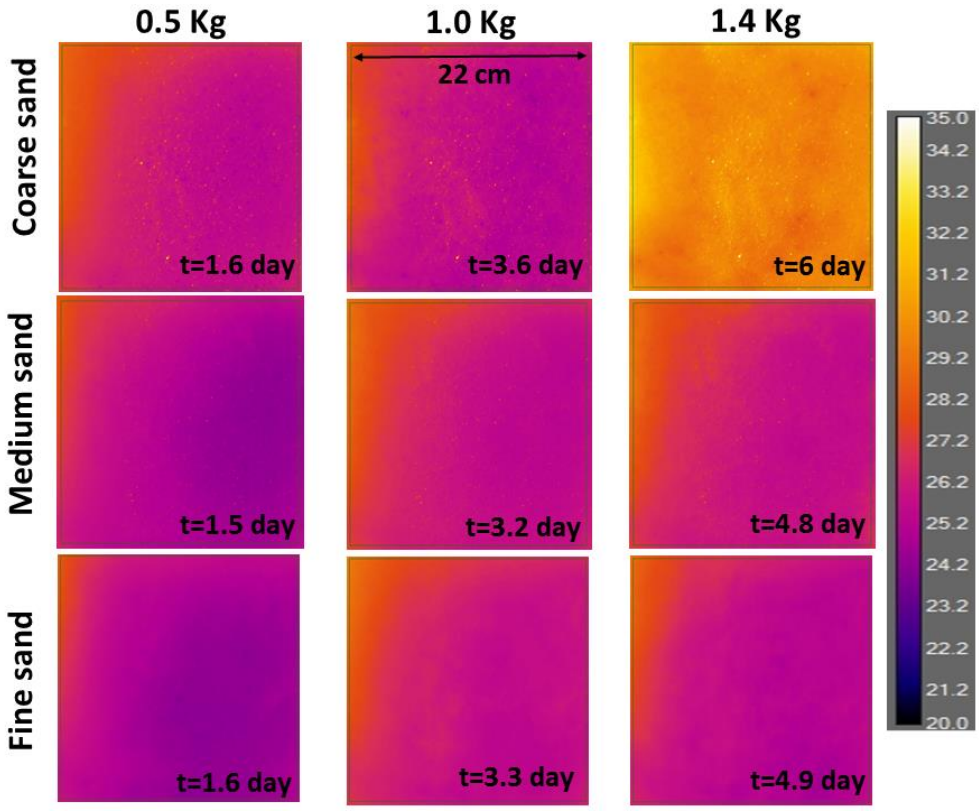

Figure 2.6. Surface temperature of the coarse (top row), medium (middle row), and fine sand (bottom row) at different times from the onset of the experiments. The numbers at the top indicate the evaporative mass losses. The colour map indicates the temperature (ºC). Results show that after the same amount of mass loss from the coarse, medium, and fine sand (1.4 Kg), the surface of the coarse sand is warmer due to the earlier transition from stage-1 to stage-2 evaporation(see Figure 2.3).

Figure 2.6 shows that as the particle size distribution increases the surface temperature increases after less mass was lost, as a result of the earlier transition from stage-1 to stage-2 of evaporation. In other words, as particle size distribution increases, the capillary length sustaining the hydraulic connections between the receding drying front and the surface (where evaporation occurs during stage-1) shortens, which results in an earlier disconnection of the hydraulic

pathways between the saturated zone at the bottom and the surface. When the liquid connections are disrupted, the evaporation surface dries out resulting in higher temperatures, and this disconnection happens earlier in coarser sand both in terms of time and in terms of accumulated evaporative loss. This is why under the same cumulative evaporative water losses, the surface temperature of the container packed with coarse sand has increased, while medium and fine sand after 1.4 Kg mass loss still are in stage-1 of evaporation and thus the surface temperature is significantly cooler, as illustrated in Figure 2.6.

Figure 2.7 shows the evolution of the temperature at top and bottom of the container packed with the drying porous media together with the associated temperature of the bare roof.

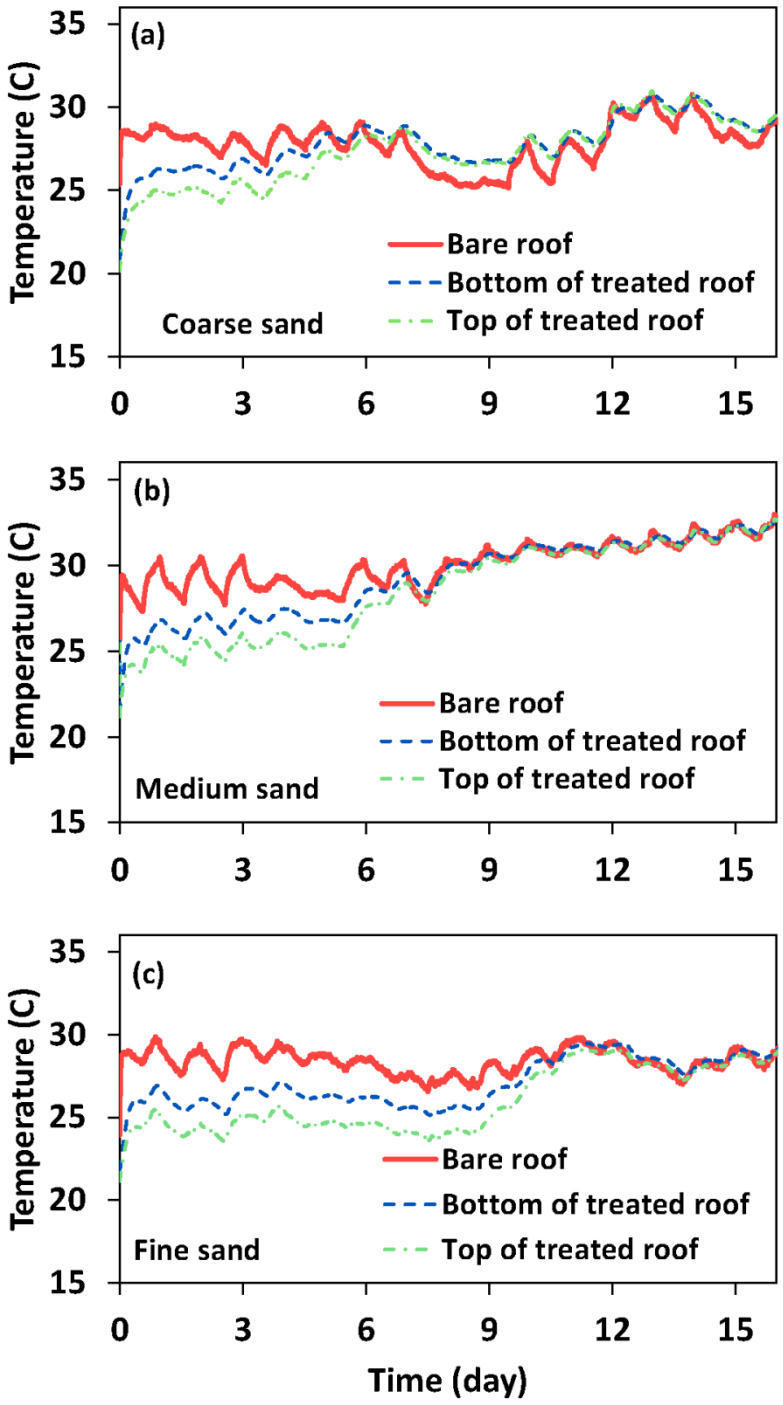

Figure 2.7. The measured temperature at top and bottom of the container packed with drying coarse (a), medium (b) and fine (c) sand referred to as "treated roof" in the legend. Also presented is the measured temperature at the surface of the bare roof (i.e. the container without porous media).

The results show that in all cases, the temperature at the roof underlying drying sand packs is less than the bare roof up to a certain time, after which the presence of the porous medium has a negligible effect on reducing the roof temperature. Additionally, Figure 2.7 shows that the finer the particle size of the drying porous medium, the longer is the period over which the surface temperature is less compared to the bare roof. This result can be interpreted in the light of the drying curves shown earlier.

Another interesting feature to note in Figure 2.7 is that for the evaporative roofs the temperature at the top of the roof is lower than the temperature at the bottom. This indicates that evaporation in this case in fact manages not only to reduce the inward heat flux, but also to reverse the flux such that the roof exterior would be cooling the building. An indication of this cooling is that the temperature at the bottom is slightly lower than the measured room air temperature (which varied from about 28 to 30 ºC); the bottom surface does not receive radiation and any deviation of its temperature from the ambient air would be related to the heat flux through the roof. A temperature lower than the ambient air at that surface indicates it is being cooled from above. This is not surprising in view of the low ambient relative humidity. Under such dry conditions, the wet bulb temperature (which one can simply define as the minimum temperature that a surface can cool to due to evaporation from its surface into the ambient environment) is significantly lower than the ambient air temperature (for our experimental conditions the wet bulb temperature can be computed from the air temperature and relative humidity and is ≈ 15ºC). An evaporating surface can cool to temperatures below those of the air, even when the surface is being heated by incoming radiation. It is clear that these conditions prevail in our experiment, and this reveals the potential of evaporative roofs not only to mitigate cooling loads (reduce

inward heat flux), but furthermore to act as passive building coolers (create an outward heat flux).

Figure 2.8 shows the dimensionless temperature at the surface and bottom of the drying porous media together with the associated measured drying curves.

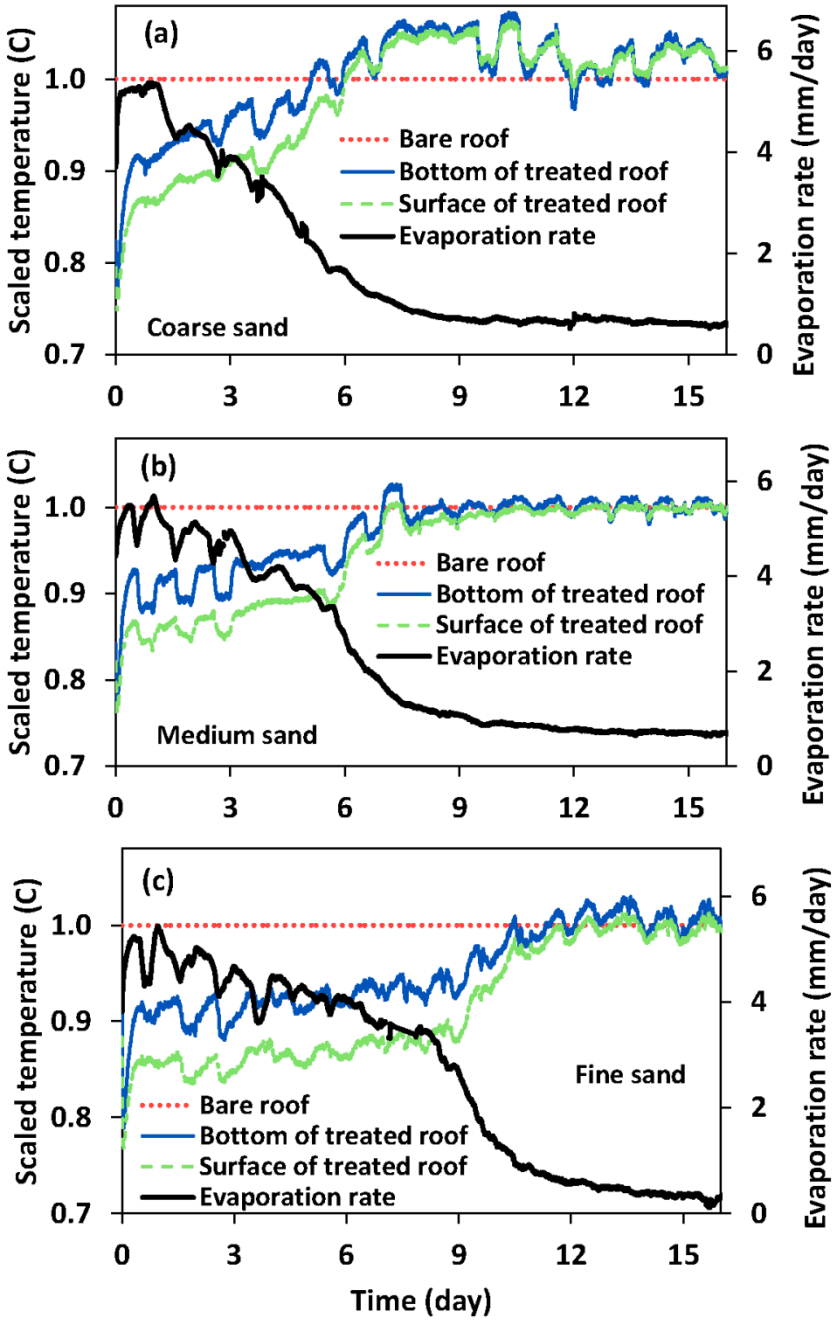

Figure 2.8. Evolution of the temperature at the surface and bottom of the treated roof filled with coarse, medium and fine sand presented in (a), (b) and (c), respectively. The temperature was scaled by the temperature of the bare roof (using the values in ºC). Results show that the temperature of the treated roof (the roof filled with the drying porous media) is lower than the bare roof as long as the evaporation process remains during stage-1 evaporation. Due to the longer stage-1 evaporation in the case of fine sand, the effectiveness of the fine-textured material to moderate the roof surface temperature is improved.

Figure 2.8 shows that as long as the evaporation process is during stage-1, the temperature at the surface of the "treated roof", i.e. the roof with the overlying drying porous media, is lower than the bare roof. As discussed earlier and shown in previous studies [32], during stage-1 evaporation the surface remains partially wet. This reduces the temperature compared to the bare roof. Figure 2.8 clearly shows that the end of stage-1 evaporation marks the time when temperature begins to rise at the surface and bottom of the drying porous media due to the loss of liquid continuity with the surface, which eventually reduces the surface water content. This Figure confirms the importance of the drying characteristics of porous media on the performance of such a roofing system. An efficient and effective porous media for such a system should present a relatively long period of stage-1 evaporation, otherwise the influence of the presence of the porous medium will be minor.

Additionally, Figure 2.8 shows that as the particle size decreases, the prolongation of stage-1 evaporation increases. Therefore, the application of a finer-textured medium will be more effective compared to the coarse-textured porous medium. It should be noted that in the range of the particle sizes used in our experiments, all three sandy media contain relatively large grains. If the drying porous medium were from a very fine-textured material, such as clay, the prolongation of stage-1 evaporation could be limited by viscous forces, which reduce the evaporation rate and also may cause desiccation cracking [24, 33]. However, these effects are

negligible in our study. In any case, Figure 2.8 shows that the application of drying porous media on the roof reduces the roof temperature by about 5 ºC relative to the bare roof. Such a reduction has the potential to reduce cooling loads and carbon footprint, as well as energy bills by requiring less energy to cool the building.

Moreover, Figure 2.8 again shows that in all cases the temperature at the bottom of the drying porous media was higher than the one at the surface, which as discussed earlier illustrates the high potential of evaporative roofs to act as passive cooling systems. This potential is further exhibited in Figure 2.9, which depicts the measured heat flux by the sensor buried in the middle of the drying porous media during each round of the experiment.

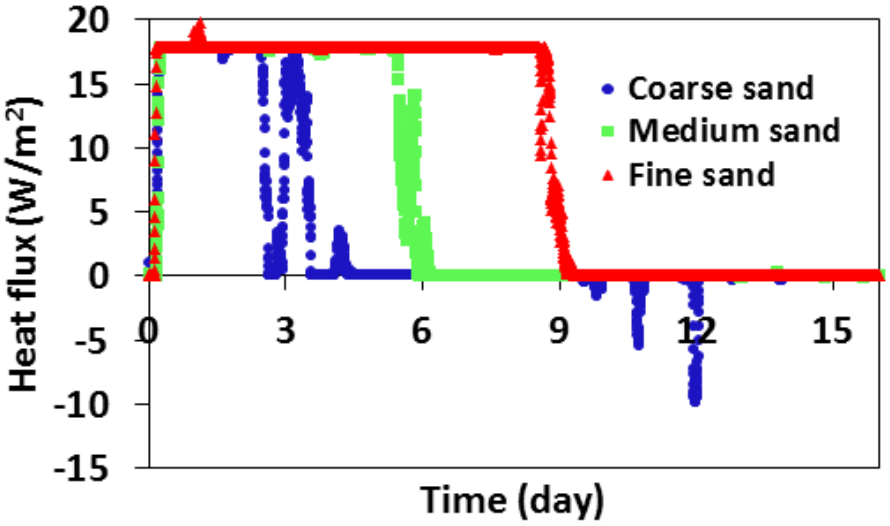

Figure 2.9. The measured heat flux through the coarse, medium and fine sand. Positive heat flux indicates upward heat transfer.

In Figure 2.9, positive values indicate upward heat flux (note that the absolute values reported in Figure 2.9 might have been influenced by the threshold used in the working range of the heat flux sensor). Since the temperature at the bottom of the drying porous media was higher than the

temperature at the surface during stage-1 evaporation in all experiments conducted in this study (Figure 2.7 and 2.8), upward heat flux was observed in all cases during stage-1. Again this is related to the low relative humidity that results in low wet bulb temperature and stronger evaporative cooling at the top surface to temperatures below the ambient air. If the roof surface is below the outdoor ambient air temperature and below the indoor desirable temperatures, the evaporation latent energy would be contributed to by the upward heat flux in the roofs as well as by a negative convective heat flux from the outdoor air towards the roof surface.

This shows the potential of such a method (i.e. adding drying porous media above the roof to moderate roof surface temperature) to reduce the roof temperatures, the building cooling loads, and the convective heat flux to the exterior air that causes the urban heat island effect, potentially cooling the city [34, 35] for analyses of the influence of surface wetness and evaporation on the outdoor urban microclimate). However, since the temperature difference between top and bottom of the drying porous media reduces at the end of stage-1 evaporation, the heat flux (driven by the temperature gradient) approaches to values close to zero and the cooling effect of the roof would become insignificant in the absence of rainfall or irrigation.

Combining the results presented in Figure 2.7, 2.8 and 2.9, it can be concluded that (i) the effectiveness of applying porous media can be improved if the stage-1 evaporation is extended over a long period because it keeps the roof surface temperature lower for a longer time and may induce upward heat flux, and (ii) strong evaporation can very effectively cool the roof surface and provide benefits in terms of building energy consumption and the local microclimate. These are important considerations in designing evaporative roofs with porous media for real world applications.

2.5. Summary and conclusions

We have conducted carefully-controlled experiments to evaluate the application of drying porous media to reduce the roof surface temperature, with a focus on the design considerations that would control the performance of such roofs. The results showed the ability of porous materials to regulate the roof surface temperature, which eventually influences the building energy efficiency via reducing energy consumptions for cooling of buildings. Reducing the surface temperature would also have positive implications for mitigating urban heat islands since it would reduce the convective heat flux from the roof surface to the outdoor air. Several factors including fluctuating temperature and humidity, radiation, wind velocity, rain fall, structure of porous media, wettability of the grains, and the physical and chemical properties of the evaporating fluid influence the drying behaviour of porous media. In this paper, we investigated how the particle size distribution of a layer of porous medium affects its drying behaviour and thermal performance. Our results showed that finer-textured porous media are more appropriate for such an application because of the prolonged stage-1 evaporation due to the efficient capillary flow connecting the wet zone at the bottom of the drying system to the surface. The thermal images, together with the data recorded by the thermocouples, established the direct connection between the drying behaviour, the recorded temperature profiles and the limit of the efficiency of the drying porous media. The end of stage-1 evaporation coincides with the time when temperature at the treated roof begins to rise making the influence of the presence of the drying porous media negligible. This result shows the need to design porous materials that result in longer stage-1 evaporation if this method is to be used to reduce roof surface temperature. Application of the drying porous media lowered the irradiated laboratory surface temperature by about 5 ºC, but reductions on real roofs where the incoming radiation is about 10 times higher

than in our laboratory experiments will be greater. The experiments also illustrated that evaporation can cool the surface to temperatures below ambient air (the theoretical limit would be the wet bulb temperature), thus reversing the heat flux and effectively extracting heat from the roof (not only reducing heat influx to the roof).

Although this study is still at an early stage, it clearly illustrates that this method has a potential to contribute toward reducing the energy consumption by buildings especially in places with hot climates. Further investigations are underway to evaluate the effects of the evaporating fluids (specifically saline water), as well as the heterogeneity of porous media on the efficiency of this method. More work is also needed, and is currently underway, to assess the performance of such roofs under real world conditions. To that end, we will implement a model of the evaporative roofs in the Princeton ROof Model (PROM, [16, 17]) and the Princeton Urban Canopy Model (PUCM, [29]), run PROM under the same experimental conditions we tested in this paper to validate our methods, and then apply the model under a wide range of real-world condition to assess the potential of evaporative roofs.

The development and use of evaporative roofs would significantly contribute towards the reduction of energy as well as water use in cities (since we could use non-fresh water), weaken the coupling of economic development and resource use, and facilitate the emergence of more sustainable cities in the future

2.6. Acknowledgement

We gratefully acknowledge funding by the The Leverhulme Trust to support this research (RPG-2014-331). We would like to thank Mr. Craig Shore and Mr. Andrew Evans for their assistance

with the experimental setup. Elie Bou-Zeid was funded by the US National Science Foundation's Sustainability Research Network Cooperative Agreement 1444758.

2.7. References

[1] T.R. Oke, Towards a prescription for the greater use of climatic principles in settlement planning, Energ Buildings 7 (1984) 1–10.

[2] e. Kalnay, E., M. Cai, Impact of urbanization and land-use change on climate, Nature 423 (2003) 528-531.

[3] D. Li, E. Bou-Zeid, Synergistic interactions between urban heat islands and heat waves: the impact in cities is larger than the sum of its parts, J. Appl. Meteor. Climatol. 52 (9) (2013) 2051-2064.

[4] A. Mavrogianni, M. Davies, M. Batty, S.E. Belcher, S.I. Bohnenstengel, D. Carruthers, et al., The comfort, energy and health implications of London's urban heat island, Building Serv. Eng. Res. Technol., 32(1) (2011) 35-52.

[5] M. Kolokotroni, X. Ren, M. Davies, A. Mavrogianni, A., London's urban heat island: Impact on current and future energy consumption in office buildings, Energy and Buildings 47 (2012) 302-311.

[6] L. Frazer, Paving paradise, Environmental Health Perspectives 113 (2005) 457-462.

[7] T. Runsheng, Y. Etzion, E. Erell, Experimental studies on a novel roof pond configuration for the cooling of buildings, Renewable Energy 28 (2003), 1513-1522.

[8] M. Kolokotroni, B.L. Gowreesunker, R. Giridharan, Cool roof technology in London: An experimental and modelling study, Energy and Buildings 67(2013) 658–667.

[9] D.J. Sailor, A green roof model for building energy simulation programs, Energy and Buildings 40(2008) 1466-1478.

[10] H.F. Castleton, V. Stovin, S.B.M. Beck, J.B. Davison, Green roofs; building energy savings and the potential for retrofit, Energy and Buildings 42(2010) 1582-1591.

[11] D. Li, E. Bou-Zeid, M. Oppenheimer, The Effectiveness of Cool and Green Roofs as Urban Heat Island Mitigation Strategies, Environ. Res. Lett. 9 (2014) 055002.

[12] S. Wanphen, K. Nagano, K. Experimental study of the performance of porous materials to moderate the roof surface temperature by its evaporative cooling effect, Building and Environment 44(2009) 338-351.

[13] R. Crawford, A.K. da Silva, A.K., Experimental testing of a passive, evaporation-based roof cooling system, Energy and Buildings 71(2014) 12-19.

[14] S.B. Sadineni, S. Madala, R.F. Boehm, Passive building energy savings: A review of building envelope components, Renewable and Sustainable Energy Reviews 15(2011) 3617-3631.

[15] D. Jain, Modeling of solar passive techniques for roof cooling in arid regions, Building and Environment 41(2006), 277-287.

[16] T. Sun, E. Bou-Zeid, G.H. Ni, To irrigate or not to irrigate: Analysis of green roof performance via a vertically-resolved hygrothermal model, Building and Environment, 73(2013) 127–137.

[17] T. Sun, E. Bou-Zeid, Z.H. Wang, E. Zerba, G.H. Ni, Hydrometeorological determinants of green roof performance via a vertically-resolved model for heat and water transport, Building and Environment 60(2013) 211–224.

[18] G.W. Scherer, Theory of drying, J. Am. Ceram. Soc. 73(1990) 3–14.

[19] A.G. Yiotis, I.N. Tsimpanogiannis, A.K. Stubos, Y.C. Yortsos, Pore-networkstudy of the characteristic periods in the drying of porous materials, J. Colloid Interface Sci. 297(2006) 738–748.

[20] K.M. Smits, V.V. Ngo, A. Cihan, T. Sakaki, T.H. Illangasekare, An evaluation of models of bare soil evaporation formulated with different land surface boundary conditions and assumptions, Water Resour. Res. 48(2012) W12526.

[21] N. Shokri, D. Or, Drying patterns of porous media containing wettability contrasts, J. Colloid Interface Sci. 391(2013) 135-141.

[22] K.F. DeCarlo, N. Shokri, Salinity effects on cracking morphology and dynamics in 3-D desiccating clays, Water Resour. Res. 50(2014) 3052-3072.

[23] N. Shokri, M. Sahimi, D. Or, Morphology, Propagation Dynamics and Scaling Characteristics of Drying Fronts in Porous Media, Geophys. Res. Lett. 39(2012) L09401.

[24] P. Lehmann, S. Assouline, D. Or, Characteristic lengths affecting evaporative drying of porous media, Phys. Rev. E 77(2008) 056309.

[25] N. Shokri, D. Or, What determines drying rates at the onset of diffusion controlled stage-2 evaporation from porous media?, Water Resour. Res. 47(2011) W09513.

[26] A.G. Yiotis, I.N. Tsimpanogiannis, A.K. Stubos, Y.C. Yortsos, Coupling between external and internal mass transfer during drying of a porous medium, Water Resour. Res. 43(2007) W06403.

[27] N. Shokri, P. Lehmann, P. Vontobel, D. Or, Drying front and water content dynamics during evaporation from sand delineated by neutron radiography, Water Resour. Res. 44(2008) W06418.

[28] M. Aminzadeh, D. Or, Energy partitioning dynamics of drying terrestrial surfaces, J Hydrol. 519(2014) 1257-1270.

[29] Z. Wang, E. Bou-Zeid, J.A. Smith, A coupled energy transport and hydrological model for urban canopies evaluated using a wireless sensor network, Quarterly Journal of the Royal Meteorological Society 139 (675) (2013) 1643-1657.

[30] N. Grapsas, N. Shokri, Acoustic characteristics of fluid interface displacement in drying porous media, Int. J. Multiphas Flow 62(2014) 30-36.

[31] N. Shokri, G. Salvucci, Evaporation from porous media in the presence of a water table, Vadose Zone J. 10 (2011), 1309-1318.

[32] N. Shokri, Pore-scale dynamics of salt transport and distribution in drying porous media, Phys. Fluids 26(2014) 012106.

[33] K.F. DeCarlo, N. Shokri, Effects of substrate on cracking patterns and dynamics in desiccating clay layers, Water Resour. Res. 50(2014) 3039-3051.

[34] P. Ramamurthy, E. Bou-Zeid, Contribution of Impervious Surfaces to Urban Evaporation, Water Resour. Res 50(4) (2014) 2889-2902.

[35] P. Ramamurthy, E. Bou-Zeid, J.A. Smith, Z. Wang, M.L. Baeck, N.Z. Saliendra, J. Hom, C. Welty, Influence of Sub-Facet Heterogeneity and Material Properties on the Urban Surface Energy Budget J., Appl. Meteor. Climatol. 53(9)(2014) 2114–2129.

Chapter 3

NEW INSIGHTS ON EFFECTS OF NACL CONCENTRATION AND PRECIPITATION ON SALINE WATER EVAPORATION FROM POROUS MEDIA

In this chapter, the interaction between the precipitated salt at the surface and the evaporative mass losses is investigated. A series of laboratory evaporation experiments using sand particles saturated with NaCl solutions differing in concentration was conducted. The sand columns are placed under evaporation conditions and the drying behaviour is recorded using digital balances controlled by a computer. Moreover, a thermal camera is used to record the dynamics of temperature at the evaporation surface.

Our results show that increasing salt concentration does not necessarily reduce the evaporation rate correlatively (although the saturated vapour pressure above the surface decreases as salt concentration increases). Sand columns with different NaCl concentrations presented relatively similar evaporation dynamics. This counter-intuitive behaviour is attributed to the effect of the presence of precipitated salt at the surface. Our microscopic imaging reveals that the precipitated salt at the surface is porous causing liquid supply to the surface via capillary flow. This keeps the precipitated salt wet at the surface which contributes to the evaporation process. High resolution thermal imaging illustrates a rapid temperature fluctuation at the surface of precipitated salt resulting in the appearance and disappearance of "cold-spots". This fluctuation causes temperature changes of ~2^{o}C every minute. This confirms the contribution of the precipitated salt to the evaporation process. The temperature fluctuation is associated with the preferential evaporation at different locations through the precipitated salt where some of the incoming energy is consumed for liquid vaporization.

Using the obtained experimental data, we could propose a conceptual evaporation curve describing saline water evaporation from porous media taking into account the contribution of the precipitated salt to the evaporation process as long as the salt crust is wet. Different phases of the saline water evaporation with the corresponding governing mechanisms are discussed.

New insights into saline water evaporation from porous media: Complex interaction between evaporation rates, precipitation and surface temperature

Salomé M.S. Shokri-Kuehni, Thomas Vetter, Colin Webb, Nima Shokri

School of Chemical Engineering and Analytical Science, The University of Manchester, Manchester, UK

This chapter has been published in Geophysical Research Letters.

Shokri-Kuehni, S.M.S., T. Vetter, C. Webb, N. Shokri (2017), New insights into saline water evaporation from porous media: Complex interaction between evaporation rates, precipitation and surface temperature, Geophys. Res. Lett., 44, 5504–5510.

3.1. Abstract

Understanding salt transport and deposition patterns during evaporation from porous media is important in many engineering and hydrological processes such as soil salinization, ecosystem functioning and land-atmosphere interaction. As evaporation proceeds, salt concentration increases until it exceeds solubility limits, locally, and crystals precipitate. The interplay between transport processes, crystallization and evaporation influences where crystallization occurs. During early stages, the precipitated salt creates an evolving porous structure affecting the evaporation kinetics. We conducted a comprehensive series of experiments to investigate how the salt concentration and precipitation influence evaporation dynamics. Our results illustrate the contribution of the evolving salt crust to the evaporative mass losses. High-resolution thermal imaging enabled us to investigate the complex temperature dynamics at the surface of precipitated salt, providing further confirmation of salt crust contribution to the evaporation. We identify different phases of saline water evaporation from porous media with the corresponding dominant mechanisms in each phase and extend the physical understanding of such processes.

3.2. Introduction

Evaporation of saline water from porous media is important in many environmental, engineering and hydrological processes including vegetation and plant growth, soil salinization, land-atmosphere interaction, functioning of the eco-system and crop production [Rodriguez-Navarro and Doehne, 1999; Suweis et al., 2010; Ott et al., 2015; Bergstad and Shokri, 2016]. This has motivated many researchers to investigate various aspects of this process including the effects of grain size, wettability, heterogeneity and external conditions [Huinink et al., 2002; Guglielmini et al., 2008; Nachshon et al., 2011a, 2011b; Eloukabi et al. 2013; Norouzi Rad et al., 2015; Jambhekar et al., 2015; Börnhorst et al., 2016; Dai et al., 2016; Shokri-Kuehni et al., 2017].

Saline water evaporation is influenced by the transport properties of the porous medium, properties of the evaporating solution, external conditions (wind, radiation, ambient temperature and relative humidity), and by the precipitation of salt crystals [Norouzi Rad et al., 2013; Shokri, 2014; Jambhekar et al., 2015; Shokri-Kuehni et al., 2017]. During evaporation, solute is transported, via capillary induced liquid flow, from a wet zone to the evaporation surface resulting in increasing solute concentration close to the vaporization plane [Guglielmini et al., 2008]. At the same time diffusion tends to spread the salt homogenously through the entire space. This competition between advection and diffusion (quantified by the Peclet number *Pe*) determines the solute distribution during the evaporation process [Guglielmini et al., 2008; Shokri, 2014] when no salt crystallization occurs.

When the salt concentration substantially exceeds the solubility limit (i.e., supersaturation exceeds a critical value) [Desarnaud et al., 2014], crystals will precipitate by first nucleating and then growing. When advection dominates (i.e., when $Pe>>1$), the concentration of salt in the liquid phase is the highest at the surface of the porous medium and hence precipitation occurs

preferentially at this surface which is called efflorescence. Depending on external conditions, temperature and humidity, the crystals formed at the surface create complex, branching structures (originating from epitaxial growth and the formation of dendrites), which can substantially increase the surface area available for evaporation. Furthermore, evaporation and crystallization give rise to heat effects: the crystallization of common salts releases heat, while evaporation of water requires heat. This can therefore lead to hot or cold spots at the surface of porous media depending on the rate of heat transfer with the surroundings. How exactly the precipitated salt at the surface or within the pores of porous media modifies the capillary liquid flow supplying the evaporative demand is not well understood.

One of the key factors influencing the evaporation process is the salt concentration [Norouzi Rad and Shokri, 2012; Gupta et al., 2014] . When the porous media surface is wet, the evaporation rate e is related to the difference between the saturated vapour pressure P_s above the surface and the vapour pressure in air P_∞ ($P_\infty = RH \times P_s$ where RH indicates relative humidity). One would expect the evaporation rate to decrease correlatively, as initial salt concentration increases, owing to the impact of salt concentration on lowering P_s in accordance to Raoult's law. However, some recent experimental studies show that increasing salt concentration does not necessarily reduce the evaporation rate [Sghaier and Prat, 2009; Norouzi Rad and Shokri, 2012; Gupta et al., 2014]. A commonly used scenario to describe this paradoxical behaviour is to (qualitatively) relate the evaporation rate to the increased surface area due to efflorescence [Sghaier and Prat, 2009].

Despite advances in analysis of saline water evaporation from porous media, the understanding of how exactly efflorescence and salt concentration influences the drying rate and dynamics is surprisingly not very advanced. This aspect has rarely been elaborated in the literature partly due to the complexity of the processes involved. Without such knowledge, our modelling efforts will

be largely dependent on adjusting parameters. Motivated by their importance in various applications, the specific objectives of the present study were to investigate how salt concentration and efflorescence influence the drying curve and illustrate some of the challenges involved in describing saline water evaporation from porous media.

3.3. Experimental considerations

The influence of initial salt concentration and surface salt precipitation on drying rate and the corresponding surface temperature dynamics were investigated by conducting a series of evaporation experiments. Cylindrical glass columns (150 mm in height, 80 mm diameter with all boundaries closed to mass transfer except the top, which was exposed to air) were packed with quartz sand grains with average particle size of 0.27 mm. The sand packs were wetted with NaCl solutions of different concentrations ranging from 0.05 to 3.5 M. Additionally, one column was packed with solid NaCl grains and wetted with saturated NaCl solution. The columns were mounted on digital balances (accuracy of 0.01 g) to record the mass loss due to evaporation over time. Moreover, one column was filled with deionised water to measure the potential evaporation rate in the absence of any salt in each round of experiments. The ambient temperature and relative humidity were measured using two standard relative humidity and temperature sensors (HygroClip HC2-S, Rotronic Instrument Corp.). Metal halide lamps (EYE Color Arc PAR36, Iwasaki Electronic Co., Japan) were directed onto the surface of the packed columns (with an arrangement similar to that illustrated in Shokri-Kuehni et al. [2016]) to boost the evaporation process. To obtain the temporal and spatial evolution of the surface temperature [Aminzadeh and Or, 2014; Haghighi and Or, 2015], a thermal camera (FLIR T650sc, FLIR Systems, Inc.) was fixed above the sand columns and set to record an image every minute. Additionally, an imaging system was set up to take visual snapshots of the surface of sand columns every 30 min.

Furthermore, growth dynamics and structure of salt crust forming on the surface during the evaporation process was investigated in a separate experiment, using an optical microscope (LeiCaM205C, 20.5:1 zoom, 0.952 mm resolution) equipped with a high-resolution digital camera (LeiCaDFC 3000G) set to record an image every minute.

3.4. Results and discussions

3.4.1. Challenges of describing saline water evaporation from porous media

Figure 3.1 (a) shows the evaporative mass losses at different times as a function of the initial salt concentration. In Figure 3.1 (b) typical examples of precipitation patterns at the surface of the columns are shown at different times from the onset of the experiments.

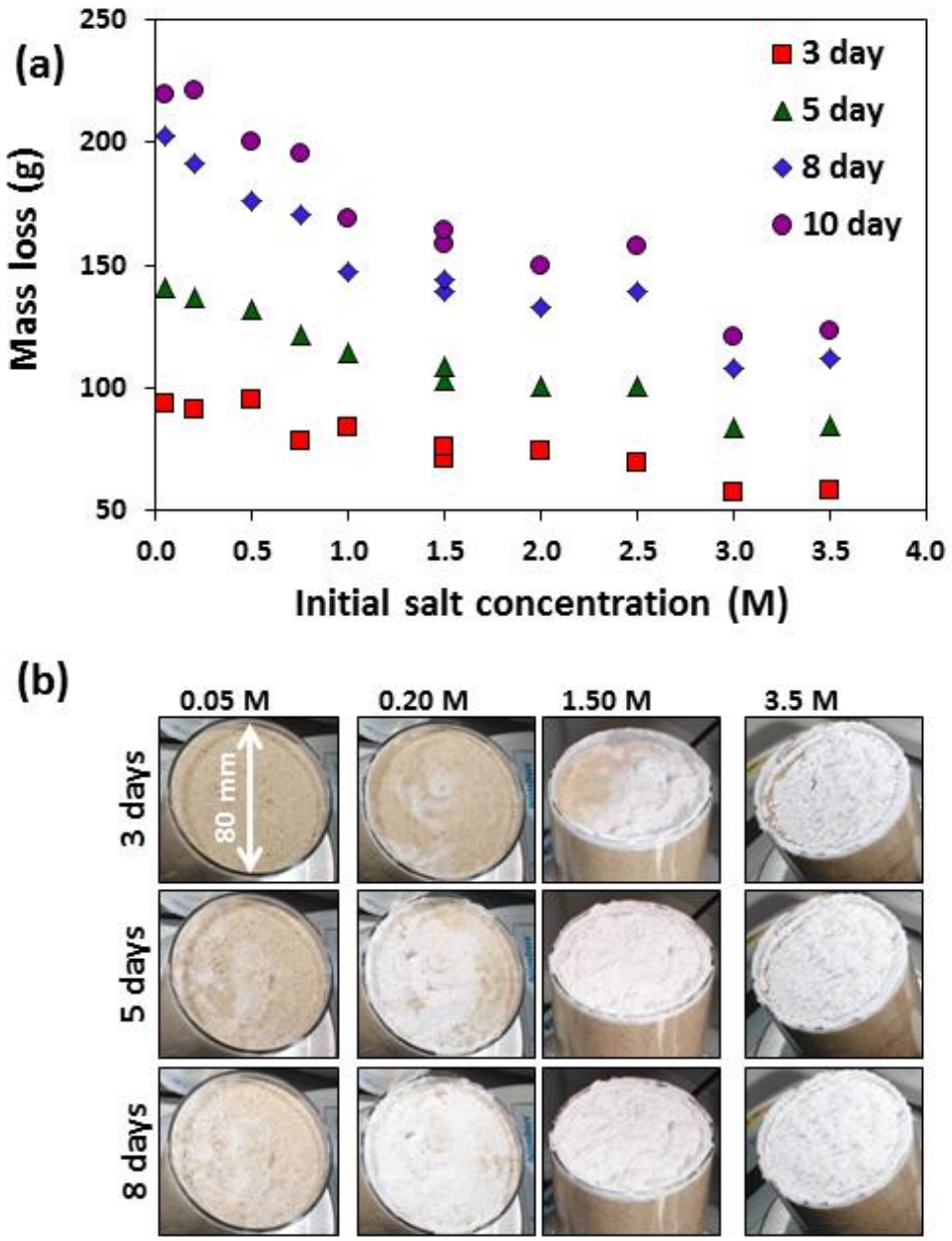

Figure 3.1. (a) Measured cumulative evaporative losses at different times from the start of experiments as a function of the initial salt concentration. (b) Typical examples of precipitation patterns at various stages, for solutions with initial salt concentrations of 0.05, 0.2, 1.5 and 3.5 M.

There are a few features in Figure 3.1 that illustrate the complexity of saline water evaporation from porous media. The first puzzling behaviour is the relationship between evaporative mass

losses and the initial salt concentrations. According to Raoult's law, one would expect to observe decreasing evaporative mass losses as the solute concentration increases especially when the surface is still wet (thus the evaporation rate is dependent on the saturated vapour pressure and controlled by the external conditions). However, a correlative decrease is not the general trend observed in Figure 3.1(a) across the wide range of concentrations studied. Similar behaviour has recently been reported in other studies [Sghaier and Prat, 2009; Norouzi Rad and Shokri, 2012; Gupta et al., 2014].

The formation of salt crusts at top of sand columns as detailed in Figure 3.1 (b), e.g. for the 3.5 M salt concentration, does not stop, or even slow down the evaporation shown in Figure 3.1 (a). In fact, the cumulative mass loss almost doubled, in this case, from 58.1g at 3 days to 112.0 g after 8 days. This observation exemplifies the complex interplay of effects and, clearly, the question of what is controlling the evaporation rate, in addition to the salt concentration or the atmospheric conditions, is paramount for any accurate predictions of the process.

Figure 3.2 shows the measured evaporation rates from the sand columns saturated with varying initial salt concentrations versus time (the evaporation rate was scaled by the potential evaporation rate, i.e., the one observed in the drying experiment carried out in the absence of salt and sand). The observed fluctuation in the measured evaporation rate from the sand column saturated with pure water at the early stage might be due to the fluctuation of the external conditions (ambient temperature and relative humidity). Figure 3.2 shows the columns with notably different initial concentrations and surface precipitation patterns may have very close evaporative fluxes. For example, sand columns saturated with 0.5 and 2.5 M experience essentially similar drying rate after ~3.5 days from the onset of the experiment which is not an intuitive result. Next, we will discuss about the possible reason behind this behaviour.

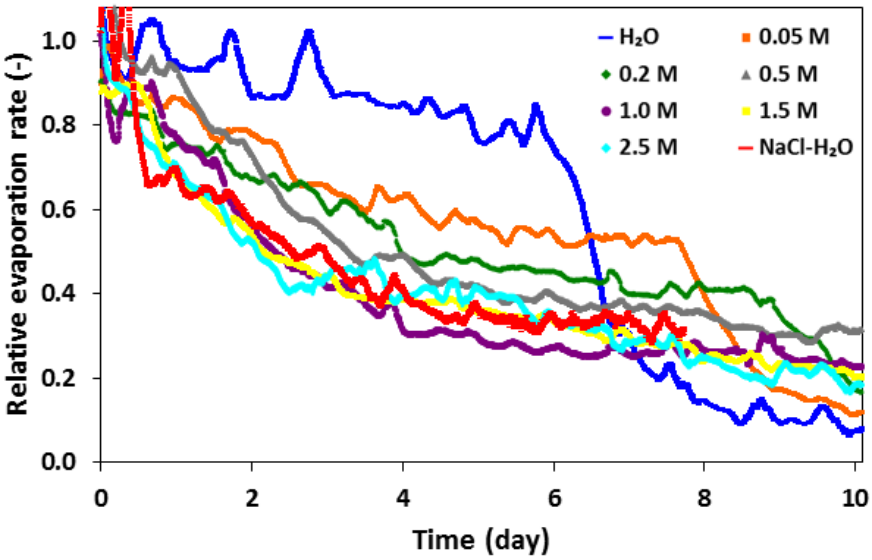

Figure 3.2. Relative evaporation rate (defined as the evaporation rate divided by the potential evaporation rate) versus time as influenced by the initial salt concentrations indicated in the legend. Also presented is the evaporation curve measured from the columns saturated with pure water (H_2O in the legend) as well as the column packed with salt grains saturated by salt solution (NaCl-H_2O in the legend). The observed fluctuations in the early stages might be due to the fluctuations in ambient temperature and relative humidity.

3.4.2. Effects of the precipitated salt at the surface on the evaporative fluxes

Closer inspection of drying curves in Figure 3.2 and surface precipitation patterns presented in Figure 3.1 (b) indicates that precipitated salt covering the surface of the column does not necessarily lead to diffusive-controlled evaporation through a dry salt layer. For example, in the case of the column wetted with 0.2 M NaCl solution, although the surface of the sand column is covered by salt after ~5 days, for a long time after this the evaporation rate remains much higher than expected from a diffusive-controlled flux through the dry salt crust. Comparing the measured evaporation rates with the recorded dynamics of the precipitation patterns at the surface confirms the significant contribution of the precipitated salt to the evaporative fluxes (see for example Figure 3.1(b) at 3.5 M and the corresponding curve in Figure 3.1(a)). Interestingly,

the evaporation rate measured from the column packed with salt grains saturated with salt solution is very similar to the evaporation rate measured from the sand columns saturated with salt solutions with varying initial concentrations. This is an important result, because it shows that the evaporation rates might be controlled by the porous structure and dynamics of the precipitated salt formed at the surface. This explains why the measured rates in the early stages of the evaporation process from the sand columns saturated with 0.5, 1.0, 1.5 and 2.5 M are almost the same (because in all cases crust forms at the surface controlling the drying process). This conclusion is in-line with the results presented recently by Bergstad and Shokri [2016]. They showed that the evaporative mass losses from porous media saturated with salt solutions with varying wettability conditions were nearly the same regardless of the wettability condition due to the effect of the presence of precipitated salt at the surface.

To have a closer look at the precipitation dynamics, we visualized salt precipitation at the surface during drying of sand pack at the micro-scale with typical results presented in Figure 3.3(a).

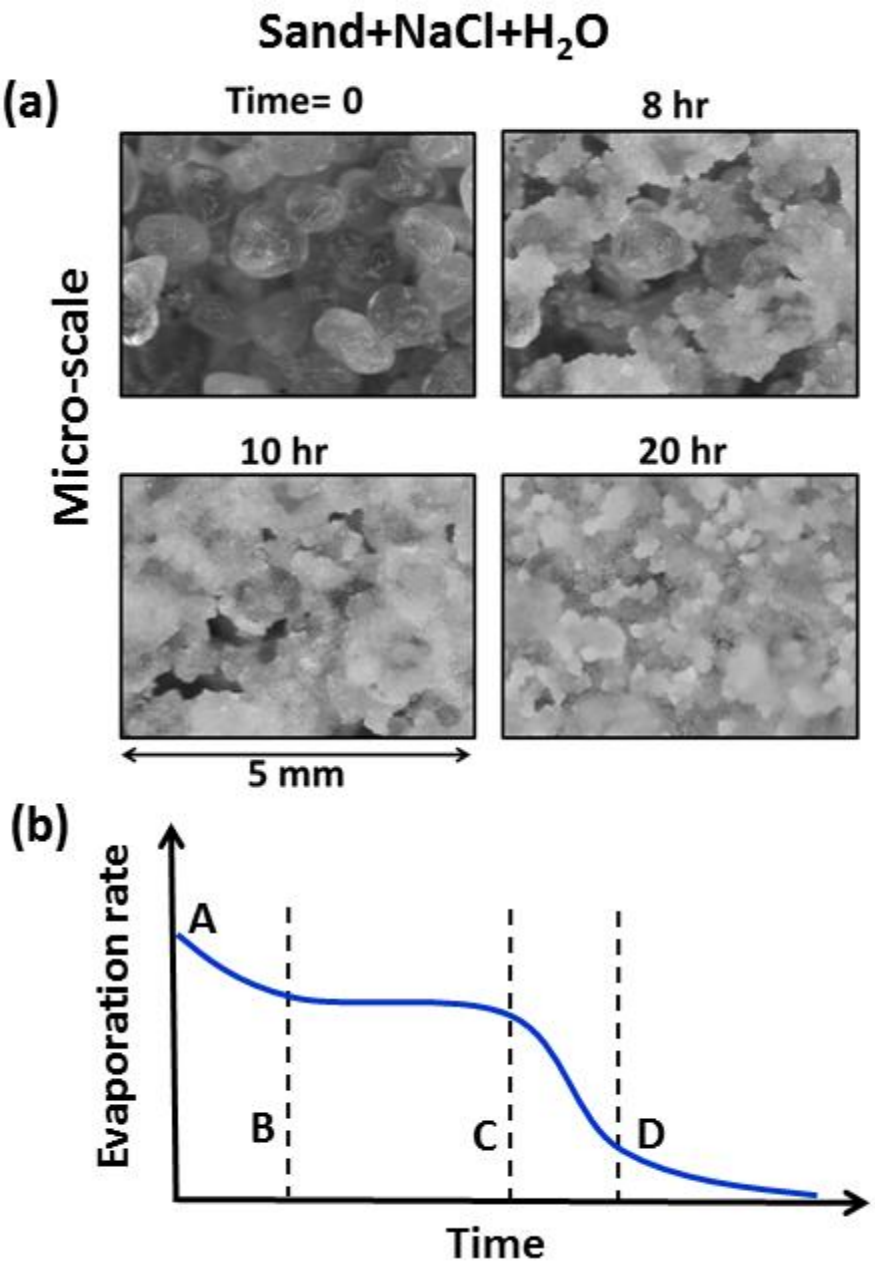

Figure 3.3. (a) Microscopic images illustrating precipitation dynamics at the surface of sand grains saturated with saline solution. Numbers at top indicate the elapsed time from the onset of the experiment. As time passes, salt crystals appear at the surface (distinguished by the bright colour). (b) The schematic illustrates conceptually the typical trend of the saline water evaporation from porous media with the following stages: Phase A-B: Increase in salt concentration and formation of salt crust govern the initial decrease in the evaporation rate. Phase B-C: Drying rate is largely controlled by liquid transport through the evolving porous salt crust. During this phase, the

precipitated salt remains wet. Phase C-D: Gradual drying of the precipitated salt at the surface significantly decreases the evaporation rate. Phase D-onward: Vapour diffusion through the sand and the dry precipitated salt limits the evaporation rate.

The microscopic images reveal that the salt crust formed at the surface of porous media is itself porous and evolves in a highly dynamic way due to the complex interplay of crystallization and evaporation at the crystal-liquid, crystal-crystal, liquid-air, and the crystal-air interfaces [Shahidzadeh et al., 2015]. This is in agreement with the results reported recently by Dai et al. [2016] showing that NaCl "preferentially precipitates in cubic-shaped crystals that are packed heterogeneously to form a very porous structure". The recorded images also indicate that formation of salt does not necessarily clog the pores; the continued growth of salt crystals above the precipitated salt indicates further water evaporation with vaporization occurring at the salt surface. Microscopic analysis suggests that the presence of porous salt at the surface causes top-supplied creeping of the solution, feeding the growth of subsequent crystals. Our results suggest that the precipitated salt at the surface is an ever changing porous medium with its own unique properties and chemical interactions as long as the surface of the underlying porous sand packing remains wet.

In the literature, the drying curve from porous media saturated with salt solutions is normally described in terms of three stages [Jambhekar et al., 2015]: The first stage includes a decreasing drying period (as a result of increasing salt concentration at the surface) when the drying rate is relatively high followed by a transition period (second stage) to a stage when the evaporative flux is much smaller than the first stage limited by the vapour diffusion through the salt crust (third stage). However, our observations suggest that this description needs revising: an additional stage should be included (at least for the cases studied in this article) in which the

evaporation rate is largely controlled by liquid transport and evaporation through the evolving porous salt layer formed at the surface.

3.4.3. Evolving precipitated salt layers at the surface and their effect on the evaporation rate

Based on our observations and the results presented in Figure 3.1 and 3.2, we propose a characteristic curve (presented in Figure 3.3(b)) to describe the various stages of saline water evaporation from porous media. Phase 1, A-B represents the stage during which the evaporation rate is largely dependent on external conditions (e.g. ambient temperature, relative humidity, radiation) and the saturated vapour pressure of the solution. The decreasing evaporation rate during this stage is due to the increasing salt concentration close to the surface (which reduces the vapour pressure and thus the driving force for evaporation). Furthermore, the formation of the salt crust is initially causing an increased mass transfer resistance for the liquid to reach the evaporation surface. However, when the evolving salt layer covers a substantial portion of the surface of the sand column, the steady decrease in the evaporation rate ceases. This marks the end of phase 1. During Phase 2 (B to C in Figure 3.3 (b)), the evaporation rate is dependent on the properties and dynamics of this new formed surface (the salt layer). The rate remains relatively constant, as long the precipitated salt is porous and remains wet (fed by capillary flow). Further precipitation onto this salt layer and the formation of complex dendritic structures increase the surface area available for evaporation. While the driving force for evaporation continues to decrease, it is approximately counterbalanced by this increased surface area, hence the relatively constant rate. In most cases (Figure 3.2), this phase is observed from about 4 days until about 8 days and is quite similar to the so-called stage-1 evaporation from porous media saturated by pure water [Shokri and Or, 2011]. During this phase, the salt crust does not

disconnect the liquid pathways from the saturated zone to the surface and the evaporative demand is largely met by the liquid transport through the evolving porous salt crust; Phase 3 (C-D in Figure 3.3 (b)) represents a stage during which the capillary liquid supply through the salt crust becomes disrupted, resulting in gradual drying of the salt layer, which in turn reduces the evaporation rate. This phase can be considered as a transition phase from evaporation controlled by the wet crust to evaporation controlled by the dry crust (Phase 4, D-onward) during which the flux is limited by the vapour diffusion through the dry precipitated salt. Similar transition periods are commonly observed from the stage-1 evaporation (a period when the surface of porous media remains wet) to stage-2 evaporation (a period when the porous media surface is dried and the process is controlled by vapour diffusion through a dry surface layer [Shokri and Or, 2011]).

3.4.4. Thermal signature of the contribution of precipitated salt to the evaporative rate

One of the key messages of the present work is the significant role of water evaporation through the wet precipitated salt during evaporation; a process that must be taken into account for a reliable description and prediction of saline water evaporation from porous media. As discussed in other studies (e.g. Veran Tissoires et al. [2014]), salt crystallization in drying porous media is a dynamic process in which a growing crystal can consume the supersaturation which may lead to dissolution of nearby crystallites. This influences the dynamics of surface temperature during evaporation which is investigated in this section. To do so, high resolution thermography was used to delineate the thermal signature of saline water evaporation from porous media. Figure 3.4 (a) shows the evolution of surface temperature by the minute, starting at 2.6 day after commencing the experiment alongside a photograph of the salt crust within this period (where the surface is entirely covered by the precipitated salt).

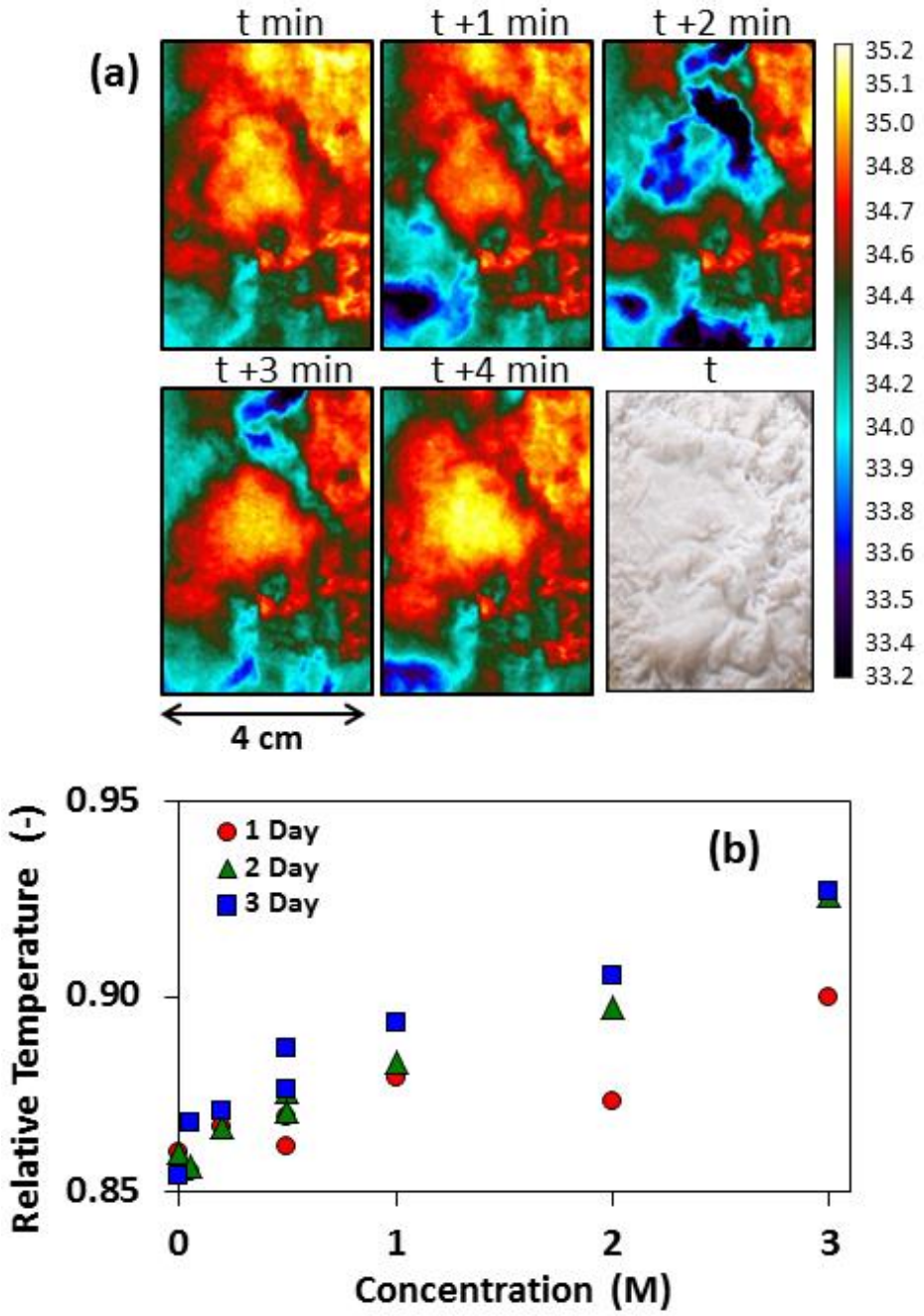

Figure 3.4. (a) Fluctuation of salt crust temperature at the surface of a sand column. The visualized salt crust has an area of 24 cm^2. The temperature of the surface was recorded every minute. The colormap indicates temperature in centigrade. The closer to blue (darker colour) the lower the temperature. The initial NaCl concentration was 2.5 M and *t* stands for time = 2.6 day from the start of the experiment. The last image shows the actual salt crust for which the temperature fluctuations were recorded. (b) Average surface temperature at different stages of the experiment

(indicated in the legend) as a function of the initial salt concentration. Temperature was scaled by a reference temperature measured at the surface of the bench in each round of experiments.

Rapid surface temperature fluctuations were found to be a characteristic behaviour coinciding with phase 2 of the saline water evaporation in all cases examined in our experiments. As explained earlier, during this period, the surface is visibly covered by a salt crust but the evaporation rate is relatively constant and higher than the flux expected if it were controlled by the vapour diffusion through the dry crust. During phase 2, the surface temperature changes rapidly, as shown in Figure 3.4(a) resulting in the appearance and disappearance of "cold-spots". The figure shows temperature changes as much as ~2ºC every minute. Such a rapid fluctuation was not observed when the sand column was saturated by pure water; see Figure 3.S1 in the supporting information. Additionally, it should be noted that the rapid temperature fluctuation at the surface was only observed during phase 2 of saline water evaporation and it was not observed during phase 1, 3 and 4 proposed in Figure 3.3 (see Figures 3.S2, 3.S3 and 3.S4 in the supporting information).

The appearance of localized cold spots (a phenomenon that is not observed during pure water evaporation from porous media) is associated with preferential evaporation at different locations through the precipitated salt where some of the incoming energy is consumed for liquid vaporization. Preferential evaporation increases the concentration of salt locally, which in turn leads to an increased rate of salt precipitation shortly after the occurrence of the cold spot. Since precipitation releases heat, the temperature at the cold spot should subsequently increase at this locus. This complex interplay between evaporation and precipitation leads to the observed temperature oscillations in Figure 3.4 (a). This experimental data provides additional confirmation for the contribution of precipitated salt to the evaporative mass losses. This analysis

reveals the need to develop more sophisticated models to describe the evolution of porous salt crust at the surface and its contribution to the evaporation process (Malmir et al., 2016).

In addition to the microscopic analysis of the salt effects on surface temperature dynamics with the associated preferential evaporation from the evolving crust, we studied the impact of the presence of salt on the surface temperature at the macroscopic scale. To do so, we calculated the average surface temperature at different times as a function of the initial salt concentration. Figure 3.4 (b) shows that in the early stages of the process, the average surface temperature increases with initial salt concentration. This correlates well with the reduced evaporation rates shown in Figure 3.2 and schematically depicted in Figure 3.3 (b). This finding shows that the presence of salt influences the surface temperature, which is not normally considered in hydrological modelling or water and energy balance analysis. Higher temperature as a result of the presence of salt may impact biological activities and biodiversity in soil.

3.5. Summary and conclusions

Our results confirm that precipitation of salt at the surface does not necessarily clog the pores and evaporation continues via water flow through the evolving porous crust structure. This mechanism plays a central role in defining the evaporative fluxes from porous media saturated with NaCl solutions. Without clear understanding of how the structure of the crystalized salt evolves at the surface during evaporation and how it limits the corresponding water flow, modelling efforts will largely rely on adjusting parameters which oversimplifies this process and masks the true physics governing saline water evaporation from porous media. Thermal imaging together with simultaneous imaging of the surface precipitation patterns and recording the drying dynamics enabled us to extend our physical understanding of the process. We have proposed a conceptual evaporation curve that highlights different phases with the corresponding dominant

mechanisms in each phase. Additionally, we discussed the complex temperature fluctuations at the surface due to efflorescence, which has rarely been illustrated in the past. Also, our results confirmed higher surface temperatures in the case of higher initial salt concentrations. This finding suggests that soil salinity not only affects crop production, vegetation etc. but also influences surface temperature, which may be relevant to biological activities in soil.

This study highlights the importance of the role of the precipitated salt on water flow and subsequent evaporation dynamics and we believe that future research must be directed toward further analysis and characterisation of how exactly the structure of the precipitated salt evolves during drying. This ultimately determines the dynamics of the evaporative water losses and will be relevant to modelling of many hydrological processes, land-atmosphere interaction and water management.

3.6. Acknowledgement

We gratefully acknowledge funding by the Leverhulme Trust to support this research (RPG-2014-331) and the equipment funding from the Royal Society (RG140088). The data used in this manuscript will be available freely via sending a request to the corresponding author. The first and last author would also like to acknowledge the contribution and cooperation of Delphi Everest Dana Shokri-Kuehni during this research.

3.7. References

Aminzadeh, M., and D. Or (2014), Energy partitioning dynamics of drying terrestrial surfaces, J. Hydrol., 519, 1257-1270.

Bergstad, M., N. Shokri (2016), Evaporation of NaCl solution from porous media with mixed wettability, Geophys. Res. Lett., 43, 4426–4432.

Börnhorst, M., P. Walzel, A. Rahimi, A. Kharaghani, E. Tsotsas, N. Nestle, A.Besser, F. Kleine Jäger and T. Metzger (2016), Influence of pore structure and impregnation–drying conditions on the solid distribution in porous support materials, Drying Technol., 34(16), 1964-1978, DOI: 10.1080/07373937.2016.1147048.

Dai, S., H. Shin, and J.C. Santamarina (2016), Formation and development of salt crusts on soil surfaces, Acta Geotech., 11, 1103-1109. doi:10.1007/s11440-015-0421-9.

Desarnaud, J., H. Derluyn, J. Carmeliet, D. Bonn, N. Shahidzadeh (2014), Metastability limit for the nucleation of NaCl crystals in confinement, J. Phys. Chem. Lett., 5(5), 890–895.

Eloukabi, E., N. Sghaier, S. Ben Nassrallah, and M. Prat (2013), Experimental study of the effect of sodium chloride on drying of porous media: The crusty–patchy efflorescence transition, Int. J. Heat Mass Transfer, 56, 80–93.

Guglielmini, L., A. Gontcharov, A. J. Aldykiewicz Jr., and H. A. Stone (2008), Drying of salt solutions in porous materials: Intermediate-time dynamics and efflorescence, Phys. Fluids, 20, 077101, doi:10.1063/1.2954037.

Gupta, S., P.H. Huinink, M. Prat, L. Pel, and K. Kopinga (2014), Paradoxical drying of a fired-clay brick due to salt crystallization, Chem. Eng. Sci., 109, 204–211.

Haghighi, E., and D. Or (2015), Thermal signatures of turbulent airflows interacting with evaporating thin porous surfaces, Int. J. Heat Mass Transfer, 87, 429-446.

Huinink, H. P., L. Pel, and M. A. Michels (2002), How ions distribute in a drying porous medium: A simple model, Phys. Fluids, 14, 1389–1395,doi:10.1063/1.1451081.

Jambhekar, V.A., R. Helmig, Natalie Schroder, N. Shokri (2015), Free-flow-porous-media coupling for evaporation-driven transport and precipitation of salt, Trans. Porous. Med., 110(2), 251-280.

Malmir, H., M. Sahimi, and M.R. Rahimi Tabar (2016), Microstructural characterization of random packings of cubic particles, Sci. Rep. 6, 35024, doi:10.1038/srep35024.

Nachshon, U., E. Shahraeeni, D. Or, M. Dragila, and N. Weisbrod (2011a), Infrared thermography of evaporative fluxes and dynamics of salt deposition on heterogeneous porous surfaces, Water Resour. Res., 47, W12519, doi:10.1029/2011WR010776.

Nachshon, U., N. Weisbrod, M. Dragila, and A. Grader (2011b), Combined evaporation and salt precipitation in homogeneous and heterogeneous porous media, Water Resour. Res., 47, W03513, doi:10.1029/2010WR009677.

Norouzi Rad, M., N. Shokri, and M. Sahimi (2013), Pore-scale dynamics of salt precipitation in drying porous media, Phys. Rev. E, 88, 032404.

Norouzi Rad, M., N. Shokri, A. Keshmiri, and P. Withers (2015), Effects of grain and pore size on salt precipitation during evaporation from porous media: A pore-scale investigation, Trans. Porous. Med., 110(2), 281-294.

Ott, H., M. Andrew, J. Snippe, and M. J. Blunt (2015), Microscale solute transport and precipitation in complex rock during drying, Geophys.Res. Lett., 41, 8369–8376, doi:10.1002/2014GL062266.

Rodriguez-Navarro, C., and E. Doehne (1999), Salt weathering: Influence of evaporation rate, super saturation and crystallization pattern, Earth Surf. Processes Landforms, 24, 191–209.

Sghaier, N. and M. Prat (2009), Effects of efflorescence formation on drying kinetics of porous media, Transp. Porous Med., 80, 441-454, doi: 10.1007/s11242-009-9373-6.

Shahidzadeh, N., M.F.L. Schut, J. Desarnaud, M. Prat, and D. Bonn (2015), Salt stains from evaporating droplets, Sci. Rep.5, 10335; doi: 10.1038/srep10335.

Shokri, N. (2014), Pore-scale dynamics of salt transport and distribution in drying porous media, Phys. Fluids, 26, 012106.

Shokri, N., and D. Or (2011), What determines drying rates at the onset of diffusion controlled stage-2 evaporation from porous media?, Water Resour. Res., 47, W09513.

Shokri-Kuehni, S.M., E. Bou-Zeid, C. Webb, and N. Shokri (2016), Roof cooling by direct evaporation from a porous roof layer, Energy and Buildings, 127, 521-528.

Shokri-Kuehni, S.M., M. Norouzirad, C. Webb, N. Shokri (2017), Impact of type of salt and ambient conditions on saline water evaporation from porous media, Adv. Water Resour., 105, 154–161.

Suweis, S., A. Rinaldo, S. E. A. T. M. Van der Zee,E. Daly, A. Maritan, and A. Porporato (2010), Stochastic modelling of soil salinity, Geophys. Res. Lett., 37, L07404, doi:10.1029/2010GL042495.

Veran-Tissoires, S., and M. Prat (2014), Evaporation of a sodium chloride solution from a saturated porous medium with efflorescence formation, J. Fluid Mech., 749, 701-749, doi:10.1017/jfm.2014.247.

3.8. Supporting Information

Geophysical Research Letters

Supporting Information for

New insights into saline water evaporation from porous media: Complex interaction between evaporation rates, precipitation and surface temperature

Salomé M.S. Shokri-Kuehni, Thomas Vetter, Colin Webb, Nima Shokri

School of Chemical Engineering and Analytical Science, The University of Manchester, Manchester, UK

Contents of this file

Figures 3.S1, 3.S2, 3.S3, 3.S4

Introduction

Figure 3.S1 illustrates the surface temperature of sand saturated with pure water at the similar elapsed time and location used in Figure 3.4. Additionally, Figures 3.S2, 3.S3 and 3.S4 illustrate the surface temperature of the sand column illustrated in Figure 3.4 at different times corresponding to different phases proposed in Figure 3.3. These supporting Figures confirm that the rapid and complex temperature fluctuation was observed only during phase 2 of saline water evaporation from sand (as illustrated in Figure 3.4) and such a rapid temperature changes was neither present in the case of sand saturated with pure water nor during phase 1, phase 3 and phase 4 (illustrated conceptually in Figure 3.3) of evaporation of NaCl solution from sand.

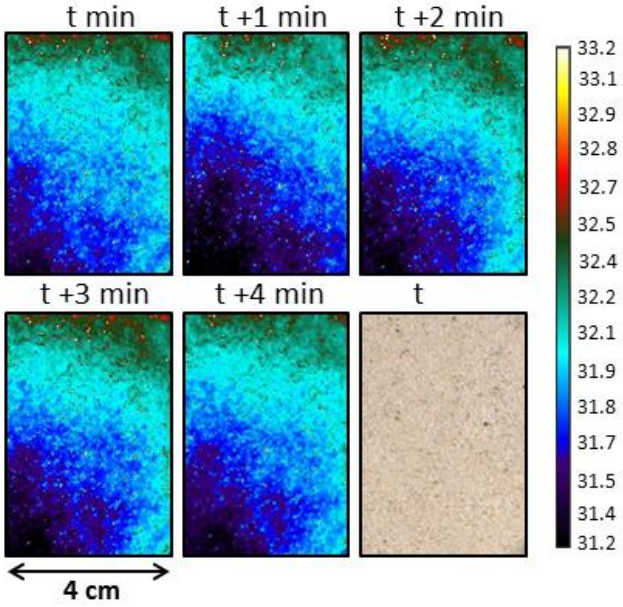

Figure 3.S1. A typical example of temporal and spatial distribution of temperature at the surface of sand saturated with pure water during evaporation. The temperature of the surface was recorded every minute. The colormap indicates temperature in centigrade. The closer to blue (darker colour) the lower the temperature. *t* stands for time = 2.6 day from the start of the experiment (similar to the elapsed time used in Figure 3.4). The last image shows the actual surface for which the temperature dynamics were recorded. In contrary to Figure 3.4, no rapid temperature change was observed in this case.

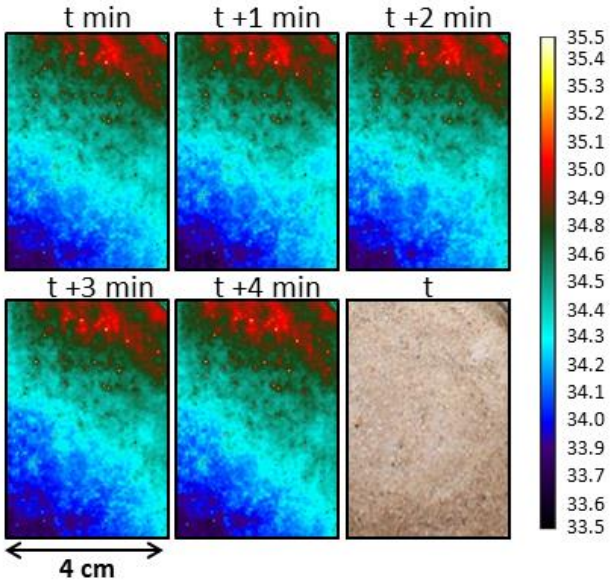

Figure 3.S2. A typical example of temporal and spatial distribution of temperature at the surface of sand saturated with 2.5 M NaCl solution after 0.95 day from the onset of experiment (corresponding to "phase 1" of the process conceptually presented in Figure 3.3). The colormap indicates temperature in centigrade. The last image shows the actual surface for which the temperature dynamics were recorded. In contrary to Figure 3.4, no rapid temperature change was observed in this case.

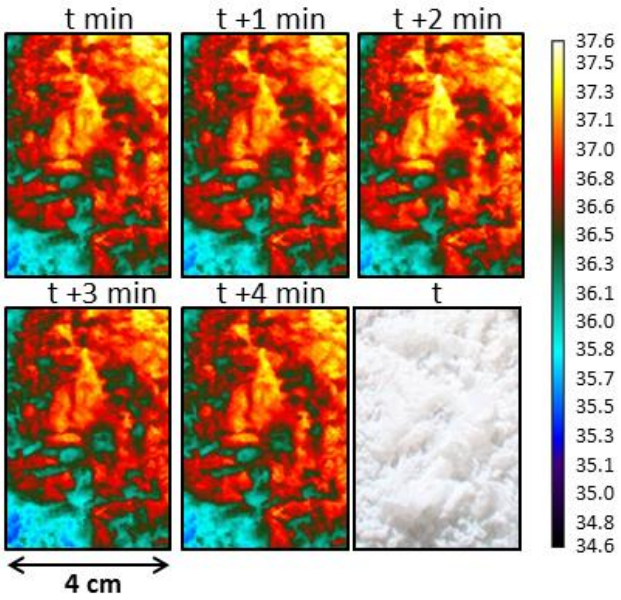

Figure 3.S3. A typical example of temporal and spatial distribution of temperature at the surface of sand saturated with 2.5 M NaCl solution after 7.9 day from the onset of experiment (corresponding to "phase 3" of the process conceptually presented in Figure 3.3). The colormap indicates temperature in centigrade. The last image shows the actual surface for which the temperature dynamics were recorded. In contrary to Figure 3.4, no rapid temperature change was observed in this case.

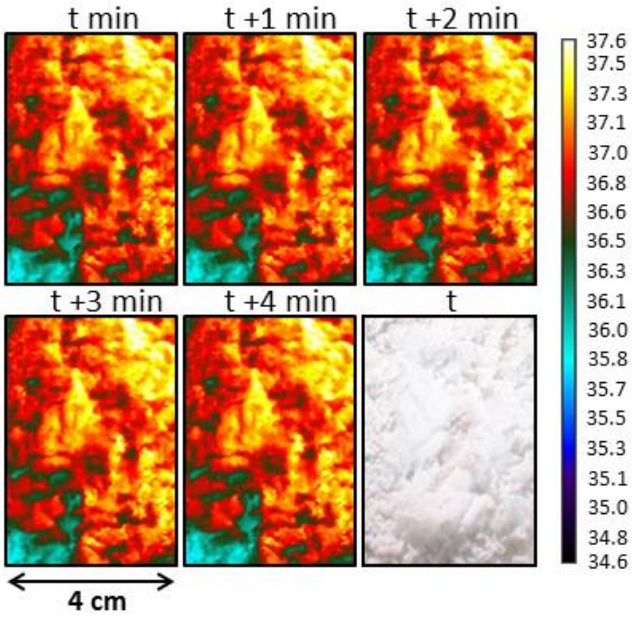

Figure 3.S4. A typical example of temporal and spatial distribution of temperature at the surface of sand saturated with 2.5 M NaCl solution after 10.4 day from the onset of experiment (corresponding to "phase 4" of the process conceptually presented in Figure 3.3). The colormap indicates temperature in centigrade. The last image shows the actual surface for which the temperature dynamics were recorded. In contrary to Figure 3.4, no rapid temperature change was observed in this case.

Chapter 4

IMPACT OF TYPE OF SALT AND AMBIENT CONDITIONS ON SALINE WATER EVAPORATION FROM POROUS MEDIA

In this chapter, saline water evaporation from porous media under different boundary conditions was investigated. A simple but effective model was proposed enabling us to quantify the effects of several parameters such as salt concentration, relative humidity, ambient temperature and type of salt on the saline water evaporation rates. To evaluate the proposed model, a comprehensive series of evaporation experiments were conducted under well-controlled conditions using sand packs saturated with saline solutions. An environmental chamber was used to evaluate the effects of ambient temperature and relative humidity on the saline water evaporation from porous media. In addition to the different environmental conditions, three different salts were used in the evaporation experiments with varying concentrations.

The obtained results confirmed the capability of the proposed model to describe the measured evaporation rates under different boundary conditions. Furthermore, the obtained results clearly showed that the presence of precipitated salt at the surface did not necessarily stop the evaporation process. Imaging of the surface of porous media during evaporation combined with the recorded mass losses revealed that the evaporation may continue even though the surface of porous media is fully covered by salt. This phenomenon is attributed to the contribution of precipitated salt to the evaporation process via capillary flow through the porous structure of salt which keeps the precipitated salt wet. Therefore the evaporation rate is not limited by the presence of precipitated salt at the surface. We could represent all evaporation curves measured

in our experiments under different drying conditions using a single curve when the measured evaporative water losses were plotted versus the scaled time introduced in this paper.

Impact of type of salt and ambient conditions on saline water evaporation from porous media

Salomé M.S. Shokri-Kuehni(1), Mansoureh Norouzirad(2), Colin Webb(1), Nima Shokri*(1)

(1) School of Chemical Engineering and Analytical Science, The University of Manchester, Manchester, UK

(2) Carl Zeiss Microscopy LLC, CA, The USA

This chapter has been published in Advances in Water Resources.

Shokri-Kuehni, S.M.S., M. Norouzirad, C. Webb, N. Shokri (2017), Impact of type of salt and ambient conditions on saline water evaporation from porous media, Adv. Water Resour., 105, 154-161.

4.1. Abstract

Saline water evaporation from porous media is important in many processes such as soil salinization, CO_2 sequestration, crop production and water management. This process is influenced by the transport properties of porous media, properties of the evaporating solution and external conditions. In this work, we investigated the effects of external conditions and type of salt on the drying behaviour of sandy media and on the dynamics of surface salt precipitation. To do so, a comprehensive series of evaporation experiments were conducted using 33 columns packed with sand saturated with salt solutions. The evaporation experiments were conducted in an environmental chamber to investigate the effects of relative humidity, ambient temperature and type of salt on the evaporation process. Sodium Chloride, Calcium Chloride and Potassium Iodide with a wide range of concentration were used to saturate the sand columns mounted on digital balances. A digital camera was fixed at the surface of the sand packs to record the dynamics of salt precipitation at the surface. The results provide further confirmation that ambient conditions are the controlling factors during stage-1 evaporation of pure water. Additionally, the minor impact of the presence of precipitated salt at the surface on the saline water evaporation during the early stages of the process is discussed. It was shown that covering the evaporation surface by precipitated salt does not necessarily stop the evaporative mass losses. The results obtained from different types of salt highlight the significant influence of the relationship between the saturated vapour pressure and salt concentration on the general dynamics of the process.

4.2. Introduction

Saline water evaporation from porous media is an important topic in many hydrological processes which influence plant growth and vegetation, water balance, soil stability, beach intertidal zone processes and land-atmosphere interaction (Odeh and Onus, 2008; Deinlein et al., 2014; González-Alcaraz ET AL., 2014; Jambhekar et al., 2015; Geng et al., 2016). It is controlled by complex interactions between type of salt, transport properties of the porous medium and external conditions (e.g. ambient temperature and relative humidity, wind, solar radiation). This has motivated many researchers to look into the effects of various parameters such as wettability [Sghaier and Prat, 2009; Bergstad and Shokri, 2016], particle size distribution [Eloukabi et al., 2013; Noruzirad et al., 2015], relative humidity [Gupta et al., 2014] and mixture of salt [Jambhekar et al., 2016] on the general dynamics of saline water evaporation from porous media.

An issue that has not received much attention in the literature is the effect of ambient conditions and the type of salt on the saline water evaporation from porous media. Sodium chloride (NaCl) has been used as the model salt in the majority of previous papers to understand processes occurring during salty water evaporation from porous media. However, depending on the type of salt, the thermodynamics of the evaporating solution will be modified and this impacts the drying dynamics. Therefore, the findings regarding NaCl cannot necessarily be generalised for other types of salt in porous media. Considering the variety of salts available in the environment, it is essential to understand how water evaporation is modified when other salts are present in porous media.

Furthermore, compared to the effects of transport properties of porous media, far fewer studies have been performed to understand the effects of external conditions on saline water evaporation

from porous media. A small increase in ambient temperature modifies soil water evaporation thus influencing salt transport and distribution in soil. Although the effects of atmospheric conditions on pure water evaporation from porous media are relatively well-understood [Smits et al., 2012; Haghighi et al., 2013; Aminzadeh and Or, 2013; Salvucci and Gentine, 2013; Ben Neriah et al., 2014; Vanderborght et al., 2017], their effects on saline water evaporation and the associated salt precipitation patterns are surprisingly not very advanced. Such knowledge will become even more important in the near future with the advent of climate change. Fluctuations in saline water evaporation and the potential change in salt balance in the environment caused by rising temperature (as a result of climate change) is complex and requires multidisciplinary research to understand the various aspects of this process [Austin et al., 2010].

Motivated by the importance of saline water evaporation from soil and its consequences on various hydrological processes, the specific objectives of the present study were to determine the effects of ambient temperature and relative humidity together with type of salt on water evaporation from porous media. Within this context, we have conducted several rounds of evaporation experiments using different types of salt in a climate chamber where we could control the ambient conditions accurately. These experiments have enabled us to understand how the relative humidity and ambient temperature, as well as the type of salt, influence the evaporation process from porous media.

4.3. Theoretical considerations

4.3.1. Pure water evaporation from porous media

As illustrated in other papers, for a given porous medium the rate of water evaporation is limited by the properties of the evaporating solution and the atmospheric conditions. As a first approximation, by neglecting the advective effects [Schlünder, 1988], the rate of volume change

of the liquid V (m^3) across the surface of porous media under isothermal conditions can be expressed using Fick's law [Gupta et al., 2014]:

$$\frac{dV}{dt} = D\frac{A}{\rho}\frac{M}{RT}\frac{P_s - P_\infty}{\delta} \tag{4.1}$$

where D is the diffusion coefficient of the liquid in air (m^2 s), A (m^2) is the surface area available for evaporation, ρ is the density of the liquid (kg m^{-3}), M is the molecular mass of water (kg mol^{-1}), R is the gas constant (kg m^2 s^{-2} K^{-1} mol^{-1}), T is the temperature (K), P_s and P_∞ correspond to the saturated vapour pressure above the evaporation surface and the vapour pressure in the surrounding environment respectively and δ is the thickness of the viscous boundary layer formed above the surface through which the diffusion of water vapour into ambient air takes place [Shokri et al., 2008]. Note that P_s and P_∞ are related via $P_\infty = RH \times P_s$ where RH corresponds to the relative humidity of the ambient air (%).

According to Eq. (4.1), water evaporation depends on the vapour pressure gradient which is influenced by the temperature. The dependency of the saturated vapour pressure of water as a function of temperature T can be expressed using the following empirical expression [Buck, 1981]:

$$P_s(T) = 0.61 \exp\left(\frac{17.27T}{T + 237.3}\right) \tag{4.2}$$

In Eq. (4.2), the units of T and P_s are °C and kPa, respectively. In addition to the saturated vapor pressure, the diffusion coefficient also depends on temperature, with the following equation describing this dependency [Ben Neriah et al., 2014]:

$$D = 2.23 \times 10^{-5} \left(\frac{T + 273.15}{273.15} \right) \tag{4.3}$$

In Eq. (4.3), the units of T and D are °C and m^2/s^{-1}, respectively. Note that Eq. (4.1) can be used to estimate the evaporation rate in the early stages of the process, during so-called stage-1 evaporation [Shokri et al., 2009]. During this period, capillary induced liquid flow from large pores, at the receding interface between the saturated and unsatuarted zones to the fine pores at the surface, keeps the surface wet and the evaporative demand is mainly supplied by liquid vaporization occurring at the surface of porous media. However, when the liquid continuity with the surface is disconnected, the liquid vaporization occurs inside the medium and the drying process will be limited by vapour diffusion through the dry layer formed close to the surface of the porous medium [Shokri et al., 2009].

Under a constant ambient temperature, P_s remains constant. In such cases, the humidity will be the main factor determining the magnitude of the evaporation [Gupta et al., 2014]. Here we use P_s, T, and D for water to scale time $\tilde{t}$ (in unit m^2) as:

$$\tilde{t} = \frac{MD(1 - RH)P_s}{\rho RT} t \tag{4.4}$$

Using Eq. (4.4) and defining the constant β as A/δ, Eq. (4.1) becomes:

$$\frac{dV}{d\tilde{t}} = \beta \tag{4.5}$$

Since β is not a function of temperature, Eq. (4.5) implies that all water evaporation data obtained at different humidities and temperatures should result in the single value β (Soulié et al., 2015) if plotted versus the scaled t introduced in Eq. (4.4). Note that this is valid only during

stage -1 evaporation where the surface is wet and the bulk of the evaporative demand is supplied by the liquid vaporization at the interface between the air and the porous media surface.

4.3.2. Saline water evaporation from porous media

The same approach explained in section 2.1 can be used to estimate saline water evaporation from porous media. However, there are some additional factors that must be taken into account, since the properties of the saline solution (e.g. saturated vapour pressure, diffusion coefficient and density) not only change because of the variation of temperature but also because of changes in the concentration of solute.

In the present study, we have worked with three different salts namely NaCl, $CaCl_2$ and KI. The salts were chosen for their non-toxicity, solubility in water, and how the vapour pressure of water is affected with increasing concentration of the salts. In the case of $CaCl_2$, there is a significant dependency of the saturated vapour pressure on salt concentration, compared to NaCl and KI, for which the increasing concentration affects the vapour pressure much less. We obtained the following empirical equation to estimate saturated vapour pressure as a function of salt concentration using the values derived from Patil et al. (1991) and Clarke and Glew (1985):

$$P_s = a_0 + a_1 C + a_2 C^2 + a_3 C^3 \tag{4.6}$$

with C indicating the salt concentration in molality and P_s in kPa. The fitting parameters a_1, a_2 and a_3 for NaCl, $CaCl_2$ and KI at 35°C are listed in Table 4.1 and are used later in our analysis. More details about how the fitting parameters in Table 4.1 were obtained using Eq. (4.6) are presented in the appendix.

Table 4.1. Parameters required to relate P_s to salt concentration for the cases of NaCl, $CaCl_2$, and KI at 35°C.

Salt	a_0	a_1	a_2	a_3
NaCl	5.98	- 0.40	0.0086	0.0018
$CaCl_2$	5.16	- 0.11	- 0.14	0.012
KI	5.55	- 0.067	- 0.029	0.0016

Additionally, the density and diffusion coefficient of salt are modified as the concentration of salt and ambient temperature changes. Published data on the dependency of diffusion coefficient of water molecules into air in the presence of ions in solution and its variation with respect to the type of salt and temperature are scarce, even for NaCl (note that here we are not referring to the self-diffusion coefficient of ions in liquid). Thus for salt solutions, the scaled time proposed in Eq. (4.4) will be useful only if the relationship between the salt concentration and the diffusion coefficient at a given temperature and solution density is known. If it is not, in the case of salt solution, one can scale time (in unit of day) using Eq. (4.7) expressed as:

$$\tilde{t}_s = \frac{M(1-RH)P_s}{\rho RT} t \tag{4.7}$$

Substituting Eq. (4.7) into Eq. (4.1) leads to:

$$\frac{dV}{d\tilde{t}_s} = \beta D \tag{4.8}$$

For Eq. (4.7), the change in density of solution as a result of the presence of salt was considered negligible for the sake of this calculation. Note that if the variation of diffusion coefficient with respect to salt concentration could be neglected, as is the case for pure water, cumulative mass loss curves measured at different temperature and relative humidity under different salt concentrations should be represented by a single curve (as long as the vaporization occurs at the surface of porous media and the presence of a salt crust does not limit the process).

When salt is present in the evaporating liquid, its concentration increases over time as a result of evaporation. When the salt concentration substantially exceeds the solubility limit (i.e., supersaturation exceeds a critical value), crystals will precipitate by first nucleating and then growing. One of the key objectives of this paper was to investigate how the presence of precipitated salt influences the validity and applicability of the above analysis (Eqs. 4.5 and 4.8). The remainder of this paper evaluates the relative importance of ambient temperature and humidity on the evaporation from porous media in the absence and presence of three different salts.

4.4. Experimental considerations

Six sets of experiments were conducted in an environmental chamber in which the relative humidity and ambient temperature were controlled accurately and kept constant at the desired values in each set (Table 4.2). NaCl, $CaCl_2$ and KI with a wide range of concentration (Table 4.2) were used in our experiments to prepare salty solutions. Glass Hele-Shaw cells (80 mm in width, 260 mm in height and 10 mm in thickness) and cylindrical glass columns (85 mm in diameter and 230 mm in height) were used in our experiments to pack sand particles saturated with either water or salty solutions. All boundaries of sand columns were closed except the top which was open to air for evaporation. The sand columns were mounted on digital balances

(accuracy 0.01 g) connected to a computer to record the mass of the evaporating sand packs every 5 minutes. A digital camera was fixed at the surface of the cylindrical column to record the dynamics of precipitation at the surface each hour. The camera was connected to a computer for automatic image acquisition. A total of 33 columns were packed with saturated sand packs to investigate the saline water evaporation under a variety of conditions in terms of relative humidity, ambient temperature and salt compound. More details about the boundary conditions in each experiment are presented in Table 4.2.

Table 4.2. Experimental conditions in each set of experiment. Note that in set # 1, 2, and 3 the average sand particle size was 0.61 mm and in set # 4, 5, and 6 it was 0.7 mm.

# of set	Evaporating liquid	Salt concentration (M)	Ambient temperature and relative humidity	Dimension of the column
1	Pure water	0	Round 1: At 25°C and RH of 30%, 50% and 70% Round 2: At 35°C and RH of 30%, 50% and 70%	Hele-Shaw cell (80 mm in width, 260 mm in height and 10 mm in thickness)
2	NaCl solution	1 Molal	Round 1: At 25°C and RH of 30%, 50% and	Hele-Shaw cell (80 mm in width, 260 mm in height and

			70% Round 2: At 35°C and RH of 30%, 50% and 70%	10 mm in thickness)
3	NaCl solution	3 Molal	Round 1: At 25°C and RH of 30% and 50% Round 2: At 35°C and RH of 30% and 50%	Cylindrical column (85 mm in diameter, 230 mm in height)
4	NaCl solution	0.5, 1, 2, 3, 4, 5 Molal	At 35°C and RH of 25%	Cylindrical column (83 mm in diameter, 153 mm in height)
5	KI solution	0.5, 1, 2, 5, 7 Molal	At 35°C and RH of 25%	Cylindrical column (83 mm in diameter, 153 mm in height)
6	$CaCl_2$ solution	0.5, 1, 2, 3.5, 5, 6.5 Molal	At 35°C and RH of 25%	Cylindrical column (83 mm in diameter, 153 mm in height)

4.5. Results and discussion

4.5.1. Scaling behaviour of pure water evaporation

Figure 4.1 (a) illustrates the measured cumulative water evaporation from the Hele-Shaw cells packed with sand grains saturated with pure water. The experiments were conducted under 6 different ambient conditions (i.e. at 25 °C and relative humidity of 30, 50 and 70% and at 35 °C and relative humidity of 30, 50 and 70%).

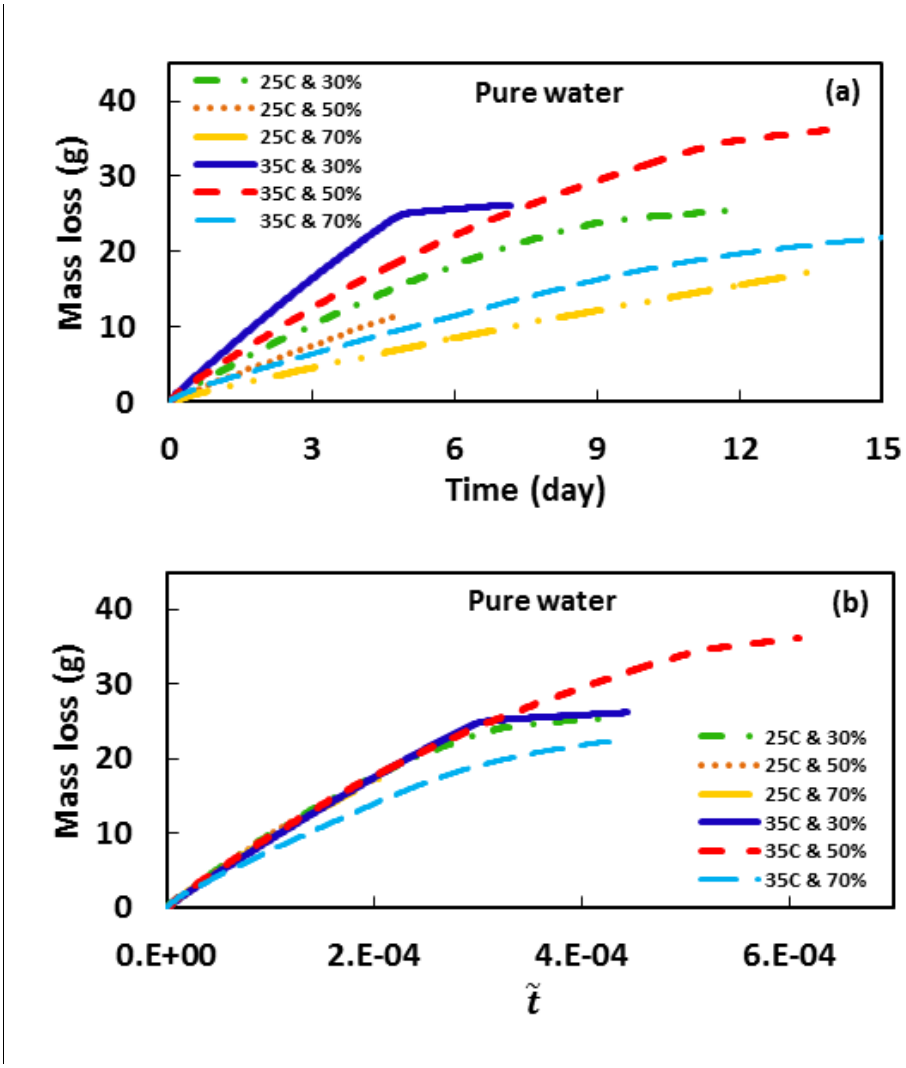

Figure 4.1. Cumulative evaporative water loss measured during the evaporation process from a Hele-Shaw cell packed with sand grains saturated with pure water versus (a) time and (b) scaled

time (in unit of m^2) introduced in Eq. (4.4). The legend indicates ambient temperature and relative humidity in each round of experiments.

The evaporation rate (i.e. the slope of the mass loss curve) in all cases remains relatively constant in the early stages of the evaporation processes depicted in Figure 4.1(a). This is typical trend observed during stage-1 evaporation where the evaporative demand is supplied by liquid transfer from the interior of the porous medium to the surface via capillary induced liquid flow and liquid vaporization at the surface. Similar behaviour has been reported in many other studies (e.g. see Lehmann et al. [2008]; Shokri-Kuehni et al. [2016]). Stage-1 evaporation will eventually end when the liquid connection with the surface is disrupted due to the competition between capillary, gravity and viscous forces [Lehmann et al., 2008]. This marks the onset of the stage-2 evaporation when the evaporative flux is limited by vapour diffusion through porous media [Shokri and Or, 2011] resulting in much smaller evaporative fluxes. This explains the change of the slope in some of the curves presented in Figure 4.1(a). Figure 4.1(b) shows the measured mass losses versus $\tilde{t}$, Eq. (4.4). This figure shows that the measured cumulative mass losses from the sand columns saturated with pure water under different relative humidity and ambient temperature coincide very well if plotted versus $\tilde{t}$. It must be noted that such a scaling behaviour is valid only during stage-1 evaporation (when the process is mainly controlled by the liquid vaporization at the surface). Figure 4.1(b) confirms that the changes in the evaporative mass losses depicted in Figure 4.1(a) are the result of the change in relative humidity and ambient temperature and the process is controlled by the external conditions.

4.5.2. Scaling behaviour of saline water evaporation

Figure 4.2 shows the measured cumulative mass losses from the Hele-Shaw cells packed with sand grains saturated with 1 M NaCl solution under different ambient temperature and relative

humidity. The highest and lowest measured evaporation correspond to the highest (35 °C and 30%) and lowest (25 °C and 70%) evaporative demands, respectively. During saline water evaporation, the NaCl concentration increases continuously close to the surface. Therefore, the saturated vapour pressure above the surface decreases continuously, Eq. (4.6). Thus, contrary to the case of pure water, the evaporation rate from the beginning of the experiments with saline water decreases over time (because the driving force $P_s - P_\infty$ decreases as a result of the increasing salt concentration).

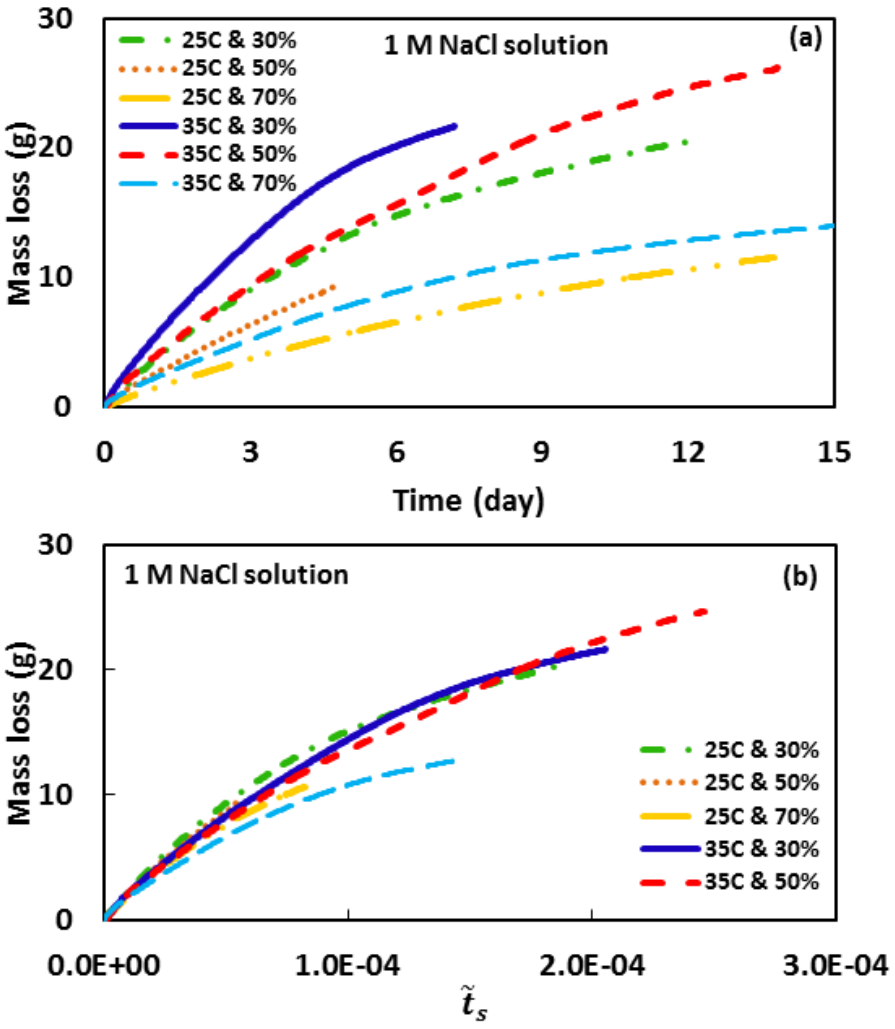

Figure 4.2. Cumulative evaporative water loss measured during saline water evaporation from a Hele-Shaw cell packed with sand grains saturated with 1 M NaCl solution versus (a) time and (b) scaled time (in unit of day) introduced in Eq. (4.7). The legend indicates ambient temperature and relative humidity in each round of experiments.

Figure 4.2(b) illustrates the recorded mass losses under different external conditions (indicated in the legend) versus the rescaled time $\tilde{t}_s$. It is remarkable to have all the curves in Figure 4.2(b) coincided quite well when plotted as a function of the scaling parameter $\tilde{t}_s$. This is not an intuitive result because one would expect the formation and growth of precipitated salt at the surface to influence and limit the evaporation flux but this is not what we observed in our data (note that the slight differences among the curves illustrated in Figure 4.2(b) could be related to the changes in the saturated vapour pressure above the surface over time due to the increasing salt concentration at the surface). Figure 4.3 shows the comparison between the measured evaporation rates during the first 2 days of the experiments (i.e. the slopes of the mass loss curves presented in Figures 4.1 and 4.2 averaged over the first two days) under different external conditions for pure and saline water.

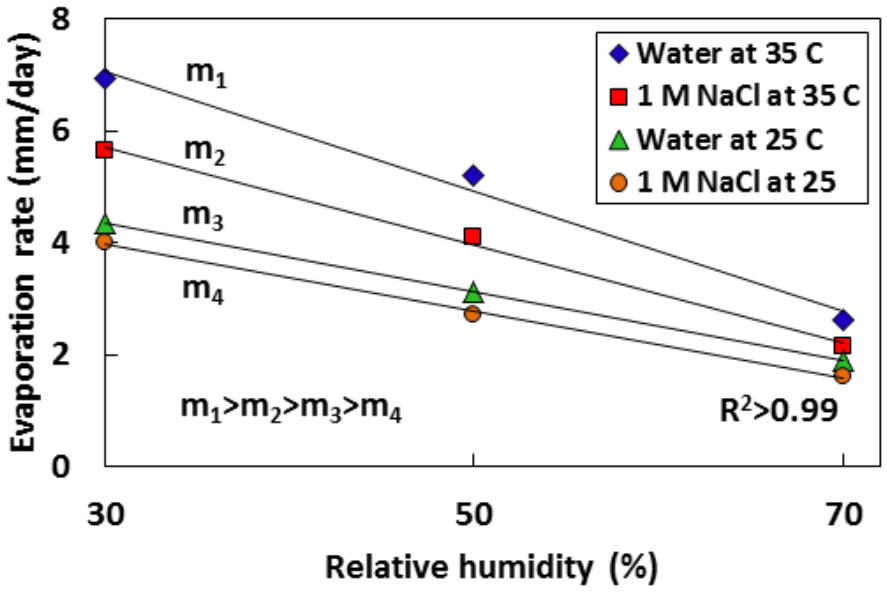

Figure 4.3. Evaporation rate during the first two days from the onset of the experiments. The value of the evaporation rate was calculated using the slope of the lines fitted to the cumulative mass loss curves presented in Figures 4.1 and 4.2. The legend indicates the ambient temperature in each round of the experiment and the liquid (water or 1 M NaCl solution) used to saturate the sand columns. The solid lines indicate the linear fit to the data (in all cases R^2>0.99). The slopes of the lines are represented by m_1, m_2, m_3 and m_4.

Figure 4.3 shows that increasing relative humidity results in decreasing evaporation flux. Under the same ambient temperature, adding salt reduced the evaporative water losses due to the reduced saturated vapour pressure above the surface. The difference between drying rates of pure and saline water increased as temperature increased from 25 °C to 35 °C. This is due to the nonlinear dependency of the saturated vapour pressure and the diffusion coefficient into air on ambient temperature. In any case, the results presented in Figures 4.2 and 4.3 illustrate a relatively linear relationship between the evaporation rate from saline solution and the external condition and that the evaporative flux is mainly limited by the external conditions; similar to

what is observed in the case of pure water (Figure 4.1). To have a closer look at the evaporation process from saline porous media, another set of experiments (set#3; Table 4.2) were conducted in which cylindrical columns were used and the dynamics of evaporative mass losses together with the salt precipitation at the surface were investigated.

4.5.3. Precipitation dynamics and the evaporative mass losses

A cylindrical column was packed with sand grains saturated with 3M NaCl solution. The evaporation experiments were conducted at four different external conditions (indicated as set#3 in Table 4.2). The recorded images of the surface of the porous medium were used to quantify the part of the surface covered by salt over time. Salt is represented by the white colour in the images. Therefore, one could assume the higher the pixel grey value (GV) of the images, the more area is covered by salt. We used the surface grey value of the last image as the reference value to scale the other images as:

$$Scaled\ GV = \frac{Summation\ of\ GV\ of\ all\ pixels\ in\ each\ image}{Summation\ of\ GV\ of\ all\ pixels\ in\ the\ last\ image} \quad (9)$$

"Scaled GV" will be always equal to, or less than one (because the last image has the highest GV since the entire surface is covered by salt). Based on the definition of "Scaled GV", a bigger portion of the surface is covered by salt when "Scaled GV" is closer to 1. Applying the same scaling to all images enabled us to quantify the dynamics of surface coverage by salt over the course of the experiment. Figure 4.4 illustrates the evaporative mass losses together with the precipitation dynamics at the surface.

The results show a strong relationship between dynamics of the evaporative mass losses and the surface coverage by salt. A similar correlation was observed by Norouzi Rad and Shokri [2012].

Existence of such a strong correlation may have applications beyond the focus of this paper because it may offer an opportunity to estimate the evaporative mass losses by looking into the salt precipitation dynamics at the surface. The counter-intuitive result presented in Figure 4.4 is to have a significant portion of the surface covered by salt; yet the cumulative evaporative mass losses are not influenced by the presence of this precipitated salt at the surface. This result suggests that the presence of salt crystals at the surface does not necessarily stop the evaporation process (at least during the early stage of the process). The same conclusion was reached in some recent studies on building materials and glass beads packing (e.g. Eloukabi et al., 2013; Gupta et al., 2014). The reason for this is the porous nature of the precipitated salt (Norouzi Rad et al., 2013). Liquid flows through the precipitated salt via capillary flow keeping the crystals at the surface wet, which contributes to the evaporation. This explains why the evaporative flux is not limited significantly by the presence of the precipitated salt at the surface (as long as it remains wet) and that the curves could be scaled in Figure 4.2(b).

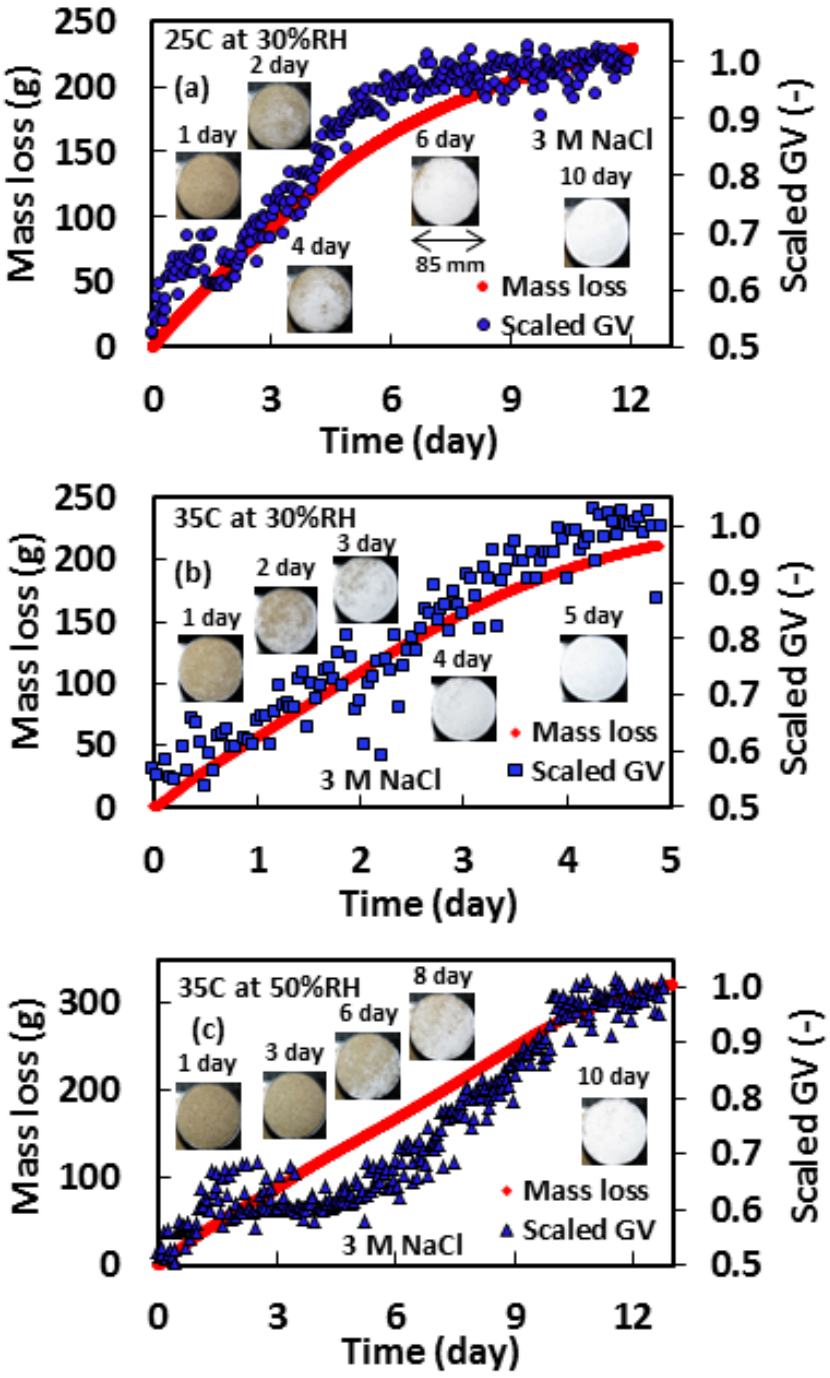

Figure 4.4. Cumulative evaporative mass losses versus time measured during evaporation from a cylindrical sand column saturated with 3M NaCl solution at a) 25°C and relative humidity (RH) of 30%, b) 35°C and relative humidity of 30% and c) 35°C and relative humidity of 50%. Also presented is the scaled grey value (GV) at the surface of porous media, indicating the surface

coverage by precipitated salt. Values closer to 1 indicate a greater fraction of the surface is covered by salt. The insets illustrate typical salt precipitation patterns at different times from the onset of the experiments. The white colour represents precipitated salt at the surface.

To further investigate this, the measured mass losses during evaporation from the columns saturated with 3 M NaCl solution at an ambient temperature of 25°C and relative humidity of 30 and 50% are presented in Figure 4.5.

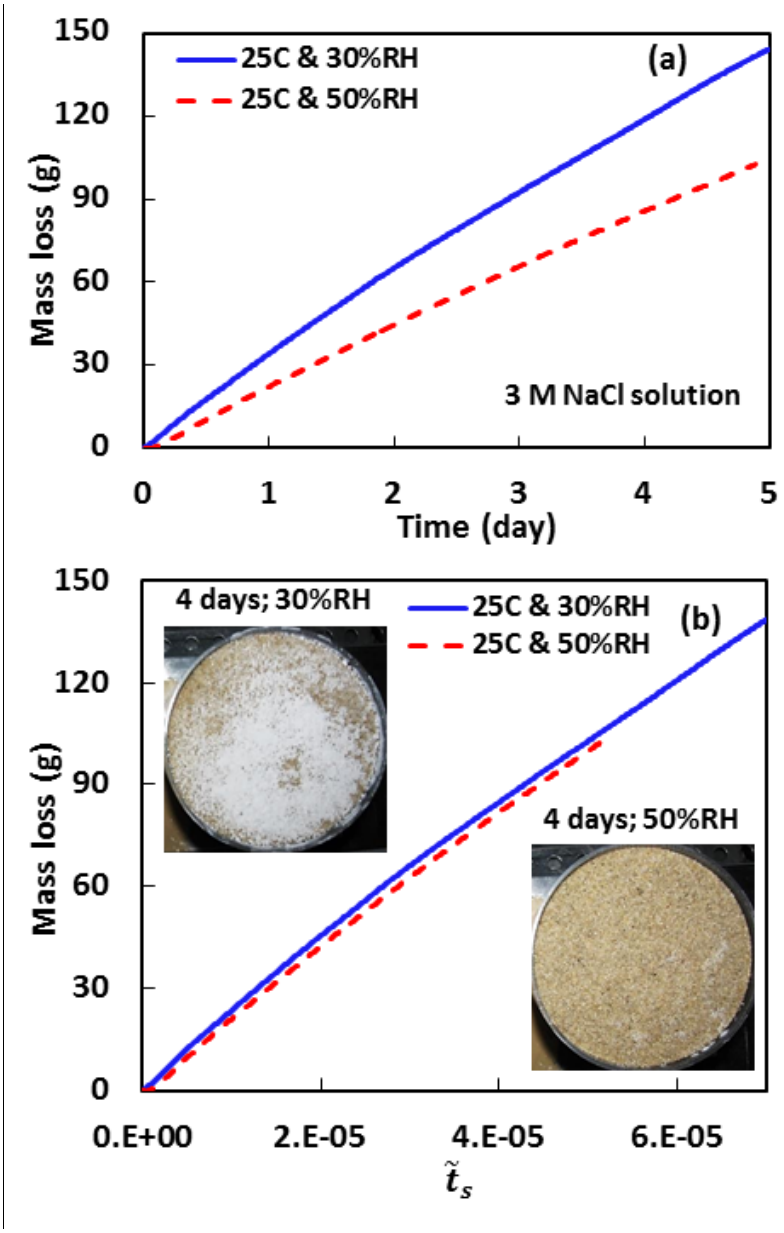

Figure 4.5. (a) The cumulative mass loss measured during evaporation from cylindrical columns packed with sand saturated with 3 M NaCl solutions. The experiments were conducted at the constant temperature of 25°C and relative humidity of 30 and 50%. (b) The cumulative mass losses presented in section (a) plotted versus the scaled time $\tilde{t}_s$ (in unit of day) introduced in Eq. (4.7). The insets illustrate the precipitation patterns at the surface after 4 days from the onset of the experiment. White corresponds to precipitated salt.

The cumulative mass loss from the column placed under 50% relative humidity is less than that under 30%; this is expected as the driving force for the evaporation is less (Eq. 4.1). Therefore much more salt was precipitated at the surface of the column placed under 30% relative humidity. The inset of Figure 4.5 shows the surface of these two sand columns after 4 days from the onset of the experiment confirming the above statement. Although these two columns have completely different precipitation patterns at the surface, the cumulative mass losses are very close if plotted against the scaled time $\tilde{t}_s$ introduced in Eq. (4.7). This confirms that the different cumulative mass losses observed in Figure 4.7(a) are due to the different external conditions and not to the presence or absence of precipitated salt at the surface and that the precipitated salt does not necessarily limit the liquid transfer toward the surface because of its porous nature (at least in the early stages of the process).

4.5.4. Effects of type of salt on the evaporation behaviour

The data obtained from the experiments with NaCl, KI, and $CaCl_2$ are presented in this section. See Table 4.2 for detail of the boundary conditions in each round of experiments. Figure 4.6 illustrates the measured cumulative mass losses. Results show that as salt concentration increased the evaporative mass losses decreased in all cases. When plotting against the scaled time $\tilde{t}_s$, the cumulative mass losses recorded during early stages of the process coincide very well in the case of NaCl and KI. This means the observed differences in the recorded mass loss curves are governed by the effects of salt concentration on lowering the vapour pressures (Eq. 4.6) as other parameters were kept the same in the experiments.

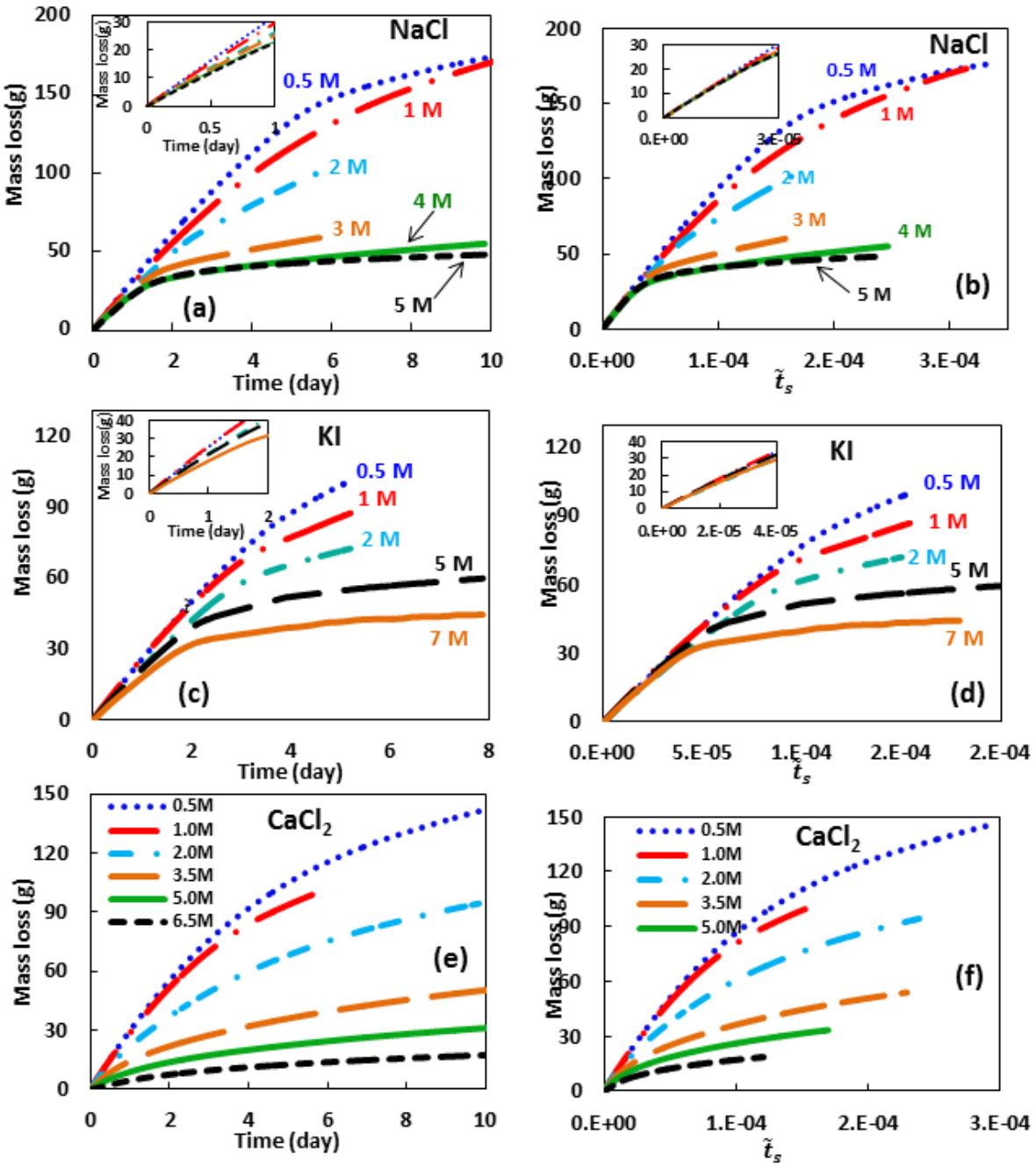

Figure 4.6. The cumulative mass loss measured during evaporation from the cylindrical columns packed with sand saturated with (a) NaCl, (c) KI and (e) $CaCl_2$ solutions. (b), (d) and (f) show the same data (i.e. cumulative mass losses) versus the scaled time $\tilde{t}_s$ (in unit of day) introduced in Eq. (4.7). All experiments were conducted at the constant temperature of 35°C and relative

humidity of 25%. Legends indicate the initial salt concentration used to saturate the sand columns. The insets in (a-d) show the same cumulative mass loss data as the main curve but zoomed in to illustrate the trend in the early stages of the process.

Note that in the previous sections variation of the external conditions caused the changes in the evaporative mass losses but in this case it is the change in properties of the solution modifying the evaporation process but all of these effects are already incorporated in the scaled times introduced in Eqs. (4.4) and (4.7). In the case of NaCl and KI, although the curves coincide very well using the scaled times during the early stages of the process (the insets in Figure 4.6(b) and 4.6(d)), they cannot be represented by a single curve during the later stages of evaporation. This is likely due to drying of the precipitated salt at the surface which results in the change of the vaporization plane from the surface of the precipitated salt to deeper depths (located either at the interface between the porous medium and the precipitated salt or depths below the surface of the porous medium). Therefore, the process is no longer controlled by vapour diffusion from the wet salt surface to the air but by a combination of capillary flow from the interface between the wet and partially wet zones in the porous medium up to this new vaporization plane, liquid vaporization at that level and then vapour diffusion through the porous medium and the dried precipitated salt to the air.

$CaCl_2$ shows a different drying behaviour to those observed in the case of NaCl and KI. Figure 4.6(e) and (f) show that the recorded cumulative mass losses in the case of $CaCl_2$ do not coincide either in the early or later stages of the evaporation using the scaled time. On top of that, variation of the evaporative mass losses versus salt concentration is much more significant in the case of $CaCl_2$ compared to the other two salts considered in this study. One of the reasons for

such behaviour could be attributed to the significant dependency of the saturated vapour pressure on salt concentration in the case of $CaCl_2$ compared to NaCl and KI.

As evaporation proceeds, the salt concentration increases close to the surface; thus the saturated vapour pressure decreases over time. This influences the driving force for evaporation especially in the early stages of the process (when the process is still limited by the external conditions). If P_s changes significantly versus concentration, the driving force for liquid vaporization in the early stages of the process changes notably thus resulting in continuous lowering of the evaporation rates. However, if P_s does not change significantly versus concentration, then one could describe the evaporation process in the early stages using the scaled times (Eq. 4.4 and 4.7). Figure 4.7(a) shows the variation of P_s versus concentration of NaCl, KI and $CaCl_2$ at 35 °C using Eq. (4.6).

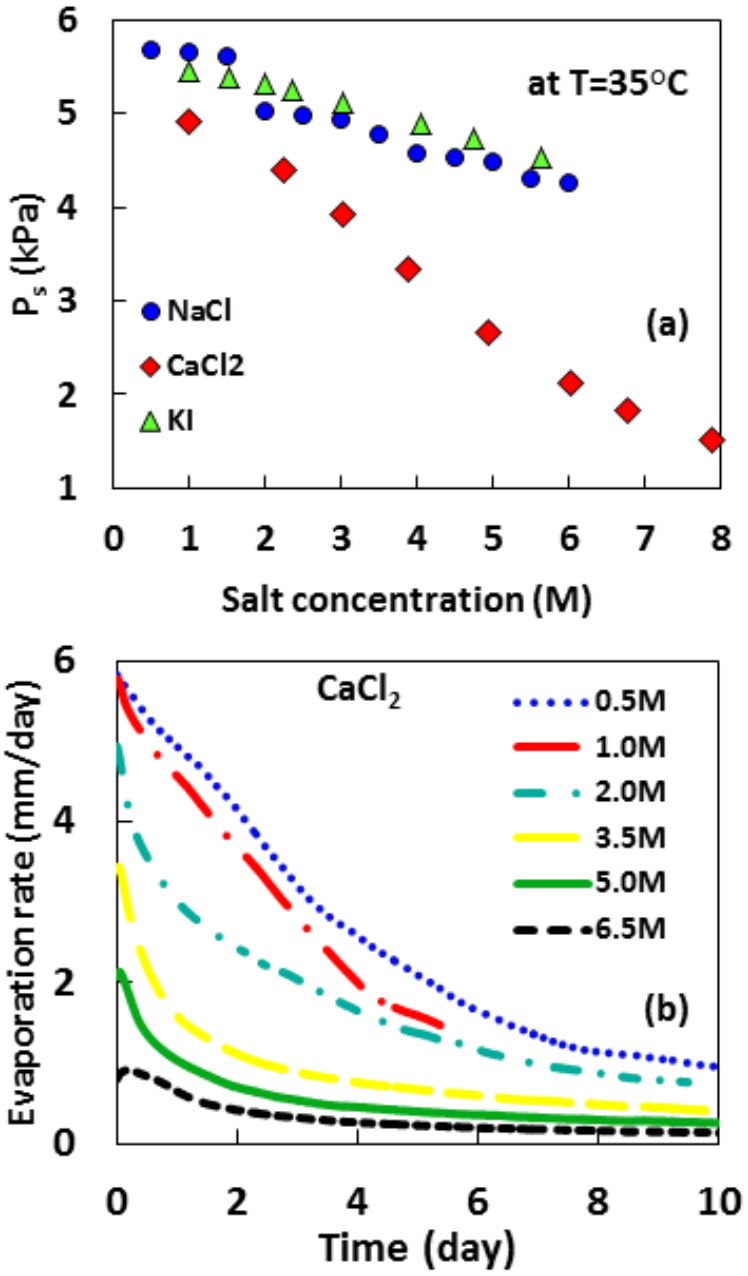

Figure 4.7. (a) Variation of the saturated vapour pressure P_s versus salt concentration at 35°C. The legend indicates the type of salt. The data were obtained using Eq. (4.6) and the data presented in Table 4.1. (b) The evaporation rate versus time measured during evaporation from the sand column saturated with $CaCl_2$ solution. The legend indicates the initial salt concentration in each case.

According to Figure 4.7(a), P_s changes significantly as concentration changes in the case of $CaCl_2$ as opposed to NaCl and KI. This has significant impact on its evaporation behaviour and causes continuous decrease of the evaporation rate from the beginning of the experiment as illustrated in Figure 4.7(b).

4.6. Summary and conclusions

A comprehensive series of evaporation experiments (using 33 sand columns) was conducted under well-controlled ambient temperatures and relative humidities to understand the effects of external condition as well as type of salt on saline water evaporation from porous media. Our results confirm that during stage-1 evaporation of pure water, the process is mainly controlled by the ambient conditions. The recorded mass losses in the case of pure water under 6 different external conditions could be represented by a single curve using scaled time $\tilde{t}$.

In addition, our results illustrate the minor impact of the presence of precipitated NaCl at the surface on saline water evaporation during the early stages of the process. This is because of the porous nature of the precipitated salt at the surface keeping the salt wet (via capillary flow) that contributes to the evaporation process. The recorded mass losses from the columns packed with saline solution with different NaCl concentrations that experienced different ambient temperature and relative humidity could be represented by a single curve using the scaled time $\tilde{t}_s$. The scaling behaviour is valid as long as the surface or the precipitated salt remains wet. This analysis confirms that it is a necessity to understand how the porous structure of precipitated salt evolves during evaporation from porous media and how it influences the subsequent flow and transport processes. Modelling tools introduced in some recent studies [Malmir et al., 2016a; 2016b] will be useful to describe such a phenomenon.

Additionally, using NaCl, KI and $CaCl_2$ enabled us to investigate the impact of the properties of the evaporating solution on the evaporation dynamics. Our results highlight the important effect of the relationship between the saturated vapour pressure and salt concentration on the general dynamics of the evaporation process. Significant variation of the saturated vapour pressure with respect to the salt concentration in the case of $CaCl_2$ led to decreasing evaporation rate from the very beginning of the experiments because any small increase in salt concentration at the surface (as a result of evaporation) has a notable impact on the saturated vapour pressure in the case of $CaCl_2$ that influences the driving force for vaporization.

4.7. Acknowledgement

We gratefully acknowledge funding by the Leverhulme Trust to support this research (RPG-2014-331). We would like to thank Kaicheng Ding, a MEng student in Nima Shokri's research group, for her help with conducting some of the experiments. The data presented in this manuscript will be available freely via sending a request to the corresponding author. The first and last author would also like to acknowledge the contribution and cooperation of Delphi Everest Dana Shokri-Kuehni during this research.

4.8. Appendix

Eq. (4.6) was fitted to the values derived from Patil et al. (1991) and Clarke and Glew (1985) to obtain the empirical parameters presented in Table 4.1. Specifically speaking, in the case of KI and $CaCl_2$, Eqs. (4.1) to (4.4) of Patil et al. (1991) were used to obtain saturated vapour pressure as a function of salt concentration at 35°C. Then Eq. (4.6) was fitted to the values derived from Patil et al. (1991). As for NaCl, the values of saturated vapour pressure at various temperatures (but not at 35°C) as a function of NaCl concentration were given as tabulated values in Clarke

and Glew (1985). We have used those values to estimate saturated vapour pressure at 35°C. Then Eq. (4.6) was fitted to these values to obtain the empirical parameters presented in Table 4.1.

4.8. References

Aminzadeh, M., and D. Or (2013), Temperature dynamics during nonisothermal evaporation from drying porous surfaces, Water Resour. Res., 49, 7339–7349.

Austin, J., L. Zhang, R.N. Jones, P. Durack, W. Dawes, P. Hairsine (2010), Climate change impact on water and salt balances: an assessment of the impact of climate change on catchment salt and water balances in the Murray-Darling Basin, Australia, Climatic Change, 100, 607-631.

Ben Neriah, A., S. Assouline, U. Shavit, N. Weisbrod (2014), Impact of ambient conditions on evaporation from porous media, Water Resour. Res., 50, 6696–6712.

Bergstad, M., N. Shokri (2016), Evaporation of NaCl solution from porous media with mixed wettability, Geophys. Res. Lett., 43, 4426–4432.

Buck, A. L. (1981), New equations for computing vapor pressure and enhancement factor, J. Appl. Meteorol., 20(12), 1527–1532,

Clarke, E.C.W., D.N. Glew (1985), Evaluation of the Thermodynamic Functions for Aqueous Sodium Chloride from Equilibrium and Calorimetric Measurements below 154 °C, j. Phys. Chem. Ref. Data, 14(2), 489-610.

Deinlein, U., A.B. Stephan, T. Horie, W. Luo, G. Xu, J.I. Schroeder (2014), Plant salt-tolerance mechanisms, Trends in Plant Science, 19(6), 371–379.

Eloukabi, E., N. Sghaier, S. Ben Nassrallah, and M. Prat (2013), Experimental study of the effect of sodium chloride on drying of porous media: The crusty–patchy efflorescence transition, Int. J. Heat Mass Transfer, 56, 80–93.

Geng, X., M.C. Boufadel, N.L Jackson (2016), Evidence of salt accumulation in beach intertidal zone due to evaporation, Sci. Rep., 6, 31486; doi: 10.1038/srep31486.

González-Alcaraz, M.N., F.J. Jiménez-Cárceles, Y. Álvarez, J. Álvarez-Rogel (2014), Gradients of soil salinity and moisture, and plant distribution, in a Mediterranean semiarid saline watershed: a model of soil–plant relationships for contributing to the management, Catena, 115, 150-158.

Gupta, S., H.P. Huinink, L. Pel, K. Kopinga (2014), How Ferrocyanide Influences NaCl Crystallization under Different Humidity Conditions, Cryst. Growth Des., 14 (4), 1591–1599.

Haghighi, E., E. Shahraeeni, P. Lehmann, and D. Or (2013), Evaporation rates across a convective air boundary layer aredominated by diffusion, Water Resour. Res., 49, 1602–1610.

Jambhekar, V.A., R. Helmig, Natalie Schroder, N. Shokri (2015), Free-flow-porous-media coupling for evaporation-driven transport and precipitation of salt, Trans. Porous. Med., 110(2), 251-280.

Jambhekar, V.A., E. Mejri, N. Schröder, R. Helmig, N. Shokri (2016), Kinetic approach to model reactive transport and mixed salt precipitation in a coupled free-flow-porous-media system, Trans. Porous. Med., 114(2), 341–369.

Lehmann, P., S. Assouline, and D. Or (2008), Characteristic lengths affectingevaporative drying of porous media, Phys. Rev. E, 77, 056309,doi:10.1103/PhysRevE.77.056309.

Malmir, H., M. Sahimi, M.R. Rahimi Tabar (2016a), Microstructural characterization of random packings of cubic particles, Sci. Rep., 6, 35024, DOI: 10.1038/srep35024.

Malmir, H., M. Sahimi, M.R. Rahimi Tabar (2016b), Packing of nonoverlapping cubic particles: Computational algorithms and microstructural characteristics, Phys. Rev. E, 94, 062901.

Norouzi Rad, M., N. Shokri (2012), Nonlinear effects of salt concentrations on evaporation from porous media, Geophys. Res. Lett., 39, L04403.

Norouzi Rad, M., N. Shokri, M. Sahimi (2013), Pore-Scale Dynamics of Salt Precipitation in Drying Porous Media, Phys. Rev. E, 88, 032404.

Odeh, I.O.A., A. Onus (2008), Spatial Analysis of Soil Salinity and Soil Structural Stability in a Semiarid Region of New South Wales, Australia, Environmental Management, 42, 265-278.

Or, D., P. Lehmann, E. Shahraeeni, N. Shokri (2013), Advances in soil evaporation physics – a review, Vadose Zone J., 12(4), doi:10.2136/vzj2012.0163.

Patil, K.R., A.D. Tripathi, G. Pathak, S.S. Katti (1991), Thermodynamic properties of aqueous electrolyte solutions. 2. Vapor pressure of aqueous solutions of sodium bromide, sodium iodide, potassium chloride, potassium bromide, potassium iodide, rubidium chloride, cesium chloride, cesium bromide, cesium iodide, magnesium chloride, calcium chloride, calcium bromide, calcium iodide, strontium chloride, strontium bromide, strontium iodide, barium chloride, and barium bromide, J. Chem. Eng. Data, 1991, 36 (2), 225–230

Salvucci, G.,D., and P. Gentine (2013), Emergent relation between surface vapor conductance and relative humidity profiles yields evaporation from weather data, Proc. Natl. Acad. Sci. U.S.A., 110 (16), 6287-6291.

Schlünder, E.-U. (1988), On the mechanism of the constant drying rate period and its relevance to diffusion controlled catalytic gas phase reactions, Chem. Eng. Sci., 43, 2685– 2688.

Sghaier, N., and M. Prat (2009), Effect of efflorescence formation on drying kinetics of porous media, Transp. Porous Med., 80, 441-454.

Shokri-Kuehni, S.M., E. Bou-Zeid, C. Webb, N. Shokri (2016), Roof cooling by direct evaporation from a porous roof layer, Energy and Buildings, 127, 521-528.

Shokri, N., P. Lehmann, P. Vontobel, D. Or (2008), Drying front and water content dynamics during evaporation from sand delineated by neutron radiography, Water Resour. Res., 44, W06418.

Shokri, N., and D. Or (2011), What determines drying rates at the onset of diffusion controlled stage-2 evaporation from porous media?,Water Resour. Res., 47, W09513, doi:10.1029/2010WR010284.

Shokri, N., P. Lehmann, D. Or (2009), Critical evaluation of enhancement factors for vapor transport through unsaturated porous media, Water Resour. Res., 45, W10433.

Smits, K. M., V. V. Ngo, A. Cihan, T. Sakaki, and T. H. Illangasekare (2012), An evaluation of models of bare soil evaporation formulated with different land surface boundary conditions and assumptions, Water Resour. Res., 48, W12526, doi:10.1029/2012WR012113.

Soulié, V. S. Karpitschk, F. Lequien, P. Prené, T. Zemb, H. Moehwald, H. Riegler (2015), The evaporation behavior of sessile droplets from aqueous saline solutions, Phys. Chem. Chem. Phys.,17, 22296-22303.

Vanderborght, J., T. Fetzer, K. Mosthaf, K. M. Smits, and R. Helmig (2017), Heat and water transport in soils and across the soil-atmosphere interface: 1. Theory and different model concepts, Water Resour. Res., 53, doi:10.1002/2016WR019982.

Chapter 5

IODINE K-EDGE DUAL ENERGY IMAGING REVEALS THE INFLUENCE OF PARTICLE SIZE DISTRIBUTION ON SOLUTE TRANSPORT IN DRYING POROUS MEDIA

In this chapter, 4D pore-scale data (3D space + time) obtained by synchrotron X-ray tomography using Iodine K-edge dual energy imaging method was used to delineate the dynamics of solute transport during saline water evaporation from porous media. Two sand columns differing in particle size distribution were saturated with salt solution with well-defined properties and the dynamics of ion transport during evaporation was visualized with high spatial and temporal resolutions. Using this technique, we could delineate the governing mechanisms controlling ion transport during evaporation from porous media.

Pore-scale 4D imaging indicated higher average salt concentration at the surface of the coarse-grained sand compared to the fine-grained sand. As mentioned in this chapter, this is counter-intuitive because in both sand columns the initial concentration, porosity and, more importantly, the evaporation rate were nearly the same, yet the ion distributions at the surface were significantly different, influencing salt deposition patterns. This behaviour is attributed to preferential solute deposition at the smaller pores at the surface of porous media while the larger pores are preferentially invaded by air.

Moreover, using the measured concentration profiles and the analytical solution of convection-dispersion equation (CDE), allowed for a semi-quantitative estimate of the effective dispersion coefficient during evaporation from porous media. We were able to investigate both, the impact of particle size distribution on the dispersion coefficient, and the evolution of the dispersion

coefficient during evaporation. The results show the effective dispersion coefficient increases during evaporation as liquid saturation decreases. With decreasing water saturation, the flow paths become increasingly more tortuous and longer, hence extending the mixing zone considerably. The liquid saturation above the drying front depends on the pore-size distribution of porous media. Due to preferential air invasion through larger pores, two porous media with different particle-size distribution may have similar saturation above the drying front, but very different drying front depth. The longer solute travel distance leads to more dispersion under similar average saturation above the drying front. The data confirms, the effective dispersion coefficient depends not only on the saturation, but also on the complex liquid network and its morphology formed during the evaporation process. This study extended the physical understanding of the mechanisms controlling the dynamics of solute transport in porous media during evaporation.

Iodine k-edge dual energy imaging reveals the influence of particle size distribution on solute transport in drying porous media

Salomé M.S. Shokri-Kuehni (1), Mina Bergstad (1), Muhammad Sahimi (2), Colin Webb (1), Nima Shokri (1)

(1) School of Chemical Engineering and Analytical Science, The University of Manchester, Manchester, UK

(2) Mork Family Department of Chemical Engineering and Materials Science, University of Southern California,Los Angeles, California 90089-1211, USA

This manuscript is currently under review.

5.1. Abstract

Increasing salinity in groundwater and soil poses a threat to water and land resources. With the expectation of major changes to the hydrological cycle through climate change, the need for understanding the fundamental processes governing solute transport through soil has grown significantly. We provide experimentally verified insights into the influence of particle size distribution on solute transport in porous media during evaporation at the pore- and macro-scales. To do so, we utilized four-dimensional (space plus time) synchrotron X-ray tomography for iodine k-edge dual energy imaging to obtain solute concentration profiles in every single pore during saline water evaporation from coarse- and fine-grained sands. Close to the surface of the coarse-grained sand significantly higher salt concentrations were observed when compared to fine-grained sand with the same porosity under similar cumulative evaporative mass losses. The physics behind this behaviour was delineated using the recorded data with high spatial and temporal resolutions. Moreover, the measured data enabled us to quantify the variations of the effective dispersion coefficient during evaporation and how it is influenced by the particle size distribution. We show that, contrary to common assumption in modelling of solute transport during evaporation, the effective dispersion coefficient varies as a function of liquid saturation and the length of the invaded zone during evaporation from porous media, and that it increases as liquid saturation decreases.

5.2. Introduction

Water and land quality have long been issues of global concerns. Increasing salinity in groundwater and soil poses a threat to the ecosystem functioning, water quality and evaporation, and crop production[1-6]. Understanding solute transport in the flow of water through soil entails studying the phenomenon through partially saturated zone during evaporation, which is a complex process. During evaporation of saline water from porous media, solutes are transported to the vaporization plane via capillary-induced liquid flow, while diffusion tends to homogenise the concentration laterally throughout the pore space. The interaction between the two determines the dynamics of solute distribution in porous media[7,8]. Numerous studies have been conducted in the past to look into the effects of various parameters, such as particle size, wettability, heterogeneity, and the type of salt[9-16] , on saline water evaporation from porous media. Much less attention has, however, been paid to experimental study of how solutes are transported and distributed throughout the pore space during evaporation, and how transport properties, such as the effective dispersion coefficient D^* in porous media, vary as drying proceeds. As is well known, dispersion is convective mixing of two miscible fluids, which is modified by molecular diffusion, particularly in the slow zones of the pore space. The effective dispersion coefficient, which is usually used in the description of solute transport in porous media by the convective-dispersion equation (CDE), represents the combined effect of the two at the macroscale. Surprisingly, the majority of previous studies that modelled saline water evaporation from porous media either assumed a constant D^* or one that decreases with decreasing saturation [8,17-21].

The focus of the present work is on providing new deep insights into the influence of particle size distribution on the physics of solute transport in porous media during evaporation. In

particular, the specific objective of this paper is to understand how the effective dispersion coefficient varies during evaporation from porous media and how it is influenced by the particle size distribution. To do so, we utilize four-dimensional (4D, space plus time) synchrotron X-ray tomography and iodine k-edge dual energy imaging in order to visualize the dynamics of solute transport in a complex pore space and quantify the variations of the effective dispersion coefficient with time and saturation. This provides us with a unique opportunity to underpin the physical mechanisms controlling solute transport and deposition in porous media during evaporation.

5.3. Results and Discussion

5.3.1. Quantitative characterisation of ion transport in porous media

The experimental setup and imaging details are the same as those reported by Shokri[21]. Briefly speaking, we conducted 4D synchrotron X-ray tomography experiments with fine and coarse sands, with the particle-size distributions presented in Figure 5.1, packed in cylindrical columns of 8 mm diameter and 16 mm height. The columns were open to air from top for evaporation. The sand column was initially saturated with a salt solution containing 5% (by weight) calcium iodide. The dynamics of the evaporation process from the sand packs were visualized using synchrotron X-ray tomography in order to resolve the details of phase distribution and solute transport at pore-scale.

Image analysis and reconstruction were done using Avizo Fire 9.2 (FEI, 2017) and in-house codes developed in MATLAB. Further details of the experiments and image analysis are given in the Methods section below. Figure 5.1 shows a 3D rendering of the reconstructed volume of the packed coarse- and fine-grained sand, together with their porosity variations that were quantified using the segmented images.

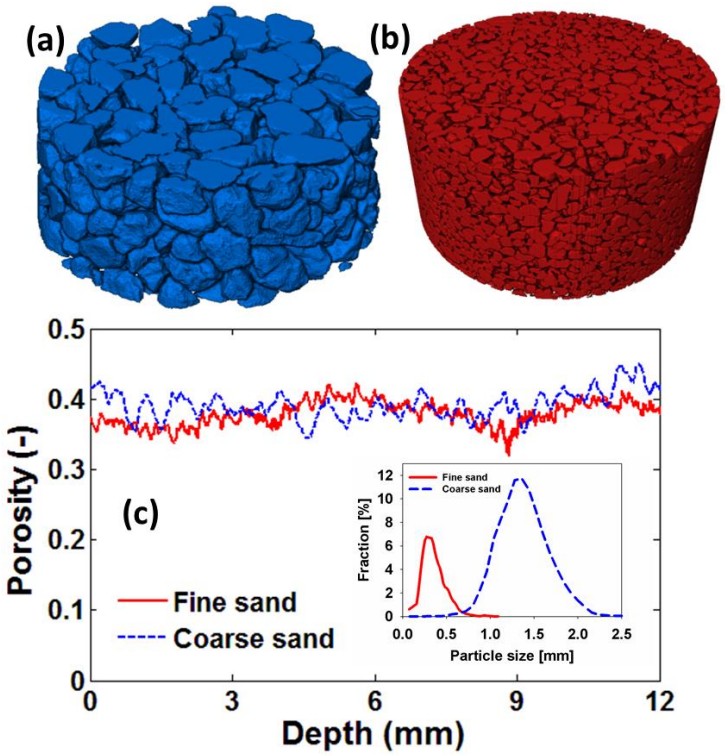

Figure 5.1. Three-dimensional rendering of the reconstructed volume of the packed (a) coarse and (b) fine sands with the corresponding porosity presented in (c). The inset illustrates the particle-size distribution of the sand grains used in the experiments.

The segmented images were used to calculate the water saturation in each cross section, from which the cumulative evaporative mass losses were calculated. Figure 5.2 shows the water saturation profiles together with the cumulative evaporative mass losses, measured during the evaporation experiments with the fine and coarse sands. The results indicate that the evaporation rates in both cases were nearly the same over the course of the experiments, despite notable differences in the measured water saturation profiles. This is expected because during early stages of the process the evaporation rate is mainly dependent on the external conditions, which were similar for both experiments. Note that the ambient temperature and relative humidity remained the same during the experiments.

The water saturation profiles depend strongly on the dynamics of the fluid front displacement during the evaporation process. The geometry and dynamics of the displacement front have been analysed in several studies[22,23] which revealed the dependence of the front dynamics on the interplay between gravity, capillarity and viscous forces. Different pore-size distributions of the fine and coarse sands influence the capillarity forces and, consequently, the liquid-phase distribution. During water evaporation, the displaced air-water interface is pinned in regions with small pores, while continuing to recede in the regions with large pores. This results in non-uniform liquid-phase distribution over time and space. For example, Figure 5.2(a) indicates that a part of the air-water interface is pinned in a region nearly 3 mm below the surface, whereas air continues to invade the medium preferentially through larger pores up to a depth of about 8 mm below the surface. Moreover, Figure 5.2 confirms the presence of more water at the surface of fine-textured sand compared to coarse-textured sand. This is due to the higher air entry pressure of fine sand compared to coarse sand, due to the presence of smaller pores. Although the cumulative mass losses are nearly the same in the case of fine- and coarse-grained sand, the liquid phase distribution above the drying front (the interface between saturated and unsaturated zone) is remarkably different. In other words, with same evaporative mass losses, the length of the unsaturated zone (the distance over which solute is transported) is different in the fine- and coarse-grained sand. This significantly influences the dynamics of solute transport which will be discussed next.

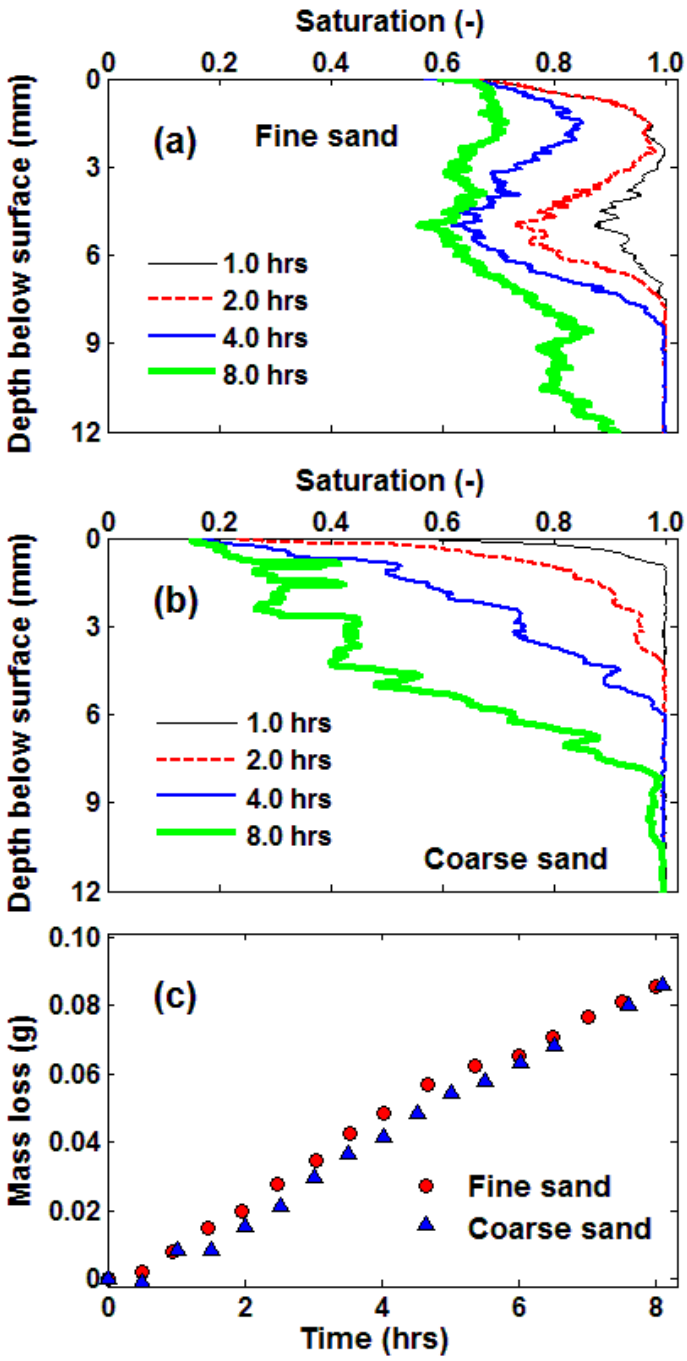

Figure 5.2. Time-dependence of the liquid saturation profiles, from the onset of the experiment (indicated in the legend) during evaporation from (a) fine- and (b) coarse-grained sands. (c) The computed cumulative mass losses over time during evaporation, computed using the segmented images obtained by synchrotron X-ray tomography.

5.3.2. Solute concentration profiles

Using iodine k-edge dual energy subtraction[21], we obtained the salt concentration profiles with high spatial and temporal resolutions, and analysed the effect of the pore-size distribution on the saline water evaporation and variation of the effective dispersion coefficient, as defined earlier. Details of the procedure used to compute the solute concentration throughout the evaporating columns using the recorded images are presented in the Method summary section. Figure 3 shows the solute concentration distribution at the surface of the two types of sand packs 6 hours after the onset of evaporation (colours closer to red indicate higher concentrations).

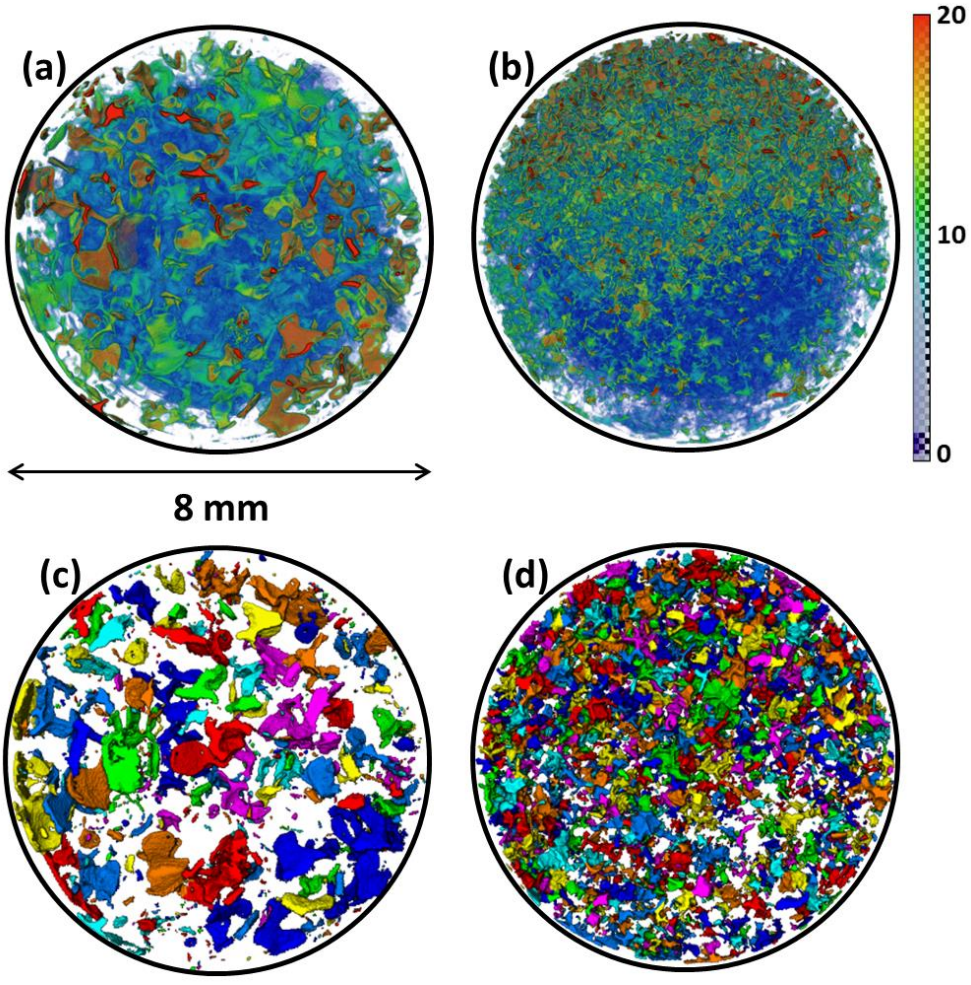

Figure 5.3. Distribution of solute concentration within the top 1 mm of (a) coarse- and (b) fine-textured sands 6 hours after the onset of the experiment. The colour map represents the solute concentration percentage, such that the closer to red, the higher the concentration. Also presented in (c) and (d) are the liquid cluster distributions within the top 1 mm of the fine- and coarse-grained sands. The clusters are defined as the liquid within pore bodies separated through pore throats. The colour represents the size of clusters.

Closer inspection of Figures 5.3(a) and 5.3(b) reveals that the average ion concentration is higher at the surface of coarse-grained sand than it is with the fine-grained sand. Note that in both cases the initial concentration, porosity and, more importantly, the evaporation rate were nearly the same, yet the solute distribution at the surface of the two sand packs are significantly different. We attribute this difference to the dominant impact of the preferential liquid evaporation from finer pores at the surface, leading to non-uniform ion distribution.

In addition, the qualitative results presented in Figure 5.3 indicate that at the surface of both sand packs, liquid clusters of the same sizes exhibit distinct solute concentrations. This suggests that the solute concentration depends not only on the pore/cluster sizes, but also on how the liquid clusters and patches are distributed at the surface. This happens due to the influence of the spacing between the liquid clusters on the corresponding evaporation rate per cluster[24,25]. Shahraeeni *et al.*[24] showed that, due to the impact of the spacing between the clusters on the formation of a diffusive vapour shell above the surface, larger spacing between wet patches at the surface of porous media results in higher evaporation per pore. As described by Bergstad and Shokri[26], such a phenomenon leads to higher salt concentrations in the wet patches, when distributed distantly. We also analysed the liquid cluster distribution within the top 1 mm of the sand columns, and the results are presented in Figures 5.3(c) and 5.3(d). These confirm the

existence of larger spacing between the liquid clusters in the coarse sand, compared to the fine packing.

Using the 4D images recorded by synchrotron X-ray tomography, we calculated the solute concentration along the sand profiles over time. The results are presented in Figure 5.4, illustrating a sharper gradient of solute concentration closer to the surface of the coarse sands compared with the fine sand. Typical examples are presented in Figures 5.4(a) and 5.4(b) that illustrate, respectively, the solute concentration after 8 hours of evaporation in the case of fine and coarse sands.

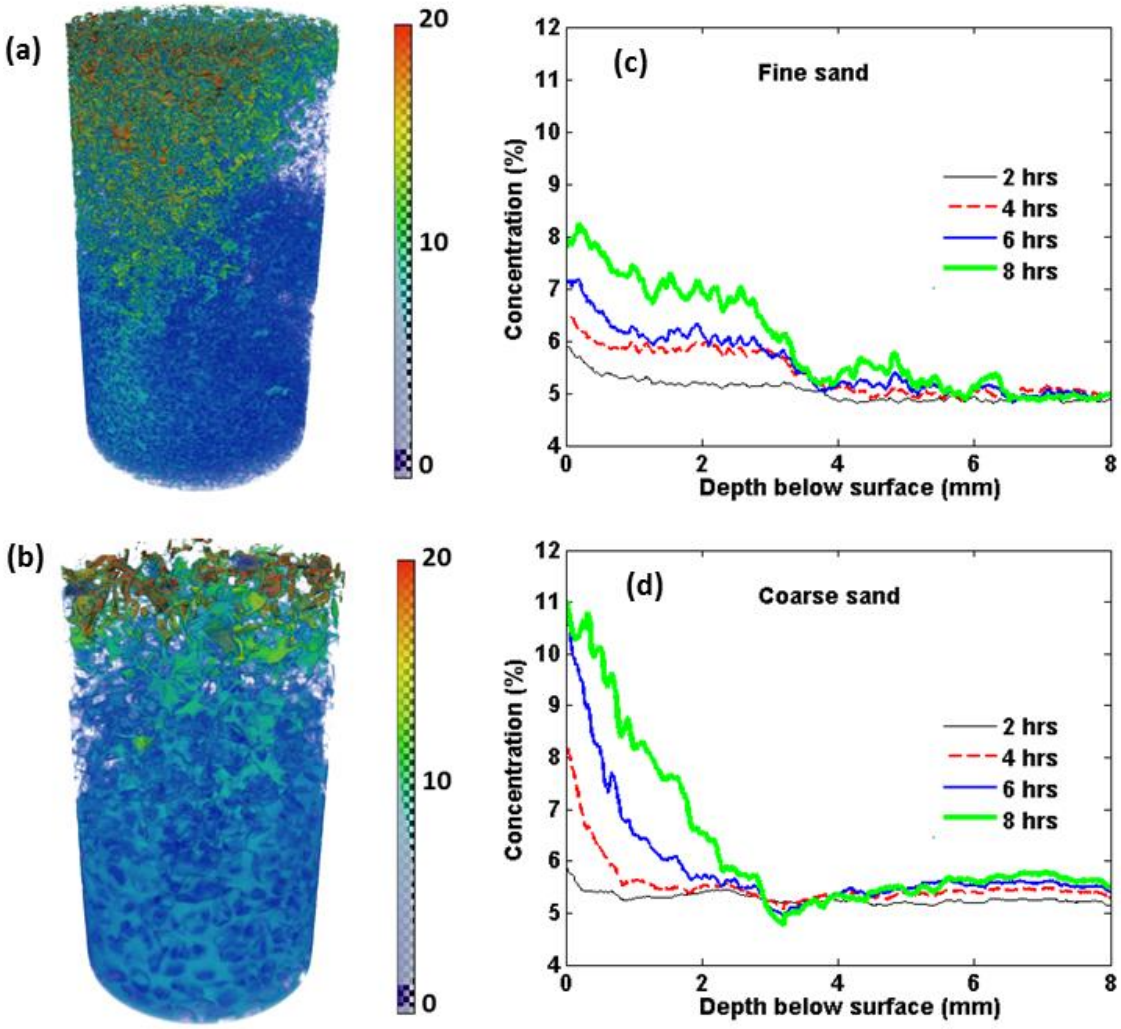

Figure 5.4. Reconstruction of the liquid phase in the top 5 mm of the (a) fine and (b) coarse sand, 8 hours after the onset of evaporation with the colour map representing the solute concentration percentages. Colours closer to red indicate higher concentrations. Also presented is the dynamics of solute distribution in (c) fine and (d) coarse sand at various times from the onset of the experiments (indicated in the legend).

Although both porous media have similar porosity and initial salt concentration, and were placed under similar evaporative demand, the pore-scale solute distributions through the two evaporating sand columns are remarkably different. Such pore-scale phenomena affect the macroscopic response, presented in Figures 5.4(c) and 5.4(d). The results indicate that, relative to the coarse sand, the solute is distributed more uniformly through the fine sand packing. This suggests that the effective dispersion coefficient is higher in the fine sand. As illustrated in Figures 5.4(a) and 5.4(b), there exist more tortuous capillary pathways in the fine sand. This leads, as a result of the existence of more junctions within the complex liquid network and the longer lengths of the flow paths, to more mixing, implying higher effective dispersion coefficients that influence the solute transport during evaporation.

5.3.2. Estimating the dispersion coefficient

Under the assumptions of negligible solute adsorption on the solid surface and a 1D vertical solute transport, the equation that governs solute transport in the evaporating liquid confined to porous media is given by: [7,18]

$$\frac{\partial(\rho\varepsilon SC)}{\partial t} = \frac{\partial}{\partial z}\left(\rho\varepsilon SD^{*}\frac{\partial C}{\partial z} - \rho\varepsilon SCU\right) \tag{5.1}$$

where $C(z,t)$, ε, ρ, t, z and S indicate, respectively, the solute mass fraction, porosity, density of the solution, elapsed time from the onset of the evaporation, depth below the surface, and the liquid saturation. U corresponds to the average liquid velocity and D^* is the effective dispersion coefficient of the solute in porous media, representing the combined effect of mixing by convection and diffusion. As mentioned earlier, in many previous studies in which Eq. (5.1) was used to describe solute transport in porous media during evaporation, D^* was assumed to be either constant or decreasing with decreasing liquid saturation.[8,17-21] Using the experimental pore-scale information, we investigate the variation of D^* during saline water evaporation from porous media.

We utilized the analytical solution developed by Guglielmini et al.[7] to estimate the dispersion coefficient using the measured salt concentration profiles. Guglielmini *et al.*[7] developed the following analytical solution to describe the dynamics of ion concentration in drying porous media at intermediate times:

$$\Omega\ (\xi,\tau) = 1 - Pe\tau + \frac{Pe^2\ \tau\ \mathrm{erfi}\left(\frac{\sqrt{Pe}(\xi-1)}{\sqrt{2-2Pe\tau}}\right)}{(Pe\ \tau - 1)\mathrm{erfi}\left(\frac{\sqrt{Pe}}{\sqrt{2-2Pe\tau}}\right)} \tag{5.2}$$

where erfi is the imaginary error function, Ω is the dimensionless effective solute density at dimensionless depth ξ below the surface, with ξ defined as $\xi = z/L$. Here, L is the length scale over which the solute transport occurs, which is the length of invaded (or unsaturated) zone, τ is the dimensionless time defined as, $\tau = tD^*/L^2$. In Eq. (5.2), Pe represents the Peclet number defined as $Pe = \frac{Le}{\rho\varepsilon D^*}$ with e representing the evaporation rate. The analytical solution was obtained with the assumption of constant S and D^*. In our experiments, for a given saturation the

system is fixed, hence the analytical solution is applicable to the state of the system at that saturation for a given scan. This allowed for a semi-quantitative estimate of the effective dispersion coefficient by fitting the analytical solution given by Eq. (5.2) to the measured concentration profiles. An example of fitting Eq. (5.2) to the experimentally-determined concentration profiles is presented in the Supplementary Information. The computed D^* in the fine and coarse sands are reported in Figure 5.5 as a function of (a) average saturation of the invaded zone S; (b) the length L of the invaded zone, and (c) S/L. The results presented in Figure 5.5 show that D^* increases during evaporation as liquid saturation decreases. This is contrary to the assumption made in previous studies regarding a constant effective dispersion coefficient or one that decreases with decreasing saturation in drying porous media.[8,17-21] The inverse relationship between D^* and liquid saturation indicated by Figure 5.5 suggests that D^* in Eq. (5.1) should be treated as an effective dispersion coefficient when this equation is used to model saline water evaporation from porous media.

That the effective dispersion coefficient increases over time is due to the fact that, as the evaporation process proceeds, water saturation decreases. Therefore, the flow paths become increasingly more tortuous and longer, hence extending the mixing zone considerably. This leads to better mixing over longer distances, resulting in larger effective dispersion coefficients. The increase in D^* at lower liquid saturations was first predicted by Sahimi *et al.*[27-29], and was subsequently confirmed in numerous experiments with various types of porous media[30-32]. Although this inverse relationship between D^* and the liquid saturation is relatively well-established and confirmed in one- or two-phase fluid displacement processes in porous media, to the best of our knowledge, a systematic analysis for delineating the relationship between D^* and liquid saturation in porous media during evaporation was not attempted before.

Figure 5.5 indicates that the effective dispersion coefficient changes almost one order of magnitude over the duration of the experiments, and that it does not necessarily change linearly with the liquid saturation, a main assumption made commonly in literature. In fact, as was first shown by Sahimi and Imdakm[33], percolation theory[34,35] predicts that as the water saturation decreases and approaches its residual value at which it becomes disconnected, D^* increases as a power law in (S-S_r), where S_r is the residual saturation, with the exponent of the power law estimated by Sahimi and Imdakm[33] to be about (-0.2) in 3D and (-2.8) in 2D porous media.

We found a strong linear relationship between D^* and the length of the invaded zone. Since the dispersivity, the ratio of the dispersion coefficient and mean flow velocity, is proportional to the length of the invaded zone, the implication is that the average macroscopic velocity remains essentially constant. As the drying front - the interface between the saturated and unsaturated zones - recedes into the porous medium, the length of the invaded zone increases. This leads to the formation of a more tortuous liquid network that contributes towards better mixing and, thus, higher D^*. Thus, the data confirm that D^* depends not only on the saturation, but also on the complex liquid network and its morphology formed during the evaporation process.

Note that, due to the receding drying front during evaporation from porous media, the length over which solute travels increases with time. The liquid saturation above the drying front depends on the pore-size distribution of porous media (among other factors). Spatial heterogeneity of pore-sizes promotes preferential air invasion through larger pores and therefore, two porous media with different particle-size distribution may have similar saturation above the drying front, but very different length of the unsaturated (invaded) zone. For example, in our experiments, under a constant liquid saturation above the drying front, the length of the unsaturated zone is longer in fine-grained sand compared to the coarse-grained sand, hence

resulting in longer solute travel distances which leads to more dispersion in the former case under similar average saturation above the drying front. Moreover, when the length of unsaturated zone is the same in coarse- and fine-grained sand, the saturation in coarse sand is less resulting in more tortuous and longer flow paths than in the fine sand which leads to more dispersion in the coarse sand as illustrated in Fig. 5.5(b). This suggests that evaluating D^* solely based on the average saturation may not capture the entire physics that controls solute transport in porous media during evaporation, and that one should simultaneously take into account the drying front depth, the length over which solute transport occurs. Based on the data presented in Figures 5.5(a) and 5.5(b), we looked into the relationship between D^* and the combined effects of saturation of the invaded zone and the length of the invaded zone, expressed as S/L. The results are presented in Figure 5.5(c).

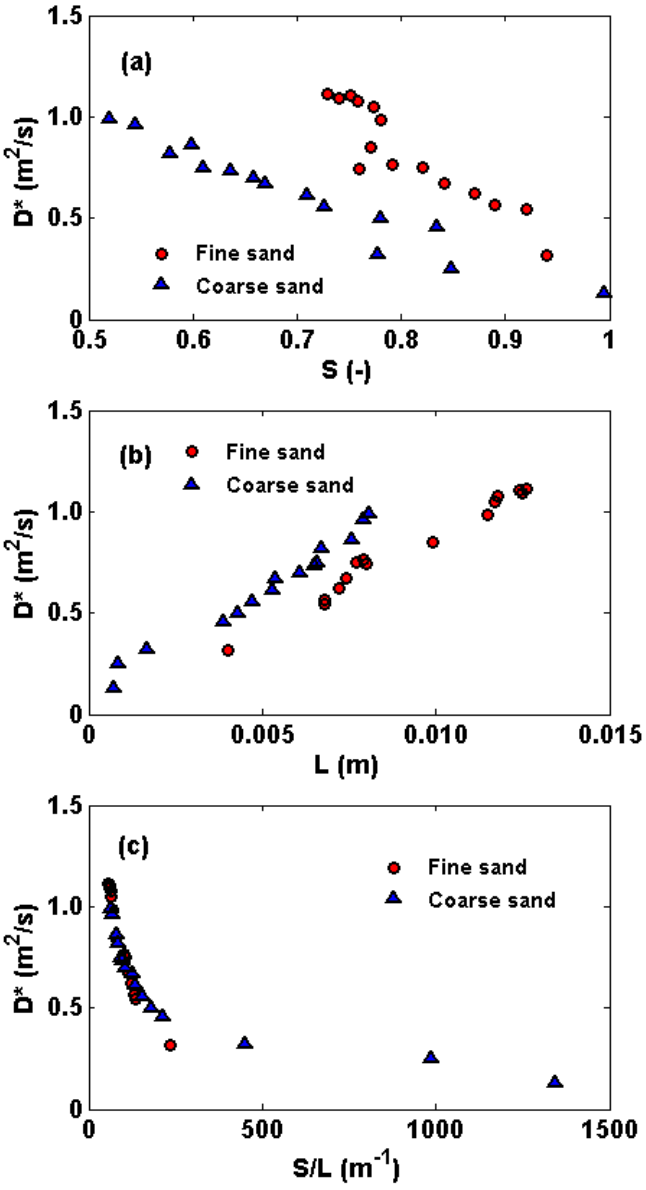

Figure 5.5. The variation of D^* versus (a) the average saturation of the invaded zone S, (b) length of the invaded (or unsaturated) zone L and (c) S/L.

Nearly similar variation of D^* in both fine and coarse sand, when plotted versus S/L, suggests that the two parameters, the average saturation of the invaded zone and the length of the invaded zone, are the key factors influencing D^* in drying porous media.

The present analysis extends the physical understanding of the mechanisms influencing solute transport in porous media during evaporation. , Moreover, the data and analysis are relevant to characterisation of drying of droplets containing salt solutions with the associated salt deposition patterns[36,37].

5.4. Methods Summary

We conducted synchrotron X-ray micro-tomography evaporation experiments with fine and coarse sands, initially fully saturated with a salt solution containing 5% calcium iodide (by weight) and packed in cylindrical plastic columns with an inner diameter of 8 mm and height of 16 mm. The experiments were conducted on the GeoSoilEnviroCARS (GSECARS) BM-13BMD beamline at the Advanced Photon Source, Argonne National Laboratory, IL. The columns were closed at all boundaries, except at the top that was open to air for water evaporation. The external conditions - ambient temperature and relative humidity - were similar and constant in both experiments. Image reconstruction was performed using programs developed by GSECARS to convert X-ray attenuation to 3D volumetric data. The resolution of the images was 12.01 microns. In this analysis, the top 13.2 mm of the sand column is used that includes 1103 reconstructed images of the 2D horizontal cross sections, with grey-scale values representing density distribution within the porous medium. The columns were scanned every 30 minutes during drying. The sand packs were visualized twice, once with X-rays with energies immediately above the K-edge (33.1694 keV) value of Iodide, and a second time with X-rays

with energies immediately below the K-edge value at 33.0690 keV. The difference in the grey value of the two scans yields the salt concentration at pore scale.

To convert the grey value to salt concentration, we followed the calibration method described by Shokri[21]. Briefly, to calibrate the grey values, CaI_2 solutions with concentration of 2%, 5%, and 25% (by mass) were imaged at the same energy levels above and below the Iodine K-edge value. A linear equation was obtained relating the known values of concentrations to the corresponding grey values of the solutions with a well-defined concentration. The linear equation was used as the calibration curve to relate the grey value at any given pixel and time during evaporation from sand columns to the salt concentration. This enabled us to delineate the temporal and spatial solute distribution at the pore-scale during evaporation.

Moreover, to quantify the liquid phase distribution and how it is influenced by the particle size distribution, the recorded pore-scale images were segmented following the procedure described by Shokri[21] and Shokri et al.[38] In-house codes were developed in MATLAB to analyse the images and distinguish between liquid, air and solid phases in each 2D cross section according to the distribution of their grey values. Threshold values were calculated to segment each phase. The segmented images were used to quantify the drying front displacement in porous media, the 3D dynamics of liquid phase distribution and the evaporative mass losses (presented in Fig. 5.2(c)). We used several segmentation algorithms for image analysis and liquid phase quantification and the estimated errors were at most as large as the size of the symbols in Fig. 5.2(c).

5.5. References

1. Rodriguez-Navarro, C., E. Doehne. Salt weathering: Influence of evaporation rate, super saturation and crystallization pattern. Earth Surf. Processes Landforms 24, 191–209 (1999).

2. Suweis, S., Rinaldo, A., Van der Zee, S.E.A.T.M., Daly, E., Maritan, A., Porporato, A. Stochastic modelling of soil salinity. Geophys. Res. Lett. 37, L07404 (2010).

3. Ott, H., Andrew, M., Snippe, J., Blunt, M.J. Microscale solute transport and precipitation in complex rock during drying. Geophys.Res. Lett. 41, 8369–8376 (2015).

4. Jambhekar, V.A., Helmig, R., Schroder, N., Shokri, N. Free-flow-porous-media coupling for evaporation-driven transport and precipitation of salt. Trans. Porous. Med. 110(2), 251-280 (2015).

5. Shokri-Kuehni, S.M.S., Vetter, T., Webb, C., Shokri, N. New insights into saline water evaporation from porous media: Complex interaction between evaporation rates, precipitation and surface temperature. Geophys. Res. Lett. 44, 5504–5510 (2017).

6. Larsen, F., Tran, L.V., Van Hoang, H., Tran, L.T., Christiansen, A.V., Pham, N.Q. Groundwater salinity influenced by Holocene seawater trapped in incised valleys in the Red River delta plain, Nature Geoscience 10(5), 376-381 (2017).

7. Guglielmini, L., Gontcharov, A., Aldykiewicz Jr., A.J., Stone, H.A. Drying of salt solutions in porous materials: Intermediate-time dynamics and efflorescence. Phys. Fluids 20, 077101 (2008).

8. Huinink, H.P., Pel, L., Michels, M.A. How ions distribute in a drying porous medium: A simple model. Phys. Fluids 14, 1389–1395 (2002).

9. Norouzi Rad, M., Shokri, N. Effects of grain angularity on NaCl precipitation in porous media during evaporation. Water Resour. Res., 50, 9020-9030 (2014).

10. Shokri-Kuehni, S.M., Norouzirad, M., Webb, C., Shokri, N. Impact of type of salt and ambient conditions on saline water evaporation from porous media. Adv. Water Resour. 105, 154–161 (2017).

11. Verran-Tissoires, S., Prat, M. Discrete salt crystallization at the surface of a porous medium. Phys. Rev. Lett. 108, 054502 (2012).

12. Naillon, A., Duru, P., Marcoux, M., Prat, M. Evaporation with sodium chloride crystallization in a capillary tube. J. Cryst. Growth 422, 52–61 (2015).

13. Bergstad, M., Shokri, N. Evaporation of NaCl solution from porous media with mixed wettability. Geophys. Res. Lett. 43, 4426–4432 (2016).

14. Derluyn, H., Moonen, P., Carmeliet, J. Deformation and damage due to drying-induced salt crystallization in porous limestone. J. Mech. Phys. Solids 63, 242–255 (2014).

15. Nachshon, U., Weisbrod, N. Beyond the Salt Crust: On Combined Evaporation and Subflorescent Salt Precipitation in Porous Media. Trans. Porous Med. 110(2), 295–310 (2015).

16. Rufai, A., Crawshaw, J. Micromodel observations of evaporative drying and salt deposition in porous media. Phys. Fluids 29, 126603 (2017).

17. Huinink, H.P., Pel, L., Michels, M.A.J. Structure and transport properties of liquid clusters in a drying porous medium. Phys. Rev. E 68, 056114 (2003).

18. Sghaier, N., Prat, M., Ben Nasrallah, S. On ions transport during drying in a porous medium. Trans. Porous Med. 67, 243–274 (2007).

19. Eloukabi, E. , Sghaier, N. , Ben Nassrallah, S. , Prat, M. Experimental study of the effect of sodium chloride on drying of porous media: the crusty–patchy efflorescence transition. Int. J. Heat Mass Transfer 56, 80–93 (2013).

20. Gran, M., Carrera, J., Olivella, S., Saaltink, M.W. Modeling evaporation processes in a saline soil from saturation to oven dry conditions. Hydrol. Earth Syst. Sci.. 15, 2077–2089 (2011).

21. Shokri, N. Pore-scale dynamics of salt transport and distribution in drying porous media. Phys. Fluids 26, 012106 (2014).

22. Méheust, Y., Løvoll, G., Ma°løy, K.J., Schmittbuhl, J. Interface scaling in a two-dimensional porous medium under combined viscous, gravity, and capillary effects. Phys. Rev. E 66, 051603 (2002).

23. Shokri, N., Sahimi, M., Or, D. Morphology, propagation dynamics and scaling characteristics of drying fronts in porous media. Geophys. Res. Lett. 39, L09401 (2012).

24. Shahraeeni, E., Lehmann, P., Or, D. Coupling of evaporative fluxes from drying porous surfaces with air boundary layer: Characteristics of evaporation from discrete pores. Water Resour. Res. 48, W09525 (2012).

25. Lehmann, P., Or, D. Effects of stomata clustering on leaf gas exchange. New Phytol. 207, 1015–1025 (2015).

26. Bergstad, M., Or, D., Withers, P.J., Shokri, N. The influence of NaCl concentration on salt precipitation in heterogeneous porous media. Water Resour. Res. 53, 1702–1712 (2017).

27. Sahimi, M., Davis, H.T., Scriven, L.E. Dispersion in disordered porous media. Chem. Eng. Commun. 23, 329-341 (1983).

28. Sahimi, M., Hughes, B.D., Scriven, L.E., Davis, H.T. Dispersion in flow through porous media: I. One-phase flow. Chem. Eng. Sci. 41, 2103-2122 (1986).

29. Sahimi, M., Heiba, A.A., Davis, H.T., Scriven, L.E. Dispersion in flow through porous media: II. Two-phase flow. Chem. Eng. Sci. 41, 2123-2136 (1986).

30. Charlaix, E., Hulin, J.-P., Plona, T.J. Experimental study of tracver dispersion in sintered glass porous materials of variable compactions. Phys. Fluids 30, 1690 (1987).

31. Charlaix, E., Hulin, J.-P., Leroy, C., Zarcone, C. Experimental study of tracer dispersion in flow through two-dimensional networks of etched capillaries. J. Phys. D 21, 1727 (1988).

32. Gist, G.A., Thompson, A.H., Katz, A.J., Higgins, R.L. Hydrodynamic dispersion and pore geometry in consolidated rock. Phys. Fluids A 2, 1533 (1990).

33. Sahimi, M., Imdakm, A.O. The effect of morphological disorder on hydrodynamic dispersion in flow through porous media. J. Phys. A 21, 3833-3870 (1988).

34. Sahimi, M. (1994) Applications of Percolation Theory, Taylor & Francis, London.

35. Sahimi, M. (2011), Flow and Transport in Porous Media and Fractured Rock, Wiley-VCH, Weinheim.

36. Shahidzadeh-Bonn, N., Rafai, S., Bonn, D., Wegdam, G. Salt crystallization during evaporation: Impact of interfacial properties. Langmuir 24, 8599–8605 (2008).

37. Shahidzadeh N., Schut, M., Desarnaud, J., Prat, M., Bonn, D. Salt stains from evaporating droplets, Sci. Rep. 5, 10335 (2015).

38. Shokri, N., Lehmann, P., Or, D. Liquid phase continuity and solute concentration dynamics during evaporation from porous media-pore scale processes near vaporization surface. Phys. Rev. E. 81, 046308 (2010).

Author Contribution

Salomé M.S. Shokri-Kuehni performed the data analysis, interpreted the data and wrote the first draft of the manuscript. Mina Bergstad helped with 3D image quantification and interpretation. Muhammad Sahimi and Colin Webb help with data interpretation and preparation of the manuscript. Nima Shokri designed the research, helped with the data interpretation and preparation of the manuscript. He supervised the general aspects and progression of the project.

Competing financial interests statement

The authors declare no competing interests as defined by Nature Research, or other interests that might be perceived to influence the results and/or discussion reported in this paper.

Data availability statement

The data presented in this manuscript will be available freely via sending a request to the corresponding author.

5.6. Acknowledgment

We gratefully acknowledge funding by the Leverhulme Trust (RPG-2014-331). Use of the Advanced Photon Source, an Office of Science User Facility operated for the U.S. Department of

Energy (DOE) Office of Science by Argonne National Laboratory, was supported by the U.S. DOE under Contract No. DE-AC02–06CH11357. The synchrotron X-ray microtomography was conducted at the GeoSoilEnviroCARS (GSECARS) BM-13BMD beamline. We would like to thank Dr. Mark Rivers for his assistance, great suggestions, and expertise in running the experiment with the synchrotron X-rays tomography. We are grateful to Mr. Peng Zhou and Nicholas Grapsas for conducting the experiments. The first and last author would also like to acknowledge the contribution and cooperation of Delphi Everest Dana Shokri-Kuehni during this research.

5.7. Supplementary Information

Fig. 5.S1 illustrates a typical example of the fitting the analytical model, Eq. (2), to the experimentally determined concentration profile to estimate the effective diffusion-dispersion coefficient presented in Fig. 5.5.

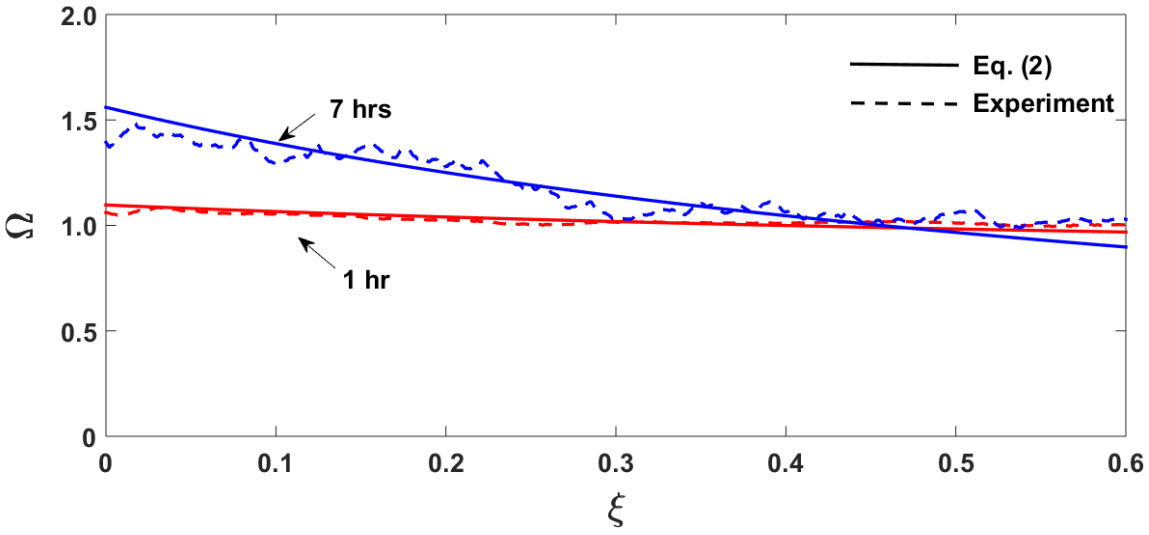

Figure 5.S1. An example of fitting Eq. (5.2) (solid lines) to the concentration profiles computed using the recorded pore-scale images (dash lines). The concentration profiles correspond to the fine-grains sand after 1 and 7 hrs from the onset of the evaporation experiments.

Chapter 6

SUMMARY AND CONCLUSIONS

This dissertation was in the so-called "alternative thesis format" which included three published papers and a fourth manuscript that is currently under review.

1. In the first paper (i.e. chapter 2), I looked into the potential application of drying porous layers for evaporative cooling practices. To do so, experiments were conducted using sand particles differing in particle size distribution saturated with pure water. The sand layers were placed under natural evaporation and the temperature distribution at the top and bottom of the drying layers were recorded using high resolution thermal imaging and temperature sensors.

   The results illustrated the ability of porous materials to regulate the temperature and its potential application for roof cooling. Strong correlations between the drying curves and the temperature dynamics were found. During stage-1, the temperature at top and bottom of the drying layers remained relatively constant. However, during the stage-2 evaporation the temperature at top of the drying layers increased because of the formation of a dry layer at the surface of porous media. The obtained results confirmed longer stage-1 evaporation periods for sand with smaller particles. Therefore, the temperature remained low for a longer time in the case of sand with smaller particles. This study illustrated the importance of the particle size of porous media when they are used in evaporative cooling practices which had not received enough attention in previous studies.

The rest of this dissertation was focused on the dynamics of saline water evaporation from porous media with a particular attention on how the evaporation rate is modified as a result of the presence of salt and the precipitated salt at the surface. I have also looked into the particle size effects on the dispersion coefficient during saline water evaporation from porous media. The main findings of these three chapters are listed below:

2. In chapter 3, a new conceptual model was presented to describe the saline water evaporation dynamics from porous media. The impact of the presence of wet and porous precipitated salt at the surface on the evaporation rate was illustrated in this chapter. Our microscopic analysis combined with the thermal imaging with high temporal and spatial resolution suggests that the presence of porous salt at the surface causes top-supplied creeping of the solution, feeding the growth of subsequent crystals. This effect contribiutes to further water evaporation and in contrary to the traditional understanding, the presence of the precipitated salt at the surface does not necessarily block the pores or cease the water evaporation because of the porous nature of the precipitated salt especially at the early stage of the process which remains wet due to the capillarity effects. As illustrated in chapter 3, the obtained results confirmed that the precipitated salt at the surface is an ever changing porous media with its own properties as long as it remains wet during evaporation.
3. In chapter 4, the effects of salt concentration and type of salt on the saline water evaporation rate from porous media was investigated. A simple but effective quantitative tool was proposed capable of describing the effects of various parameters such as ambient temperature, relative humidity, type of salt and salt concentration on the saline water evaporation rate from porous media. The proposed equation was validated against a

comprehensive series of experimental data using porous media saturated with three types of salt with varying concentrations. The evaporation curves measured under different ambient temperature, relative humidity and salt concentrations could be represented all on a single curve using the proposed equation. This further confirmed the minor impact of the presence of precipitated salt at the surface on the evaporation rate as long as the precipitated salt remains wet.

4. In chapter 5, synchrotron X-ray tomography was used to study ion transport during saline water evaporation from porous media in 4D (3D space + time). The pore-scale results revealed the effects of particle and pore size distribution on the solute transport during evaporation from porous media. Using Iodine K-edge dual energy imaging, we could quantify the ion concentration at pore scale with a high temporal and spatial resolution. The analysis illustrated that this technology can be used as a powerful tool to investigate the dynamics of solute transport in porous media. Using the measured concentration profiles and the analytical solution of the convection-dispersion equation (CDE), we could obtain a quantitative estimate of the evolution of the dispersion coefficient as influenced by the particle size distribution of porous media during evaporation. Our results confirmed that the parameter D in the CDE increases as the liquid saturation decreases during evaporation. Furthermore, we could show that the effective dispersion coefficient depends not only on the saturation, but also on the complex liquid network and its morphology formed during the evaporation process.

6.1. Future work

1. This dissertation revealed the importance of the morphology and dynamics of the precipitated salt at the surface on the overall drying behaviour. More research is required

to quantify how exactly the pore size distribution and evolution of the porous precipitated salt influences the evaporation rate. Such efforts may result in developing equations capable of describing the relationship between the precipitated salt dynamics and the evaporation rates. This will be very useful in developing reliable models to predict the dynamics of saline water evaporation from porous media. Microfluidics experiments and 4D X-ray tomography could be useful tools to investigate this relationship.

2. Another important aspect could be including vegetation and plants in the saline water evaporation studies to quantify how salinity influences the plant growth and biomass production. In addition, the findings regarding the influence of particle size distribution on the salt concentration profile can be used, to investigate the relations between particle size distributions and salinity resistance as a function of plant rooting depth.
3. Another possible extension of this work could be the inclusion of mixtures of salts instead of only one type of salt. This aspect was not investigated in the present study. It would serve as a first step to working with seawater or contaminated groundwater.
4. Considering the presence of a water table into the analysis could be another potential extension of this work. The presence of a water table influences the dynamics of water content distribution as well as the connectivity of the liquid pathways through the soil profile. In the case of shallow water tables, the surface might be in hydraulic connection with the water table via capillary induced liquid pathways. However, in the case of deep water tables, such connection may not exist anymore and the water evaporation may occur at a depth somewhere below the surface. This will significantly influence not only the evaporative mass losses but also the solute deposition patterns.